DOI:10.28974/idojaras.2024.1.1

IDŐJÁRÁS

Quarterly Journal of the HungaroMet Hungarian Meteorological Service
Vol. 128, No. 1, January – March, 2024, pp. 1–26

Strong differences in microclimate among the habitats of a forest-steppe ecosystem

Ho Vu Khanh[1,2,*], **Gabriella Süle** [3], **Bence Kovács** [3], and **László Erdős** [3,4]

[1]*Doctoral School of Environmental Sciences, University of Szeged*
6720 Szeged, Rerrich Béla tér 1, Hungary

[2]*Faculty of Natural Resources-Environment, Kien Giang University*
Kien Giang, Vietnam

[3]*Institute of Ecology and Botany, HUN-REN Centre for Ecological Research*
2163 Vácrátót, Alkotmány u. 2-4., Hungary

[4]*HUN-REN-UD Functional and Restoration Ecology Research Group*
4032 Debrecen, Egyetem sqr. 1., Hungary

**Corresponding author E-mail: hvkhanh@vnkgu.edu.vn*

(Manuscript received in final form June 23, 2023)

Abstract— Microclimate has a substantial impact on plant composition, survival, and growth, as well as ecosystem processes. Although microclimatic conditions in anthropogenically fragmented ecosystems have received considerable scientific attention, they are understudied in naturally fragmented ecosystems, including forest-steppes. In addition, earlier investigations in these mosaics only measured microclimate parameters for a very short period (i.e., 24 hours on a single summer day). In the present study, the long-term microclimatic conditions were described in multiple habitat types, both woody and non-woody, in a sandy forest-steppe ecosystem in the Kiskunság, central Hungary. The aim of this study was to answer (1) how air humidity and temperature conditions differ among the studied habitats during the growing season and (2) which habitats are more stressed to vegetation growth regarding vapor pressure deficit (VPD). Wireless sensors recording air temperature and humidity values were used to monitor microclimatic parameters. VPD values were calculated based on the obtained air temperature and humidity, and two thresholds at 1.2 and 3.0 kPa were defined. To compare mean air temperature and humidity variables, as well as above-threshold VPD rate among habitat types, general linear models were used. Our results indicated that open grasslands were the warmest and driest habitats. Among woody habitats, south-facing edges had the harshest microclimatic conditions. The current work also found that small forest patches and larger

forest patches had similar air temperature and humidity variables. Regarding VPD, open grasslands were the most stressed for vegetation growth from May to October. During the summer season, forest patches had a small moderating effect at the limiting threshold of 1.2 kPa VPD, but a stronger moderating effect at the 3.0 kPa threshold. With ongoing climate change, this role of forest patches is expected to become increasingly important in forest-steppes. Therefore, it is suggested that the remaining near-natural forest stands in sandy forest-grassland ecosystems should be prioritized for protection, and that scattered trees or groups of trees of native species should be established in extensive treeless grasslands.

Key-words: air humidity, air temperature, climate change, drought, forest edges, forest-steppes, grasslands, vapor pressure deficit (VPD).

1. Introduction

Globally, increasing temperature has been observed during the last few decades, and this trend is expected to continue in the 21st century (*IPCC,* 2018), potentially having severe consequences on the structure, composition, and function of plant communities (*Suggitt et al.,* 2011; *Bellard et al.,* 2012; *Hofmeister et al.,* 2019; *Aalto et al.,* 2022). This tendency is seriously threatening biodiversity as it may result in species and habitat loss (*Kappelle et al.,* 1999; *Araújo et al.,* 2011; *Bellard et al.,* 2012; *Erdős et al.,* 2018a). Climate change has been reported to have a major effect on vegetation dynamics globally (*Bakkenes et al.,* 2002; *Walther et al.,* 2002; *Krishnaswamy et al.,* 2014; *Zhan et al.,* 2022). Although responses of plant communities to climate change are hard to predict, ecosystems that are fragmented either by natural processes or artificially-induced factors could be especially sensitive (*Kertész* and *Mika,* 1999; *Bartha et al.,* 2008; *Travis et al.,* 2003; *Erdős et al.,* 2018b).

In the northern hemisphere, the most noticeable naturally fragmented ecosystems are forest-steppes, composed of woody and herbaceous patches (*Erdős et al.,* 2018b). It is reasonable to assume that increasing temperature and decreasing precipitation considerably inhibit the growth of woody vegetation in these ecosystems (*Erdős et al.,* 2022). A drying tendency has been observed, and is expected to become more serious in the future, in the Carpathian Basin, particularly in the Kiskunság (central Hungary) (*Bartholy et al.,* 2007; 2014; *Blanka et al.,* 2013), where forest-steppe forms the natural vegetation. The global drying tendency is additionally exacerbated by regional processes. For example, afforestation (especially with non-native evergreen trees) and the spontaneous spread of invasive species are further reducing water level in the Kiskunság (*Tölgyesi et al.,* 2020). Indeed, the groundwater level is currently declining in the whole area (*Biró et al.,* 2007; *Szabó et al.,* 2022) resulting in the increasing mortality rate of mature oak trees in forest patches (*Molnár,* 2003; *Molnár et al.,* 2012).

Microclimate can be defined as the climate condition near the ground level at a small scale, ranging from centimeters to several hundred meters (*Davies-Colley et al.*, 2000; *Zellweger et al.*, 2019; *De Frenne et al.*, 2021). It is likely to regulate plant survival, growth, distribution, and interaction (*Arnone et al.*, 2008; *Dingman et al.*, 2013; *De Frenne et al.*, 2021; *Meeussen et al.*, 2021) and has a significant impact on ecosystem processes such as vegetation dynamics and nutrient cycles (*Davies-Colley et al.*, 2000; *Riutta et al.*, 2012; *Schmidt et al.*, 2019). Air temperature and relative air humidity are the most important microclimate components, which have a profound impact on vegetation under extreme environmental conditions (*Sih et al.*, 2000; *Erdős et al.*, 2014, 2018a; *De Frenne et al.*, 2021). In addition, vapor pressure deficit (VPD), obtained from air temperature and humidity, has a noteworthy influence on how much water is necessary for plants to grow optimally (*Şahin et al.*, 2013; *Süle et al.*, 2020). The relationship between water and plant is extremely sensitive to environmental extremes (e.g., drought events or heat waves), resulting in an increase of VPD that hastens faster plant transpiration into the atmosphere (*Reyer et al.*, 2013). Hence, VPD is considered an important limiting factor for plant survival, growth, and regeneration with ongoing climate change (*Breshears et al.*, 2013; *Will et al.*, 2013; *Williams et al.*, 2013).

It is well known that vegetation has a significant effect on the climate conditions near the surface (*Geiger et al.*, 2009). Previous works have indicated that microclimatic differences among various habitat types may become more pronounced under climate change, and that canopy cover plays an important role in buffering harsh environmental conditions (*Suggitt et al.*, 2011; *Ashcroft* and *Gollan*, 2012; *Hardwick et al.*, 2015). According to *De Frenne et al.* (2013), microclimate, rather than macroclimate, may be a better predictor of how well canopy cover mitigates extreme temperature. This is especially relevant in ecosystems where tree-dominated and grass-dominated habitats coexist under the same macroclimatic condition. Although microclimate measurements in anthropogenically fragmented ecosystems have received considerable scientific attention (*Chen et al.*, 1993, 1995; *Pohlman et al.*, 2009; *Wright et al.*, 2010; *Luskin* and *Potts*, 2011; *Magnago et al.*, 2015; *Schmidt et al.*, 2019), knowledge of microclimate variables in naturally fragmented vegetation types (e.g., forest-steppes) have received less attention in previous studies (but see *Erdős et al.*, 2014; *Süle et al.*, 2020).

Forest-steppes are structured by the co-occurrence of differently sized forest and grassland patches of various types, connected by an intricate network of differently exposed edges (*Erdős et al.*, 2018b). As a result of varying vegetation cover among the habitats in forest-steppes, microclimate can vary significantly even over short distances (*Erdős et al.*, 2023). Vegetation-environment relations have been intensively studied recently, with special emphasis on soil moisture, air humidity, and air temperature patterns (e.g., *Bátori et al.*, 2014; *Erdős et al.*, 2014, 2018a; *Tölgyesi et al.*, 2018). However, earlier investigations measured microclimate parameters for only a very short period (typically 24 hours on a selected summer

day) in forest-steppes (*Erdős et al.*, 2014, 2018a; *Tölgyesi et al.*, 2018; *Milošević et al.*, 2020). These short-term measurements may not be able to capture the most critical microclimatic conditions. To gain more informative microclimate background data, repeated measurements are needed throughout the vegetation period, from spring to autumn. Furthermore, earlier studies did not take into account the full variety of forest-grassland mosaics: some works disregarded the edge habitat (e.g., *Tölgyesi et al.* 2018; *Milošević et al.* 2020), while others restricted their attention to small forest patches and a single type of grassland (e.g., *Erdős et al.* 2014; *Süle et al.* 2020). Thus, measuring microclimate in a broader spectrum of near-natural forest-steppe habitats is necessary to fill the above knowledge gap.

The aim of this study was to describe the microclimate conditions of multiple habitat types throughout the vegetation period, in a sandy forest-steppe ecosystem. Our specific questions were the following: (1) How do air temperature and humidity differ among the studied habitats during the growing season from April to October? (2) Which habitats are more stressed to vegetation growth in terms of vapor pressure deficit?

2. Materials and methods

2.1. Study area

The study was conducted in the Kiskunság Sand Ridge, a large plain between the Danube and Tisza rivers in central Hungary. For the study, an area near Fülöpháza (N 46° 51'; E 19° 25'), located in the center of the Sand Ridge, has been chosen (*Fig. 1*). This area is part of the Kiskunság National Park. The climate is subcontinental with a sub-Mediterranean influence, the mean annual temperature and precipitation are 10.5 ºC and 530 mm, respectively (*Dövényi*, 2010). The study site is made up of calcareous sand dunes that are covered by humus-poor sandy soils with low water retention capacity; however, humous sandy soils with slightly better moisture supply are found in forest patches (*Várallyay*, 1993).

The natural vegetation of the area is a mosaic of forest and grassland patches (*Fig. 2a, b*). Forests are naturally fragmented, resulting in a variety of forest patches ranging in size from a few dozen square meters to ca. one hectare. Three differently sized forest groups were defined in this study: large forest patches (> 0.5 ha), medium forest patches (0.2–0.4 ha), and small forest patches (< 0.1 ha) (*Fig. 2c-e*). Forest stands (*Junipero-Populetum albae*) have a canopy cover of approximately 50-70% and are dominated by *Populus alba* trees, with a height of 10–15 m. The shrub layer, with covers of 5–80% and heights of 1–5 m, is structured by *Berberis vulgaris, Crataegus monogyna, Ligustrum vulgare,* and *Rhamnus catharticus.* The herb layer is typically composed of *Asparagus officinalis*, *Calamagrostis epigeios*, *Carex liparicarpos*, *Euphorbia cyparissias*, and *Poa angustifolia*.

Edge is defined as the zone out of the outmost trunks of trees, below the canopy layer. The edges are commonly covered by shrubs (mainly *Crataegus monogyna*, *Juniperus communis*, and *Ligustrum vulgare*) and herbaceous species (primarily *Calamagrostis epigeios*, *Cynoglossum officinale*, *Festuca vaginata*, and *Poa angustifolia*). In this study, only north- and south-facing edges were considered (*Fig. 2f, g*) as they are expected to have significantly different environmental conditions (*Stoutjesdijk* and *Barkman*, 1992; *Ries et al.*, 2004; *Heithecker* and *Halpern*, 2007).

The most conspicuous grassland in the study area is open perennial grassland (*Festucetum vaginatae)*, with a total vascular plant cover of ca. 50–70% (*Fig. 2h*). *Festuca vaginata*, *Stipa borysthenica*, and *S. capillata* are dominant species in this grassland type. Other common species include *Alkanna tinctoria*, *Arenaria serpyllifolia*, *Centaurea arenaria*, and *Holosteum umbellatum*.

Open annual grasslands *(Secali sylvestris-Brometum tectorum)* are co-dominated by *Bromus tectorum* and *Secale sylvestre*, having a cover of approximately 20–50% (*Fig. 2i*). Other typical species occurring in this grassland include *Bromus squarrosus*, *Poa bulbosa*, *Polygonum arenarium*, *Syrenia cana*, and *Tragus racemosus*. Detailed information about the vegetation of forests, edges, and grasslands in the Kiskunság Sand Ridge is provided in the previous study of *Erdős et al.* (2023).

The names of vascular plant taxa are according to *Király* (2009), while plant community names follow *Borhidi et al.* (2012).

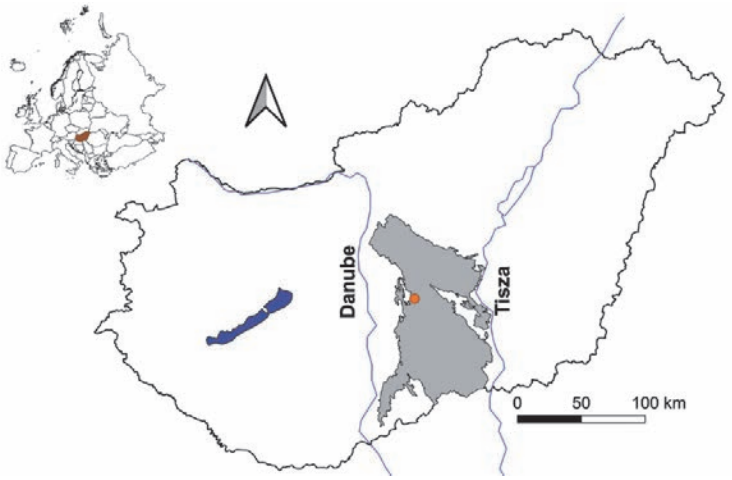

Fig. 1. The location of the Fülöpháza area (orange dot) in the Kiskunság Sand Ridge (grey), central Hungary.

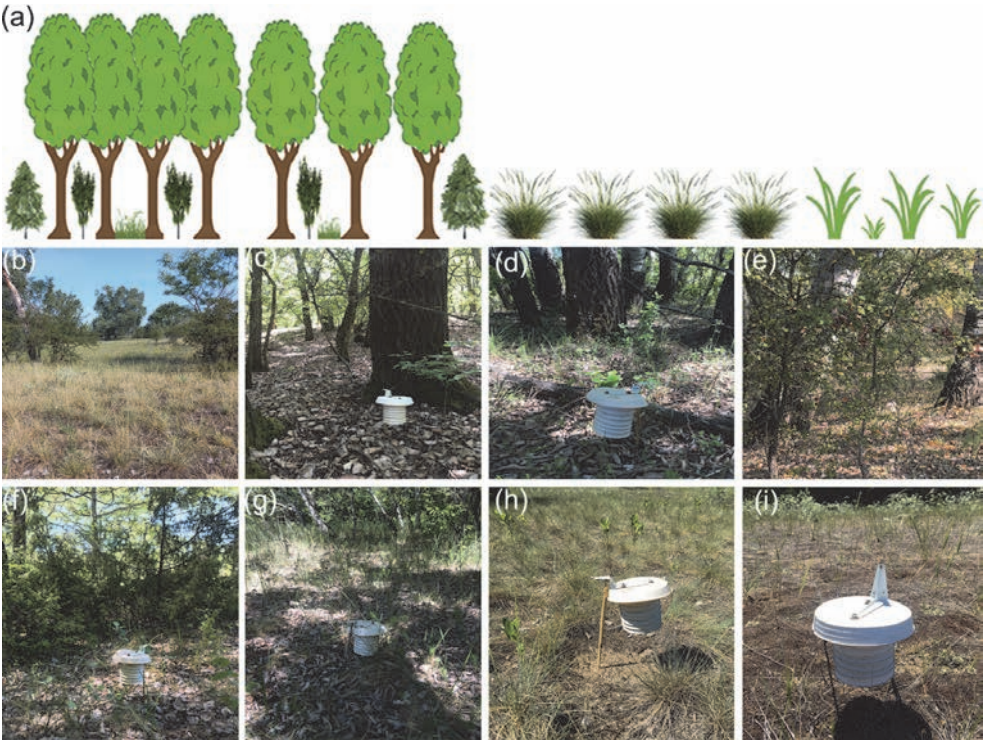

Fig. 2. (a) The model of forest-steppes, and (b) a mosaic of forests and grasslands at the Fülöpháza area. The following seven habitat types were included in this study: (c) large forest patch, (d) medium forest patch, (e) small forest patch, (f) north-facing forest edge, (g) south-facing forest edge, (h) open perennial grassland, and (i) open annual grassland.

2.2. Data collection

Microclimate measurements were carried out in the seven habitat types described above (i.e., large forest patches, medium forest patches, small forest patches, north-facing forest edges, south-facing forest edges, open perennial grasslands, and open annual grasslands). Three replicates for each habitat type were used. The air temperature (ºC) and relative air humidity (%) were measured once every month in all seven habitats from April to October 2022. They were measured synchronously 20 cm above the ground surface in the center of each habitat for 24 hours (i.e., a day per month) using MCC USB-502 data loggers (Measurement Computing Corporation, Norton, MA, USA). The resolution of the sensors was

set to once every minute; therefore, each sensor yielded 1440 temperature and 1440 humidity data records per day. The loggers were placed in naturally ventilated radiation shields in order to avoid direct solar radiation. The sampling occasions were selected under clear weather conditions, but the weather was cloudy during the second daytime periods of July and was rainy during the first couple of hours during September.

2.3. Data analysis

The following variables were computed from the obtained microclimate data: mean daily air temperature (MDAT), mean daytime air temperature (MDtAT), mean nighttime air temperature (MNtAT), mean daily relative air humidity (MDAH), mean daytime relative air humidity (MDtAH), and mean nighttime relative air humidity (MNtAH). Daytime was defined as the interval from 7:01 a.m. to 7:00 p.m., while nighttime was the interval from 7:01 p.m. to 7:00 a.m. (see *Bátori et al.*, 2014; *Erdős et al.*, 2014, 2018a). These variables were calculated for each replicate.

Vapor pressure deficit was selected as the meaningful limiting factor for plant growth and productivity (*McDowell et al.*, 2008; *Yuan et al.*, 2019; *Süle et al.*, 2020). Vascular plants may be stressed if VPD values exceed a certain threshold (*Novick et al.*, 2016; *Shamshiri et al.*, 2018; *Süle et al.*, 2020). This factor (VPD, Pa) was calculated from the air temperature (t, ^{o}C) and relative air humidity (H, %) according to *Bolton* (1980):

$$VPD = (100 - H) \times 6.112 \times e\hat{}(17.67 \times t/(t + 234.5)).$$

In this study, the exceedance rate was analyzed, which is the percentage of VPD values above an appropriate threshold (1.2 or 3.0 kPa) over a 24-hour period. This approach can help us better understand the microclimatic conditions that affect vegetation growth (*Süle et al.*, 2020). The limiting threshold for the stress effect was set at 1.2 kPa, as suggested by many previous studies (*Novick et al.*, 2016; *Shamshiri et al.*, 2018; *Süle et al.*, 2020), whereas 3 kPa threshold had a stronger inhibitory effect on plant growth and photosynthesis (*Shirke* and *Pathre*, 2004; *Shibuya et al.*, 2018; *Süle et al.*, 2020). A VPD duration curve (DC) was constructed using 1440 VPD values that were averaged over three replicates collected over the period of 24 hours for each habitat per month. This method is similar to the flow duration curve in hydrology and is thoroughly described by *Süle et al.* (2020). In addition, the DC for each replicate was also calculated. Based on this DC, the exceedance rate was calculated per replicate, which was then used for statistical analysis.

The variables related to mean daily air temperature, mean daytime air temperature, mean nighttime air temperature, mean daily relative air humidity (MDAH), mean daytime relative air humidity, and mean nighttime relative air

humidity, as well as exceedance rate were analyzed using general linear models. The fixed factor was the habitat. The “glm” function in R version 4.1.2 was used to build the models with Gaussian family (*R Core Team*, 2021). The assumptions of the models were checked by visual assessment of diagnostic plots. The general linear models were then tested using analysis of variance (ANOVA) with the “Anova” function in the car package (*Fox* and *Weisberg*, 2019). If the model had a significant proportion of variability, all pairwise comparisons of the fixed factor levels were performed using the “emmeans” function in the emmeans package in R (*Lenth*, 2022). The p-values were adjusted with the false discovery rate (FDR) method.

3. Results

3.1. Air temperature patterns

The general 24-hour patterns of air temperature were somewhat similar in all habitats in each month, with a peak around or slightly after noon and a bottom during nighttime (*Fig. 3*). The temperature did not differ largely among habitats in April (*Fig. 3a*), whereas there were larger differences between open grasslands and forests during 24 hours for the other months (*Fig. 3b-g*). A distinct tendency between differently oriented edges was found. South-facing edges had similar patterns to the grasslands during the daytime, but they were closer to the forests at nighttime. North-facing edges resembled forests during the whole day. A similar pattern was observed for the seven-month average (*Fig. 3h*). Temperatures among habitats did not vary largely in the last couple of hours of the July measurement, when the weather was cloudy (*Fig. 3d*), while they fluctuated considerably in the first few hours of the September measurement, when the weather was rainy (*Fig. 3f*).

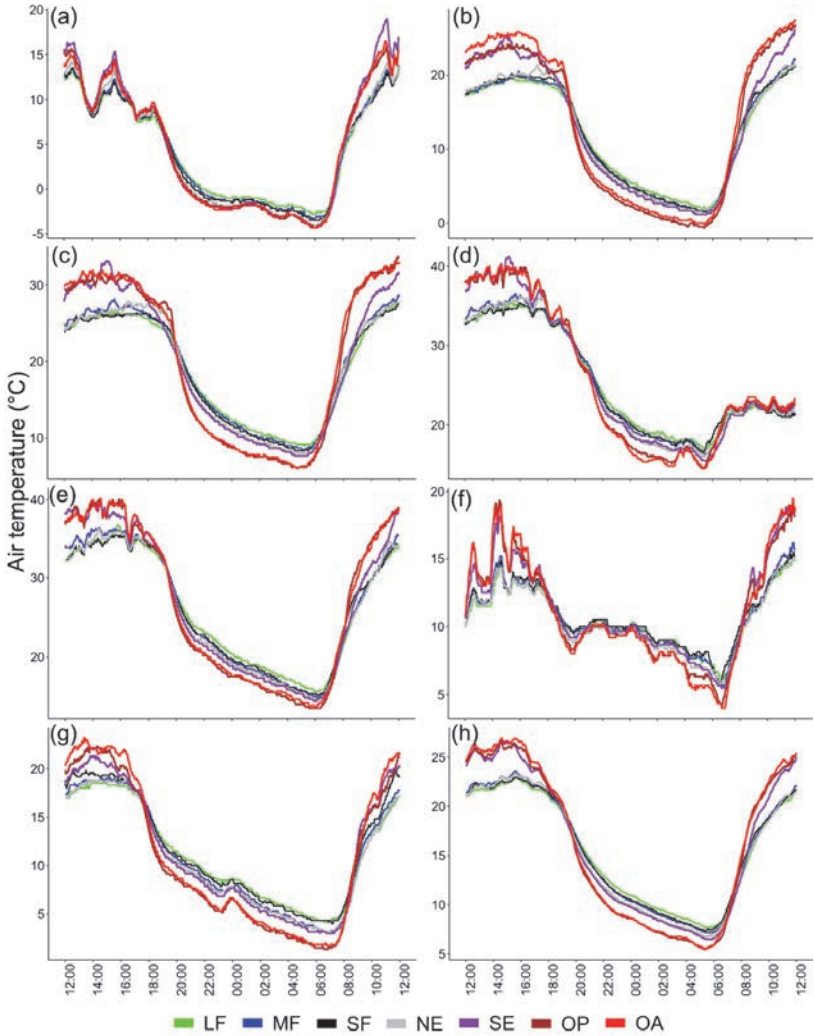

Fig. 3. Air temperature values for the various habitat types over a 24-hour period. The values for each minute are averaged over three replicates. The air temperature values were measured for the following months: (a) April, (b) May, (c) June, (d) July, (e) August, (f) September, (g) October, and (h) seven-month average. LF: large forest patches; MF: medium forest patches; SF: small forest patches; NE: north-facing forest edges; SE: south-facing forest edges; OP: open perennial grasslands; OA: open annual grasslands.

The mean daily air temperatures were very similar among the habitats in most measured months, but the daytime and nighttime values were significantly different among the habitats in each month (*Fig. 4a-g*). The diurnal range values were remarkably large in all habitats, but the largest values were observed in open

perennial and open annual grasslands. The mean daytime air temperature was the highest in south-facing edges and open grasslands, while the mean nighttime air temperature was the lowest in the open grasslands. For the seven-month averaged values, there was an increasing trend of daytime air temperatures along the vegetation gradient, while the opposite trend was seen for the nighttime air temperatures (*Fig. 4h*).

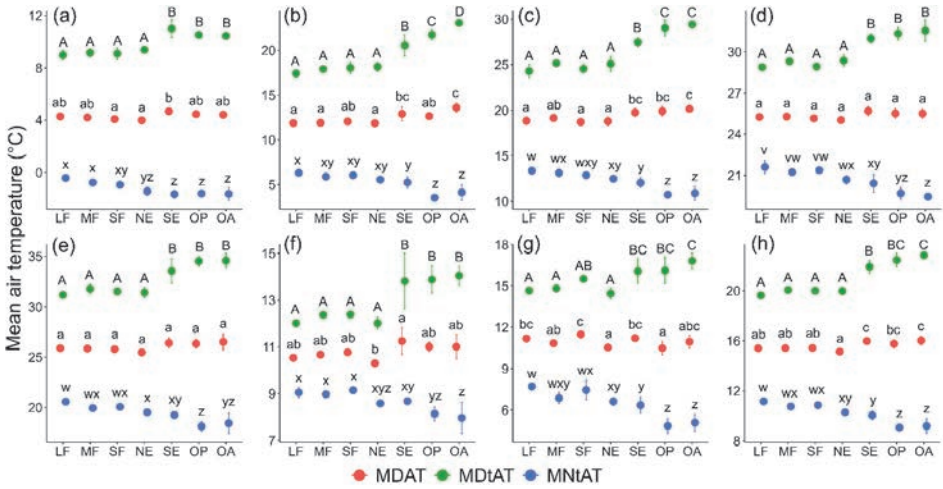

Fig. 4. Mean daily, daytime, and nighttime air temperature values of the habitat types (mean ± standard deviation). The values are averaged over three replicates (large dots). The mean air temperature values were measured for the following months: (a) April, (b) May, (c) June, (d) July, (e) August, (f) September, (g) October, and (h) seven-month average. Habitat type abbreviations are according to the caption of *Fig. 3.* Different letters indicate significant differences among habitats. MDAT: mean daily air temperature; MDtAT: mean daytime air temperature; MNtAT: mean nighttime air temperature.

3.2. Relative air humidity patterns

The 24-hour patterns of relative air humidity showed the opposite trend compared to air temperature (*Fig. 5*). In April, the values of relative air humidity measured at the same time were quite similar among habitats, although south-facing edges seemed to have somewhat lower relative air humidity than the other habitats at nighttime (*Fig. 5a*). From May to October, the driest habitats were south-facing edges, open perennial grasslands, and open annual grasslands during the daytime (*Fig. 5b-g*). However, open perennial grasslands (and sometimes north-facing edges) were the most humid during the nighttime. This pattern repeated itself for

the seven-month mean (*Fig. 5h*). The values of air humidity remained high during the second daytime period of July (*Fig. 5d*), whereas humidity fluctuated significantly in the first couple of hours of April and September (*Fig. 5a, f*).

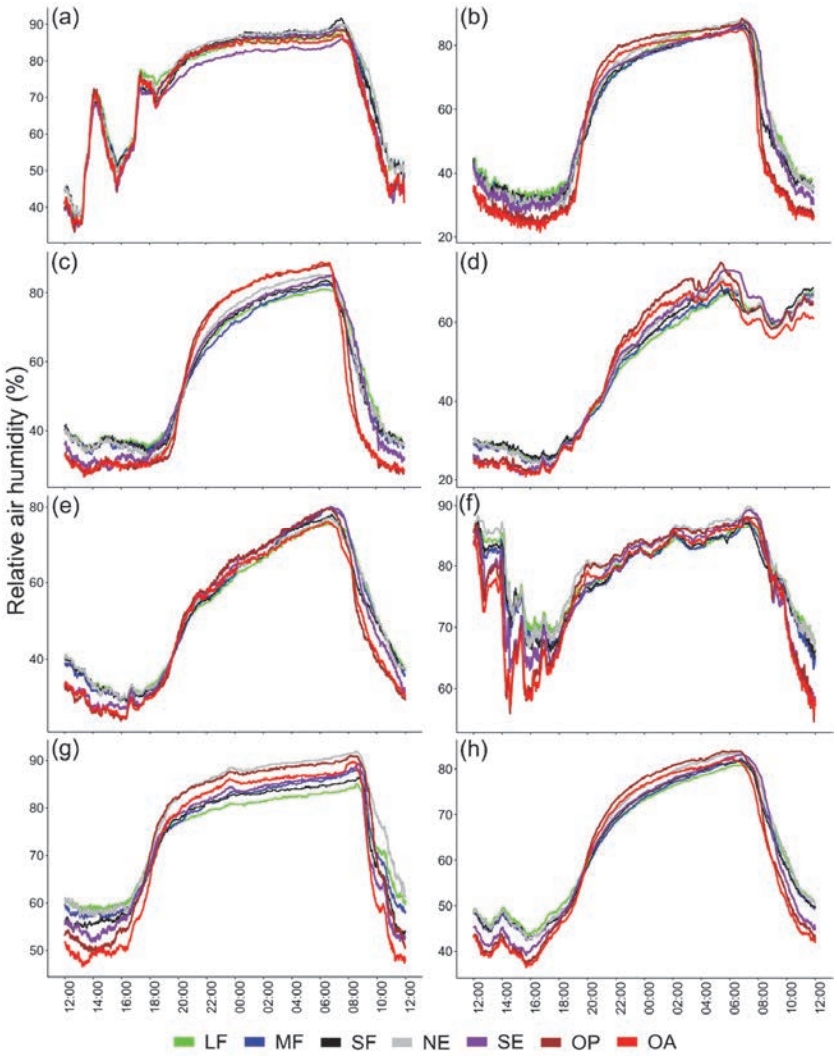

Fig. 5. Relative air humidity values for the various habitat types over a 24-hour period. The values for each minute are averaged over three replicates. The relative air humidity values were measured for the following months: (a) April, (b) May, (c) June, (d) July, (e) August, (f) September, (g) October, and (h) seven-month average. Habitat type abbreviations are according to the caption of *Fig. 3*.

The present study showed that, with the exception of May, mean daily air humidity did not differ significantly among habitats (*Fig. 6*). A similar pattern was also revealed for the mean nighttime air humidity values, but a peak was shown at open perennial grasslands in June and July (*Fig. 6c, d*). Regarding mean daytime air humidity, open grasslands were the driest habitats in most months, followed by south-facing edges (*Fig. 6a-g*). For the seven-month averaged values, both open grassland types had the lowest daytime air humidity, while open perennial grasslands had the highest air humidity at night (*Fig. 6h*). Rain generated a very similar but more pronounced jittering in the air humidity data as in the air temperature.

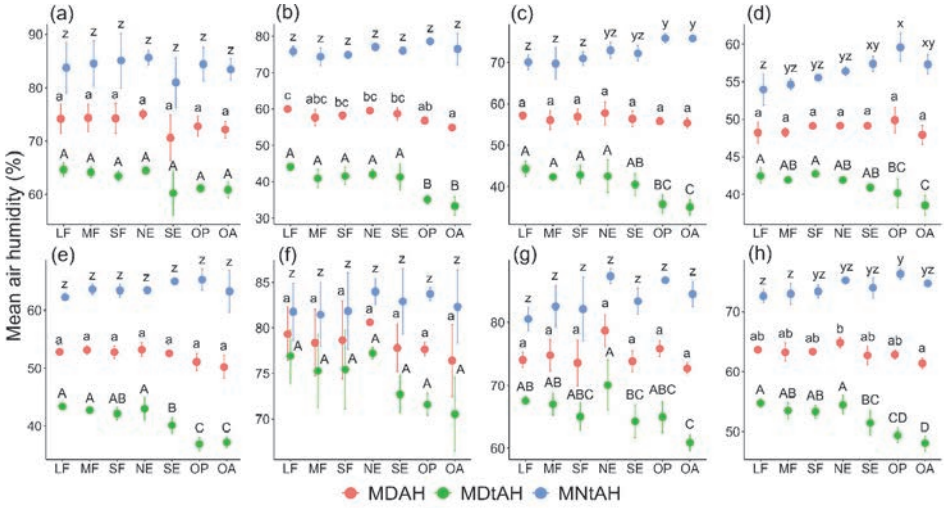

Fig. 6. Mean daily, daytime, and nighttime air humidity values of the habitat types (mean ± standard deviation). The values are averaged over three replicates (large dots). The mean air humidity values were measured for the following months: (a) April, (b) May, (c) June, (d) July, (e) August, (f) September, (g) October, and (h) seven-month average. Habitat type abbreviations are according to the caption of *Fig 3*. Different letters indicate significant differences among habitats. MDAH: mean daily air humidity; MDtAH: mean daytime air humidity; MNtAH: mean nighttime air humidity.

3.3. The patterns of vapor pressure deficit (VPD)

The VPD values calculated over 24 hours for each month and the seven-month average were quite high around noon but quite low during the nighttime (*Fig. 7a-h*). During the daytime, the VPD values of the woody habitats (i.e., forests and edges) were consistently lower than those of open grasslands, with the exception of April. Interestingly, the south-facing edges had higher VPD values than other woody

habitats and had a similar trend to grasslands, while north-facing edges seemed similar to forest interiors. The VPD values were extremely high in the summer season (from June to August), especially in July and August. There were no large differences among habitats at nighttime. A prominent effect of rain and cloudy sky on air temperature and relative air humidity was observed in July and September, which also affected the 24-hour patterns of VPD (*Fig. 7d, f*).

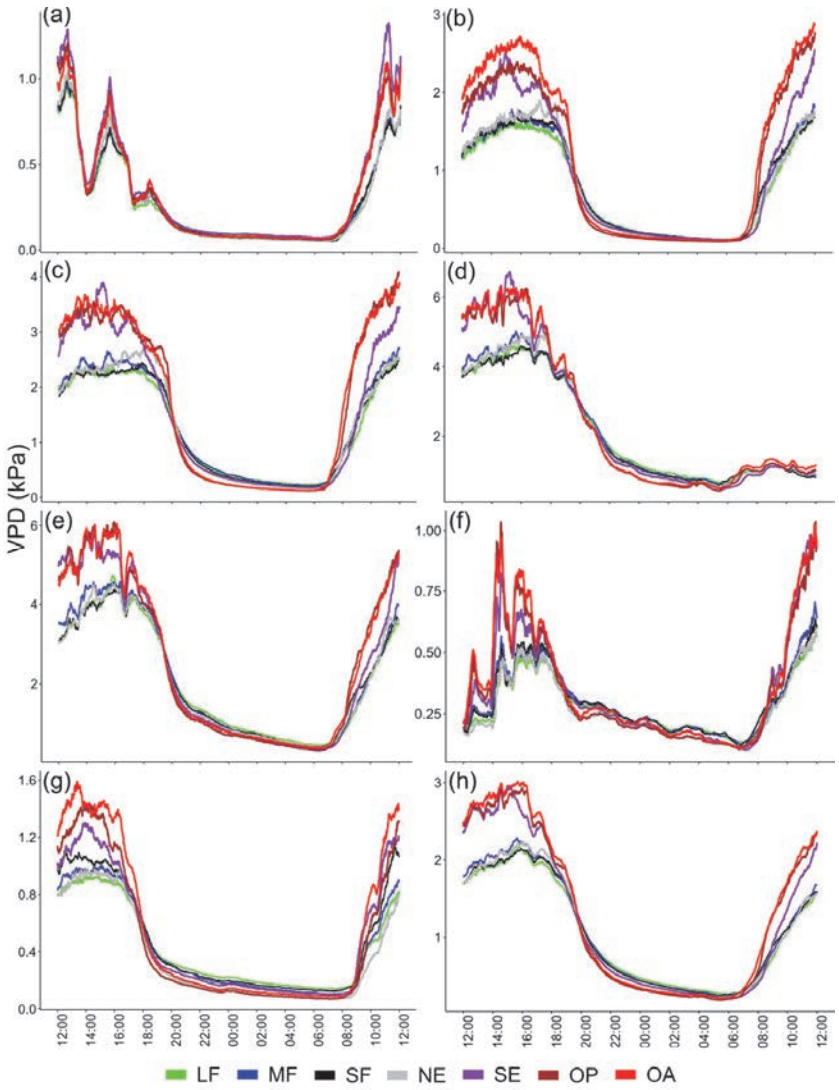

Fig. 7. VPD values for the various habitat types over a 24-hour period. The values for each minute are averaged over three replicates. The VPD values were measured for the following months: (a) April, (b) May, (c) June, (d) July, (e) August, (f) September, (g) October, and (h) seven-month average. Habitat type abbreviations are according to the caption of *Fig. 3*.

Based on the VPD duration curves (*Fig. 8*), it was found that VPD values exceeded the 1.2 kPa stress threshold for all habitats from May to August. In October, south-facing edges and open grasslands had VPD values higher than 1.2 kPa, but with a low exceedance rate from 4.64% to 23.3%. In terms of the 3 kPa threshold, the summer season seemed critical, with open grasslands and south-facing edges having higher exceedance rates than other habitats. For the seven-month average VPD values, the exceedance rate for 1.2 kPa varied between 39.3 and 46.0% in the studied habitats, while the exceedance rate for 3 kPa was less than 1%, with open annual grasslands having the highest value (*Fig. 8h*).

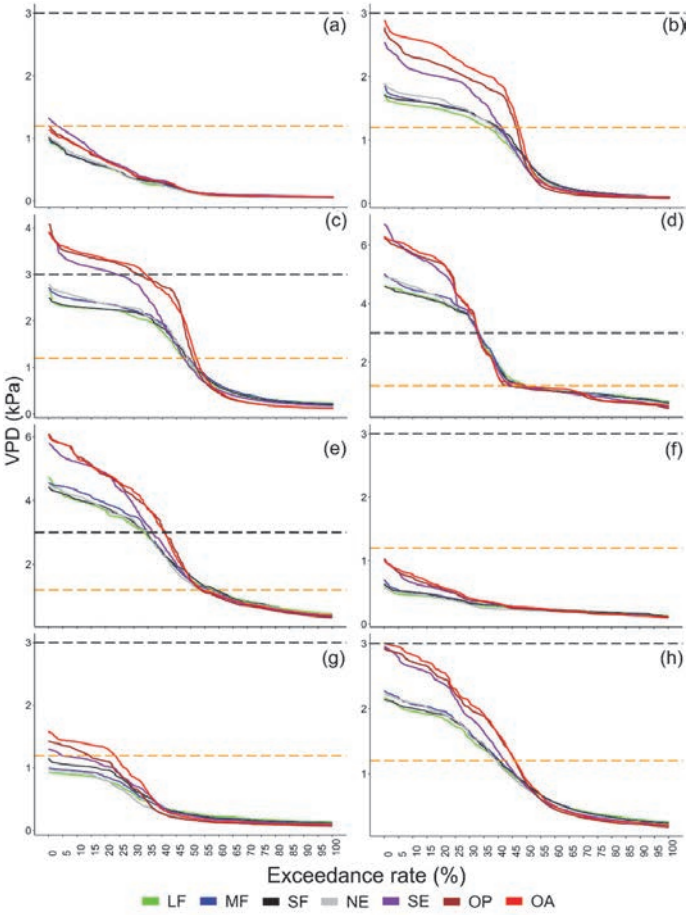

Fig. 8. VPD duration curves for habitat types from a 24-hour measurement period each month: (a) April, (b) May, (c) June, (d) July, (e) August, (f) September, (g) October, and (h) seven-month average. The VPD values for each minute are averaged over three replicates. The orange dashed line indicates the 1.2 kPa physiological threshold; the black dashed line indicates the 3.0 kPa threshold, above which the exceedance rates significantly diversified. Habitat type abbreviations are according to the caption of *Fig. 3*.

Exceedance rate was significantly different among habitats from May to October, except for July and September (*Fig. 9*). The study revealed that the exceedance rate was very low in April and September (*Fig. 9a, f*). In May, the most stressed habitats were open grasslands at a 1.2 kPa physiological threshold (*Fig. 9b*). For June, open grasslands were the most stressed, followed by south-facing edges at a 3 kPa limiting threshold (*Fig. 9c*). Interestingly, all habitats were very stressed and were thus not significantly different among habitats in July at both limiting thresholds (*Fig. 9d*), while open grasslands were the harshest habitats in August at the 3 kPa threshold and in October at 1.2 kPa threshold, respectively (*Fig. 9e, g*). Regarding the averaged values for seven months, open grasslands were the most stressed to plant growth, followed by south-facing edges only at the 1.2 kPa threshold (*Fig. 9h*).

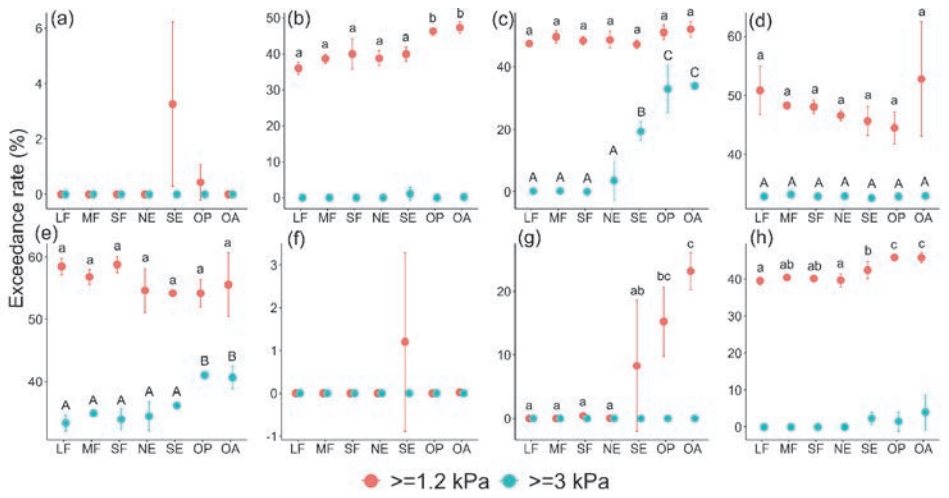

Fig. 9. Exceedance rate (%) for VPD values above 1.2 kPa and above 3.0 kPa (mean ± standard deviation). The values are averaged over three replicates (large dots). Habitat type abbreviations are according to the caption of *Fig. 3*. Different letters indicate significant differences among habitats. Exceedance rate for each month: (a) April, (b) May, (c) June, (d) July, (e) August, (f) September, (g) October, and (h) seven-month average. Due to the 5% lower mean exceedance rate and data with many zeros, statistical analysis was not applied for the exceedance rate above 1.2 kPa in April and September, and it was not used for the exceedance rate above 3 kPa in April, May, September, October, and seven-month average.

4. Discussion

4.1. Microclimate differences among the habitats

An earlier study revealed a gradient in species composition from large forest patches through smaller-sized forest patches and edges to grasslands (*Erdős et al.*, 2023). The compositional differences among the habitats were thought to be associated with differences in microclimate. The current study demonstrated that forests indeed have a strongly different microclimate than grasslands (compared to grasslands, forests are cooler during the daytime and warmer during the nighttime, and more humid during the daytime). Similar findings were reported by *von Arx et al.* (2012). In this study, especially for temperature, south-facing edges tended to be more similar to grasslands, while north-facing edges tended to be more similar to forests.

The present work confirmed that the harshest conditions were found at the end of the vegetation gradient during the growing season (*Fig. 2a*). Open grasslands were the hottest and driest at daytime, but the coolest at nighttime, resulting in the largest diurnal range in these habitats. This result is in line with the previous study of *Erdős et al.* (2014), who measured the microclimate of forest-grassland mosaics in central Hungary for a short period (only 24 hours on a single summer day). Similar results have been reported from grasslands of other biogeographical regions (*Davies-Colley et al.*, 2000; *Wright et al.*, 2010; *Peng et al.*, 2012; *Bogyó et al.*, 2015).

The importance of forests in reducing environmental extremes under semi-arid conditions of the Kiskunság Sand Ridge was shown in the present study. It is reasonable to assume that the revealed microclimatic patterns are caused by the different vegetation, most notably the differences in vegetation cover, especially canopy cover (*Chen et al.*, 1995). Trees play an essential role in driving the below-canopy microclimate: they reduce temperature variation under the canopy, as they absorb and reflect the solar radiation, they have a cooling effect near the soil surface during the daytime, and release longwave radiation during the nighttime (*Magnago et al.*, 2015; *Greiser et al.*, 2018; *Aalto et al.*, 2022). *De Frenne et al.* (2019) found that forest patches were 4.1 ºC cooler than open-habitat patches on a global scale. Similarly, canopy sites have been shown to have significantly lower maximum temperatures than non-canopy ones under sunny conditions, differences being around 5.2 ºC in Africa (*Aalto et al.*, 2022), and around 3.0–5.1 ºC in Europe (*Morecroft et al.*, 1998; *von Arx et al.*, 2012; 2013; *Milošević et al.*, 2020). On the other hand, minimum temperatures in forest patches are on average 1 ºC higher than in open-field conditions at night (*De Frenne et al.*, 2021).

Woody habitats (forests and edges) were more humid than open grasslands at daytime, and daytime air humidity, therefore, exhibited patterns opposite to that of the air temperature. Similar results were reported, among others, from the western United States (*Ma et al.*, 2010), Switzerland (*von Arx et al.*, 2012),

Hungary (*Tölgyesi et al.,* 2020), and the United Kingdom (*Morecroft et al.,* 1998). In the current study, there was no statistically significant difference in nighttime air humidity among the studied habitat types, which is similar to that reported from poplar, black locust, and pine forests as compared to adjacent grasslands (*Tölgyesi et al.,* 2020). Indeed, the significant differences in microclimate variables among habitat types occurred only between May and October, when the foliage of the dominant tree (*Populus alba*) reappears with a high canopy cover of about 50–70%, while microclimate was almost similar among habitats in April, because the foliage has not yet appeared at that time (*Caudullo* and *de Rigo,* 2016). Therefore, canopy cover may be considered the most central factor in creating strong microclimatic differences during daytime (*Godefroid et al.,* 2006).

Small forest patches are usually expected to be warmer and drier than larger forest patches, but the present study found that temperature and humidity values did not differ significantly between differently sized forest patches. Several studies generally state that small forests are largely affected by edge influence and are, in practice, very similar to edges, whereas only larger forest patches with core areas are buffered from environmental harshness (*Hofmeister et al.,* 2019; *Erdős et al.,* 2020; 2023). In the present study, the importance of maintaining tree cover (even in small forest patches or groves) in regulating the microclimate condition under semi-arid conditions was highlighted. *Aalto et al.* (2022) stated that trees outside forests (e.g., trees on farmlands, trees in cities, or small tree groups not defined as forests) have the potential in reducing climate change and regulating local and regional temperatures. Although forest fragmentation may reduce the forest's ability to mitigate climate change (*Ewers* and *Banks-Leite,* 2013), small forest patches can still regulate the environmental extremes (*Mildrexler et al.,* 2011; *Milošević et al.,* 2020), which is in good agreement with the present results. One possible explanation is that the tree/shrub canopy in all forest patches of this study is primarily composed of broadleaved trees and shrubs with a high canopy cover, creating shade and effectively reducing solar radiation reaching the ground. Microclimate conditions, therefore, were largely similar among differently sized forest patches.

One of the most interesting findings was that the mean daytime temperature of south-facing edges was very close to grasslands, while their nighttime values bear a resemblance to forests. This implied that the canopy of south-facing edges showed more resistance to cooling during nighttime than to heating during daytime. On the other hand, microclimate conditions of north-facing edges were similar to the forest interiors both daytime and nighttime. Similar results for the large temperature differences between north-facing and south-facing edges were reported in oak-chestnut forests and in Douglas-fir forests in the United States (*Matlack et al.,* 1993; *Chen et al.,* 1993). A potential reason for this phenomenon is that southern forest edges tend to receive more direct sunlight and solar radiation in daytime compared to north-facing edges (*Stoutjesdijk* and *Barkman,* 1992; *Heithecker* and *Halpern,* 2007; *Bennie et al.,* 2008). Another possibility is

that south-facing edges have lower tree density and/or canopy closure than north-facing edges (*Hofmeister et al.,* 2019).

4.2. VPD, an important limiting factor affecting plant growth

Although vapor pressure deficit is inferred from air temperature and relative air humidity, it is regarded as an important environmental factor affecting the photosynthetic process, since it provides information about how water loss influences the stomatal openness or closure, which is related to CO_2 uptake (*Stewart* and *Dwyer,* 1983; *Young* and *Mitchell,* 1994; *Bunce,* 1997; *Novick et al.,* 2016; *Shamshiri et al.,* 2018). The present results indicated that the VPD values were high during daytime and low during nighttime, showing that high transpiration rate and water stress occur during daytime, when the plants carry out photosynthesis (*Jackson* and *Volk,* 1970).

During the growing season, high VPD values were revealed in the summer months (between June and August), due to the high temperature in this season. For example, a temperature rising from 30 to 33 °C increased VPD from 1.75 to 2.54 kPa (*Will et al.,* 2013). Increased VPD is likely to exacerbate physiological stress on vegetation, leading to increased water loss or decreased carbon uptake, which influences the survival and growth of plant species (*Van Heerwaarden* and *Teuling,* 2014; *McDowell et al.,* 2008). *Yuan et al.* (2019) reported increased VPD being part of the drivers of a decrease in global-scale plant growth, particularly an increase in drought-related forest mortality. A study in western US forests showed that high VPD significantly decreases Douglas fir growth (*Restaino et al.,* 2016). Another study in the forest–grassland ecotone in the US also highlighted that increased VPD hastened greater transpiration and faster mortality of tree seedlings (*Will et al.,* 2013).

The present results showed that the VPD values were significantly lower within woody habitats than in the open grasslands at daytime, indicating that grasslands were the most stressed for plant growth and productivity. These results are in good agreement with an earlier study in central Hungary, which concluded that the VPD values of small groves were lower than those of open areas (*Süle et al.,* 2020). According to a study conducted in the northwestern United States (*Davis et al.,* 2019), the forest canopy can buffer vapor pressure deficit: VPD was found to be 1.1 kPa lower in habitats with canopy than in those without canopy. Similarly, the long-term mean moderating capacity of the forest canopy for VPD in Switzerland was reported to be up to 0.52 kPa (*von Arx et al.,* 2013).

This study indicated that south-facing edges had higher VPD values than north-facing ones during daytime, despite the fact that both are transition zones. This may be explained by the heat-reflective properties of the sunny side (*Süle et al.,* 2020). Together with air temperature and humidity, it is highlighted that south-facing edges have more unfavorable environmental conditions in comparison to north-facing edges, which may result in reduced diversity (*Erdős et al.,* 2013; 2018a; 2023).

Instead of extreme values (e.g., maximum and minimum values) that occur in a short period, the duration curve can help us to better understand the spatio-temporal VPD pattern (*Süle et al.,* 2020). In terms of the 1.2 kPa stress limiting threshold, exceedance rates of over 30% were observed in all habitats from May to August, indicating that each habitat type is strongly stressed during this period. In autumn, the studied habitats did not differ significantly from each other due to the cloudy and rainy weather conditions in September, but the exceedance rate was the highest in open grasslands in October, from 15.2 to 23.2%. Several studies have reported that for both temperature and VPD, differences between woody and non-woody habitats were larger on sunny days than on cloudy days (*Chen et al.,* 1993; *Davies-Colley et al.,* 2000). As there is little heating of soil and air on cloudy days (*Urban et al.,* 2012), the difference between woody and non-woody habitats was small or non-existent in September.

When considering the limiting threshold of 1.2 kPa only, the role of forest patches may be ignored in the extremely dry period, from June to August, as the exceedance rate was similar among habitats. However, a stronger moderating effect of the forests was clearly observed when choosing 3.0 kPa as the threshold value for the exceedance rate, which is in line with *Süle et al.* (2020). Therefore, the present study highlights the central role of forest patches in buffering vapor pressure deficit under severe conditions (*Davis et al.,* 2019).

4.3. Implications for conservation and management

It is well known that forests have a buffering function to regulate climate extremes (*Breshears et al.,* 1998; *von Arx et al.,* 2013; *Davis et al.,* 2019). The current study highlighted that even the smallest forest patches (<0.1 ha) had an important function in mitigating macroclimatic harshness. Therefore, woody habitats may become refuges for plant species that require cooler temperature and/or higher humidity. With ongoing climate change, the role of forest patches, groves, or even scattered trees is expected to become increasingly important (*Manning et al.,* 2009; *Erdős et al.,* 2018a; *Süle et al.,* 2020). In addition, forest patches in forest-grassland mosaics host a specific flora and fauna and also have considerable carbon sequestration capacity (*Foit et al.,* 2016; *Erdős et al.,* 2018b; *Ónodi et al.,* 2021; *Süle et al.,* 2021; *Tölgyesi et al.,* 2022). Thus, the remaining near-natural poplar stands should be protected throughout the study region, as well as in other forest-grassland ecosystems of the world.

Here it is important to point out that protecting the near-natural forest patches is very different from afforestation. Indeed, plantations, especially non-native plantations, cannot substitute near-natural forests, as they have serious negative effects on diversity and other ecosystem properties. For example, compared to near-natural forests, *Robinia* plantations had lower native species richness, functional and phylogenetic diversity, as well as naturalness (*Ho et al.,* 2023), while *Pinus* plantations compromise soil humus content (*Tölgyesi et al.,* 2020)

and are also associated with high fire risk (*Cseresnyés et al.*, 2011). Furthermore, creating large forest stands in sandy drylands may have negative effects on regional underground water balance (*Tölgyesi et al.*, 2020). Tree-planting attempts on ancient or near-natural grasslands are also frowned upon by proponents of open ecosystems, because they risk destroying species, habitats, and ecosystem functioning (*Feurdean et al.*, 2018). Afforestation efforts should therefore be minimized in forest-grassland ecosystems, but planting scattered trees of native species in the open grassland matrix is highly advised and is even regarded as the new standard in increasing higher biodiversity and ecosystem services in Europe (*Manning et al.*, 2009; *Tölgyesi et al.*, 2023).

***Acknowledgements*:** The authors are thankful to Gábor Ónodi and György Kröel-Dulay for their technical help during microclimate measurements. This work was supported by the National Research, Development and Innovation Office, Hungary (grant number FK 134384 for LE), the János Bolyai Research Scholarship of the Hungarian Academy of Sciences (LE), and the Stipendium Hungaricum Scholarship (KVH).

References

Aalto, I.J., Maeda, E.E., Heiskanen, J., Aalto, E.K., and *Pellikka, P.K.E.,* 2022: Strong influence of trees outside forest in regulating microclimate of intensively modified Afromontane landscapes. *Biogeosciences 19*, 4227–4247. https://doi.org/10.5194/bg-19-4227-2022

Araújo, M.B., Alagador, D., Cabeza, M., Nogués-Bravo, D., and *Thuiller, W.,* 2011: Climate change threatens European conservation areas. *Ecol. Lett. 14*, 484–492. https://doi.org/10.1111/j.1461-0248.2011.01610.x

Arnone, J.A., Verburg, P.S.J., Johnson, D.W., Larsen, J.D., Jasoni, R.L., Lucchesi, A.J., Batts, C.M., Von Nagy, C., Coulombe, W.G., Schorran, D.E., Buck, P.E., Braswell, B.H., Coleman, J.S., Sherry, R.A., Wallace, L.L., Luo, Y., and *Schimel, D.S.*, 2008: Prolonged suppression of ecosystem carbon dioxide uptake after an anomalously warm year. *Nature 455*, 383–386. https://doi.org/10.1038/nature07296

Ashcroft, M.B., and *Gollan, J.R.,* 2012: Fine-resolution (25 m) topoclimatic grids of near- surface (5 cm) extreme temperatures and humidities across various habitats in a large (200 × 300 km) and diverse region. *Int. J. Climatol. 32*, 2134–2148. https://doi.org/10.1002/joc.2428

Bakkenes, M., Alkemade, J.R.M., Ihle, F., Leemans, R., and *Latour, J.B.,* 2002: Assessing effects of forecasted climate change on the diversity and distribution of European higher plants for 2050. *Glob. Change Biol. 8*, 390–407. https://doi.org/10.1046/j.1354-1013.2001.00467.x

Bartha, S., Campetella, G., Ruprecht, E., Kun, A., Házi, J., Horváth, A., Virágh, K., and *Molnár, Z.*, 2008: Will interannual variability in sand grassland communities increase with climate change? *Community Ecol. 9*, 13–21. https://doi.org/10.1556/ComEc.9.2008.S.4

Bartholy, J., Pongrácz, R., and *Gelybó, GY.*, 2007: Regional climate change expected in Hungary for 2071–2100. *App. Ecol. Environ. Res. 5*, 1–17. https://doi.org/10.15666/aeer/0501_001017

Bartholy, J., Pongrácz, R., and *Pieczka, I.,* 2014: How the climate will change in this century? *Hungarian Geogr. Bull. 63*, 55–67. https://doi.org/10.15201/hungeobull.63.1.5

Bátori, Z., Lengyel, A., Maróti, M., Körmöczi, L., Tölgyesi, Cs., Bíró, A., Tóth, M., Kincses, Z., Cseh, V., and *Erdős, L.*, 2014: Microclimate-vegetation relationships in natural habitat islands: species preservation and conservation perspectives. *Időjárás 118*, 257–281.

Bellard, C., Bertelsmeier, C., Leadley, P., Thuiller, W., and *Courchamp, F.*, 2012: Impacts of climate change on the future biodiversity. *Ecol. Lett. 15*, 365–377. https://doi.org/10.1111/j.1461-0248.2011.01736.x

Bennie, J., Huntley, B., Wiltshire, A., Hill, M.O., and *Baxter, R.*, 2008: Slope, aspect and climate: Spatially explicit and implicit models of topographic microclimate in chalk grassland. *Ecol. Model. 216*, 47–59. https://doi.org/10.1016/j.ecolmodel.2008.04.010

Biró, M., Révész, A., Molnár, Z., and *Horváth, F.*, 2007: Regional habitat pattern of the Danube-Tisza Interfluve in Hungary, I: The landscape structure and habitat pattern; the fen and alkali vegetation. *Acta Bot. Hung. 49*, 267–303. https://doi.org/10.1556/ABot.49.2007.3-4.4

Blanka, V., Mezosi, G., and *Meyer, B.*, 2013: Projected changes in the drought hazard in Hungary due to climate change. *Időjárás 117*, 219–237.

Bogyó, D., Magura, T., Nagy, D. D., and *Tóthmérész, B.*, 2015: Distribution of millipedes (*Myriapoda, diplopoda*) along a forest interior – Forest edge – Grassland habitat complex. *ZooKeys, 510*, 181–195. https://doi.org/10.3897/zookeys.510.8657

Bolton, D., 1980: The computation of equivalent potential temperature. *Mon. Weather Rev. 108*, 1046–1053. https://doi.org/10.1175/1520-0493(1980)108<1046:TCOEPT>2.0.CO;2

Borhidi, A., Kevey, B., and *Lendvai, G.*, 2012: Plant communities of Hungary. Academic Press, Budapest.

Breshears, D.D., Adams, H.D., Eamus, D., McDowell, N.G., Law, D.J., Will, R.E., Williams, A.P. and *Zou, C.B.*, 2013: The critical amplifying role of increasing atmospheric moisture demand on tree mortality and associated regional die-off. *Front. Plant Sci.* 4, 266. https://doi.org/10.3389/fpls.2013.00266

Breshears, D.D., Nyhan, J.W., Heil, C.E., and *Wilcox, B.P.*, 1998: Effects of Woody Plants on Microclimate in a Semiarid Woodland: Soil Temperature and Evaporation in Canopy and Intercanopy Patches. *Int. J. Plant Sci.* 159, 1010–1017. https://doi.org/10.1086/314083

Bunce, J.A., 1997: Does transpiration control stomatal responses to water vapour pressure deficit? *Plant Cell. Environ. 20*, 131–135. https://doi.org/10.1046/j.1365-3040.1997.d01-3.x

Caudullo, G., and *de Rigo, D.*, 2016: Populus alba in Europe: distribution, habitat, usage and threats. In: (Eds. *San-Miguel-Ayanz, J., de Rigo, D., Caudullo, G., Houston Durrant, T., Mauri, A.*), European Atlas of Forest Tree Species. Publ. Off. EU, Luxembourg, e010368+

Chen, J., Franklin, J. F., and *Spies, T. A.*, 1993. Contrasting microclimates among clearcut, edge, and interior of old-growth Douglas-fir forest. *Agric. For. Meteorol. 63*, 219–237. https://doi.org/10.1016/0168-1923(93)90061-L

Chen, J., Franklin, J. F., and *Spies, T. A.*, 1995: Growing-season microclimatic gradients from clearcut edges into old-growth Douglas-fir forests. *Ecol. Appl. 5*, 74–86. https://doi.org/10.2307/1942053

Cseresnyés, I., Szécsy, O., and *Csontos, P.*, 2011: Fire risk in Austrian pine (*Pinus nigra*) plantations under various temperature and wind conditions. *Acta Bot. Croat. 70*, 157–166. https://doi.org/10.2478/v10184-010-0022-5

Davies-Colley, R.J., Payne, G. W., and *van Elswijk, M.*, 2000: Microclimate gradients across a forest edge. *N. Z. J. Ecol.* 24, 111–121.

Davis, K. T., Dobrowski, S. Z., Holden, Z. A., Higuera, P. E., and *Abatzoglou, J. T.*, 2019: Microclimatic buffering in forests of the future: the role of local water balance. *Ecography 42*, 1–11. https://doi.org/10.1111/ecog.03836

De Frenne, P., Lenoir, J., Luoto, M., Scheffers, B.R., Zellweger, F., Aalto, J., Ashcroft, M.B., Christiansen, D.M., Decocq, G., De Pauw, K., Govaert, S., Greiser, C., Gril, E., Hampe, A., Jucker, T., Klinges, D.H., Koelemeijer, I.A., Lembrechts, J.J., Marrec, R., Meeussen, C., Ogée, J., Tyystjärvi, V., Vangansbeke, P., and *Hylander, K.*, 2021: Forest microclimates and climate change: Importance, drivers and future research agenda. *Glob. Chang Biol. 27*, 2279–2297, https://doi.org/10.1111/gcb.15569

De Frenne, P., Rodríguez-Sánchez, F., Coomes, D.A., Baeten, L., Verstraeten, G., Vellend, M., Bernhardt-Römermann, M., Brown, C.D., Brunet, J., Cornelis, J., Decocq, G.M., Dierschke, H., Eriksson, O., Gilliam, F. S., Hédl, R., Heinken, T., Hermy, M., Hommel, P., Jenkins, M. A., Kelly, D.L., Kirby, K.J., Mitchell, F.J.G., Naaf, T., Newman, M., Peterken, G., Petrik, P., Schultz, J., Sonnier, G., Van Calster, H., Waller, D.M., Walther, G-R., White, P.S, Woods, K.D., Wulf, M., Graae, B.J., and *Verheyen, K.*, 2013: Microclimate moderates plant responses to macroclimate warming. *P. Natl. Acad. Sci. 110*, 18561–18565. https://doi.org./10.1073/pnas.1311190110

De Frenne, P., Zellweger, F., Rodriguez-Sanchez, F., Scheffers, B.R., Hylander, K., Luoto, M., Vellend, M., Verheyen, K. and *Lenoir, J.*, 2019: Global buffering of temperatures under forest canopies. *Nat. Ecol. Evol. 3*, 744–749. https://doi.org/10.1038/s41559-019-0842-1

Dingman, J.R., Sweet, L.C., McCullough, I., Davis, F.W., Flint, A., Franklin, J., and *Flint, L.E.,* 2013: Cross-scale modeling of surface temperature and tree seedling establishment in mountain landscapes. *Ecol. Process. 2*, 1–15. https://doi.org/10.1186/2192-1709-2-30

Dövényi, Z., 2010: *Magyarország kistájainak katasztere*. MTA FKI, Budapest.

Erdős, L., Ambarlı, D., Anenkhonov, O.A., Bátori, Z., Cserhalmi, D., Kiss, M., Kröel-Dulay, G., Liu, H., Magnes, M., Molnár, Z., Naqinezhad, A., Semenishchenkov, Y.A., Tölgyesi, C., and *Török, P.*, 2018b: The edge of two worlds: A new review and synthesis on Eurasian forest-steppes. *Appl. Veg. Sci. 21*, 345–362. https://doi.org/10.1111/avsc.12382

Erdős, L., Gallé, R., Körmöczi, L., and *Bátori, Z.*, 2013: Species composition and diversity of natural forest edges: Edge responses and local edge species. *Community Ecol. 14*, 48–58. https://doi.org/10.1556/ComEc.14.2013.1.6

Erdős, L., Ho, K. V., Bátori, Z., Kröel-Dulay, G., Ónodi, G., Tölgyesi, C., Török, P., and *Lengyel, A.*, 2023: Taxonomic, functional and phylogenetic diversity peaks do not coincide along a compositional gradient in forest-grassland mosaics. *J. Ecol. 111*, 182–197. https://doi.org/10.1111/1365-2745.14025

Erdős, L., Kröel-Dulay, G., Bátori, Z., Kovács, B., Németh, C., Kiss, P. J., and *Tölgyesi, C.*, 2018a: Habitat heterogeneity as a key to high conservation value in forest-grassland mosaics. *Biol. Conserv. 226*, 72–80. https://doi.org/10.1016/j.biocon.2018.07.029

Erdős, L., Tölgyesi, Cs., Horzse, M., Tolnay, D., Hurton, A., Schulcz, N., Körmöczi, L., Lengyel, A., and *Bátori, Z.*, 2014: Habitat complexity of the Pannonian forest-steppe zone and its nature conservation implications. *Ecol. Complex. 17*, 107–118. https://doi.org/10.1016/j.ecocom.2013.11.004

Erdős, L., Török, P., Szitár, K., Bátori, Z., Tölgyesi, C., Kiss, P. J., Bede-Fazekas, Á., and *Kröel-Dulay, G.*, 2020: Beyond the forest-grassland dichotomy: the gradient-like organization of habitats in forest-steppes. *Front. Plant Sci. 11*, 236. https://doi.org/10.3389/fpls.2020.00236

Erdős, L., Török, P., Veldman, J. W., Bátori, Z., Bede-Fazekas, Á., Magnes, M., Kröel-Dulay, G., and *Tölgyesi, C.*, 2022: How climate, topography, soils, herbivores, and fire control forest–grassland coexistence in the Eurasian forest-steppe. *Biol. Rev. 97*, 2195–2208. https://doi.org/10.1111/brv.12889

Ewers, R.M. and *Banks-Leite, C.*, 2013: Fragmentation Impairs the Microclimate Buffering Effect of Tropical Forests. *PLoS One 8*, e58093, https://doi.org/10.1371/journal.pone.0058093

Feurdean, A., Ruprecht, E., Molnár, Z., Hutchinson, S.M., and *Hickler, T.*, 2018: Biodiversity-rich European grasslands: ancient, forgotten ecosystems. *Biol. Conserv. 228*, 224–232. https://doi.org/10.1016/j.biocon.2018.09.022

Foit, J., Kašák, J., and *Nevoral, J.*, 2016: Habitat requirements of the endangered longhorn beetle *Aegosoma scabricorne* (Coleoptera: Cerambycidae): a possible umbrella species for saproxylic beetles in European lowland forests. *J. Insect Conserv. 20*, 837–844. https://doi.org/10.1007/s10841-016-9915-5

Fox, J., and Weisberg, S., 2019: An {R} Companion to Applied Regression, Third Edition. Thousand Oaks CA: Sage. https://socialsciences.mcmaster.ca/jfox/Books/Companion/

Geiger, R., Aron, R.H. and *Todhunter, P.*, 2009: The Climate Near the Ground. Rowman & Littlefield.

Godefroid, S., Rucquoij, S., and *Koedam, N.*, 2006: Spatial variability of summer microclimates and plant species response along transects within clearcuts in a beech forest. *Plant Ecol. 185*, 107–121. https://doi.org/10.1007/s11258-005-9088-x

Greiser, C., Meineri, E., Luoto, M., Ehrlén, J., and *Hylander, K.*, 2018: Monthly microclimate models in a managed boreal forest landscape. *Agric For Meteorol*. *250–251*, 147–158. https://doi.org/10.1016/j.agrformet.2017.12.252

Hardwick, S. R., Toumi, R., Pfeifer, M., Turner, E. C., Nilus, R., and *Ewers, R. M.*, 2015: The relationship between leaf area index and microclimate in tropical forest and oil palm plantation: Forest disturbance drives changes in microclimate. *Agric For Meteorol. 201*, 187–195. https://doi.org/10.1016/j.agrformet.2014.11.010

Heithecker, T.D., and Halpern, C.B., 2007: Edge-related gradients in microclimate in forest aggregates following structural retention harvests in western Washington. *For. Ecol. Manag. 248*,163–173. https://doi.org/10.1016/j.foreco.2007.05.003

Ho, K.V., Kröel-Dulay, G., Tölgyesi, C., Bátori, Z., Tanács, E., Kertész, M., Török, P., and *Erdős, L.*, 2023: Non-native tree plantations are weak substitutes for near-natural forests regarding plant diversity and ecological value. *For. Ecol. Manag. 531*. 120789. https://doi.org/10.1016/j.foreco.2023.120789

Hofmeister, J., Hošek, J., Brabec, M., Střalková, R., Mýlová, P., Bouda, M., Pettit, J. L., Rydval, M., and *Svoboda, M.*, 2019: Microclimate edge effect in small fragments of temperate forests in the context of climate change. *For. Ecol. Manag. 448*, 48–56. https://doi.org/10.1016/j.foreco.2019.05.069

IPCC., 2018: *Summary for Policymakers*. In: (eds. *Masson-Delmotte, V., Zhai, P., Pörtner, H.O., Roberts, D., Skea, J., Shukla, P.R., Pirani, A., Moufouma-Okia, W., Péan, C., Pidcock, R., Connors, S., Matthews, J.B.R., Chen, Y., Zhou, X., Gomis, M.I., Lonnoy, E., Maycock, T., Tignor, M.*, and *Waterfield, T.*,), Global Warming of 1.5°C. An IPCC Special Report on the impacts of global warming of 1.5°C above pre-industrial levels and related global greenhouse gas emission pathways, in the context of strengthening the global response to the threat of climate change, sustainable development, and efforts to eradicate poverty. Cambridge University Press, Cambridge, UK and New York, NY, USA, 3–24. https://doi.org/10.1017/9781009157940.001

Jackson, W.A., and *Volk, R.J.*, 1970: Photorespiration. *Annu. Rev. Plant Physio. 21*, 385–432. https://doi.org/10.1146/annurev.pp.21.060170.002125

Kappelle, M., Van Vuuren, M. M. I., and *Baas, P.*, 1999: Effects of climate change on biodiversity: A review and identification of key research issues. *Biodivers. Conserv. 8*, 1383–1397. https://doi.org/10.1023/A:1008934324223

Kertész, A., and *Mika, J.*, 1999: Aridification, climate change is South-eastern Europe. *Phys. Chem. Earth Pt. A. 24*, 913–920. https://doi.org/10.1016/S1464-1895(99)00135-0

Király G., 2009: Új magyar füvészkönyv. Aggtelek National Park.

Krishnaswamy, J., John, R., and *Joseph, S.*, 2014: Consistent response of vegetation dynamics to recent climate change in tropical mountain regions. *Glob. Change Biol. 20*, 203–215. https://doi.org/10.1111/gcb.12362

Lenth, R. V., 2022: *emmeans: Estimated Marginal Means, aka Least-Squares Means*. R package version 1.7.5. https://CRAN.R-project.org/package=emmeans

Luskin, M. S., and *Potts, M. D.*, 2011: Microclimate and habitat heterogeneity through the oil palm lifecycle. *Basic Appl. Ecol. 12*, 540–551. https://doi.org/10.1016/j.baae.2011.06.004

Ma, S.Y., Concilio, A., Oakley, B., North, M. and *Chen, J.Q.*, 2010: Spatial variability in microclimate in a mixed-conifer forest before and after thinning and burning treatments. *For. Ecol. Manag. 259*, 904–915. https://doi.org/10.1016/j.foreco.2009.11.030

Magnago, L.F.S., Rocha, M.F., Meyer, L., Martins, S.V., and *Meira-Neto, J.A.A.*, 2015: Microclimatic conditions at forest edges have significant impacts on vegetation structure in large Atlantic forest fragments. *Biodivers. Conserv. 24*, 2305–2318. https://doi.org/10.1007/s10531-015-0961-1

Manning, A.D., Gibbons, P., and *Lindenmayer, D.B.*, 2009: Scattered trees: a complementary strategy for facilitating adaptive responses to climate change in modified landscapes? *J. Appl. Ecol. 46*, 915–919. https://doi.org/10.1111/j.1365-2664.2009.01657.x

Matlack, G.R., 1993: Microenvironment variation within and among deciduous forest edge sites in the eastern United State. *Biol. Conserv. 66*, 185–194. https://doi.org/10.1016/0006-3207(93)90004-K

McDowell, N., Pockman, W. T., Allen, C. D., Breshears, D. D., Cobb, N., Kolb, T., Plaut, J., Sperry, J., West, A., Williams, D. G., and *Yepez, E. A.*, 2008: Mechanisms of plant survival and mortality during drought: Why do some plants survive while others succumb to drought? *New Phytol. 178*, 719–739. https://doi.org/10.1111/j.1469-8137.2008.02436.x

Meeussen, C., Govaert, S., Vanneste, T., Bollmann, K., Brunet, J., Calders, K., Cousins, S.A.O., De Pauw, K., Diekmann, M., Gasperini, C., Hedwall, P.O., Hylander, K., Iacopetti, G., Lenoir, J., Lindmo, S., Orczewska, A., Ponette, Q., Plue, J., Sanczuk, P., Selvi, F., Spicher, F., Verbeeck, H., Zellweger, F., Verheyen, K., Vangansbeke, P., and *De Frenne, P.*, 2021: Microclimatic edge-to-interior gradients of European deciduous forests. *Agric For Meteorol. 311*. 108699. https://doi.org/10.1016/j.agrformet.2021.108699

Mildrexler, D. J., Zhao, M., and *Running, S. W.*, 2011: A global comparison between station air temperatures and MODIS land surface temperatures reveals the cooling role of forests. *J. Geophys. Res. 116*, G03025. https://doi.org/10.1029/2010JG001486

Milošević, D.D., Dunjić, J., and *Stojanović, V.*, 2020: Investigating Micrometeorological Differences between Saline Steppe, Forest-steppe and Forest Environments in Northern Serbia during a Clear and Sunny Autumn Day. *Geogr. Pannonica 24*, 176–186. https://doi.org/10.5937/gp24-25885

Molnár, Z., 2003: A Kiskunság száraz homoki növényzete. Természetbúvár Alapítvány Kiadó, Budapest (in Hungarian).

Molnár, Z., Biró, M., Bartha, S., and *Fekete, G.*, 2012: *Past trends, present state and future prospects of Hungarian forest-steppes.* In: (Eds. *Werger, M.J.A.* and *van Staalduinen, M.A.*), Eurasian Steppes. Springer, Berlin, 209–252. https://doi.org/10.1007/978-94-007-3886-7_7

Morecroft, M.D., Taylor, M.E. and *Oliver, H.R.*, 1998: Air and soil microclimates of deciduous woodland compared to an open site. *Agric. For. Meteorol. 90*, 141–156. https://doi.org/10.1016/S0168-1923(97)00070-1

Novick, K.A., Ficklin, D.L., Stoy, P.C., Williams, C.A., Bohrer, G., Oishi, A.C., Papuga, S. A., Blanken, P.D., Noormets, A., Sulman, B.N., Scott, R.L., Wang, L., and *Phillips, R.P.*, 2016: The increasing importance of atmospheric demand for ecosystem water and carbon fluxes. *Nat. Clim. Chang. 6*, 1023–1027. https://doi.org/10.1038/nclimate3114

Ónodi, G., Botta-Dukát, Z., Winkler, D., and *Rédei, T.*, 2021: Endangered lowland oak forest steppe remnants keep unique bird species richness in Central Hungary. *J. For. Res. 33*, 343–355. https://doi.org/https://doi.org/10.1007/s11676-021-01317-9

Peng, J., Dong, W., Yuan, W., and *Zhang, Y.*, 2012: Responses of grassland and forest to temperature and precipitation changes in Northeast China. *Adv. Atmos. Sci. 29*, 1063–1077. https://doi.org/10.1007/s00376-012-1172-2

Pohlman, C. L., Turton, S. M., and *Goosem, M.*, 2009: Temporal variation in microclimatic edge effects near powerlines, highways and streams in Australian tropical rainforest. *Agric. For. Meteorol. 149*, 84–95. https://doi.org/10.1016/j.agrformet.2008.07.003

R Core Team., 2021: R: a language and environment for statistical computing. https://cran.r-project.org/bin/windows/base/

Restaino, C. M., Peterson, D. L., and *Littell, J.*, 2016: Increased water deficit decreases Douglas fir growth throughout western US forests. *Proc. Natl Acad. Sci. USA* 113, 9557–9562. https://doi.org/10.1073/pnas.1602384113

Reyer, C.P.O., Leuzinger, S., Rammig, A., Wolf, A., Bartholomeus, R.P., Bonfante, A., de Lorenzi, F., Dury, M., Gloning, P., Abou Jaoudé, R., Klein, T., Kuster, T.M., Martins, M., Niedrist, G., Riccardi, M., Wohlfahrt, G., de Angelis, P., de Dato, G., François, L., … and *Pereira, M.*, 2013: A plant's perspective of extremes: Terrestrial plant responses to changing climatic variability. *Glob. Change Biol. 19*, 75–89. https://doi.org/10.1111/gcb.12023

Ries, L., Fletcher, Jr., Battin, J., and *Sisk, T.D.*, 2004: Ecological Responses to Habitat Edges: Mechanisms, Models, and Variability Explained. *Annu. Rev. Ecol. Evol. Syst. 35*, 491–522. https://doi.org/10.1146/annurev.ecolsys.35.112202.130148

Riutta, T., Slade, E.M., Bebber, D.P., Taylor, M.E., Malhi, Y., Riordan, P., Macdonald, D.W., and *Morecroft, M.D.*, 2012: Experimental evidence for the interacting effects of forest edge, moisture and soil macrofauna on leaf litter decomposition. *Soil Biol. Biochem. 49*, 124–131. https://doi.org/10.1016/j.soilbio.2012.02.028

Şahin, M., Yıldız, B.Y., Şenkal, O., and *Peştemalci, V.*, 2013: Estimation of the vapour pressure deficit using NOAA-AVHRR data. *Int. J. Remote Sens. 34*, 2714–2729. https://doi.org/10.1080/01431161.2012.750021

Schmidt, M., Lischeid, G., and *Nendel, C.*, 2019: Microclimate and matter dynamics in transition zones of forest to arable land. *Agric. For. Meteorol. 268*, 1–10. https://doi.org/10.1016/j.agrformet.2019.01.001

Shamshiri, R.R., Jones, J.W., Thorp, K.R., Ahmad, D., Man, H.C., and *Taheri, S.*, 2018: Review of optimum temperature, humidity, and vapour pressure deficit for microclimate evaluation and control in greenhouse cultivation of tomato: A review. *Int. Agrophysics 32*, 287–302. https://doi.org/10.1515/intag-2017-0005

Shibuya, T., Kano, K., Endo, R., and *Kitaya, Y.*, 2018: Effects of the interaction between vapor-pressure deficit and salinity on growth and photosynthesis of Cucumis sativus seedlings under different CO_2 concentrations. *Photosynthetica 56*, 893–900. https://doi.org/10.1007/s11099-017-0746-8

Shirke, P. A., and *Pathre, U. V.*, 2004: Influence of leaf-to-air vapour pressure deficit (VPD) on the biochemistry and physiology of photosynthesis in Prosopis juliflora. *J. Exp. Bot. 55*, 2111–2120. https://doi.org/10.1093/jxb/erh229

Sih, A., Jonsson, B.G., and *Luikart, G.*, 2000: Do edge effects occur over large spatial scale? *Tree 15*, 134–135. https://doi.org/10.1016/S0169-5347(00)01838-3

Stewart, D.W., and *Dwyer, L.M.*, 1983: Stomatal response to plant water deficits. *J. Theor. Biol. 104*, 655–666. https://doi.org/10.1016/0022-5193(83)90253-9

Stoutjesdijk, P., and *Barkman, J.J.*, 1992: *Microclimate, vegetation and fauna*. Opulus, Uppsala.

Suggitt, A.J., Gillingham, P.K., Hill, J.K., Huntley, B., Kunin, W.E., Roy, D.B., and Thomas, C.D., 2011: Habitat microclimates drive fine-scale variation in extreme temperatures. *Oikos, 120*, 1–8. https://doi.org/10.1111/j.1600-0706.2010.18270.x

Süle, G., Balogh, J., Fóti, S., Gecse, B., and *Körmöczi, L.*, 2020: Fine-scale microclimate pattern in forest-steppe habitat. *Forests 11*, 1–16. https://doi.org/10.3390/f11101078

Süle, G., Fóti, S., Körmöczi, L., Petrás, D., Kardos, L., and *Balogh, J.*, 2021: Co-varying effects of vegetation structure and terrain attributes are responsible for soil respi ration spatial patterns in a sandy forest–steppe transition zone. *Web Ecol. 21*, 95–107. https://doi.org/10.5194/we-21-95-2021

Szabó, A., Gribovszki, Z., Kalicz, P., Szolgay, J., and *Bolla, B.*, 2022: The soil moisture regime and groundwater recharge in aged forests in the Sand Ridge region of Hungary after a decline in the groundwater level: an experimental case study. *J. Hydrol. Hydromech. 70*, 308–320. https://doi.org/10.2478/johh-2022-0019

Tölgyesi C., Valkó O., Deák B., Kelemen A., Bragina T.M., Gallé R., Erdős L., and *Bátori Z.*, 2018: Tree-herb coexistence and community assembly in natural forest-steppe transitions. *Plant Ecol. Divers. 11*, 465-477. https://doi.org/10.1080/17550874.2018.1544674

Tölgyesi, C., Kelemen, A., Bátori, Z., Kiss, R., Hábenczyus, A.A., Havadtői, K., Varga, A., Erdős, L., Frei, K., Tóth, B., and *Török, P.*, 2023: Maintaining scattered trees to boost carbon stock in temperate pastures does not compromise overall pasture quality for the livestock. *Agric. Ecosyst. Environ. 351*, 108477. https://doi.org/10.1016/j.agee.2023.108477

Tölgyesi, C., Török, P., Hábenczyus, A. A., Bátori, Z., Valkó, O., Deák, B., Tóthmérész, B., Erdős, L., and *Kelemen, A.*, 2020: Underground deserts below fertility islands? Woody species desiccate lower soil layers in sandy drylands. *Ecography 43*, 848–859. https://doi.org/10.1111/ecog.04906

Tölgyesi, C., Buisson, E., Hem, A., Temperton, V. M. and *Török, P.*, 2022: Urgent need for updating the slogan of global climate actions from “tree planting” to “restore native vegetation.”. *Restor. Ecol. 30*, e13594. https://doi.org/10.1111/rec.13594

Travis, J. M. J., 2003: Climate change and habitat destruction: A deadly anthropogenic cocktail. *Proc. R. Soc. Lond*. B. 270, 467–473. https://doi.org/10.1098/rspb.2002.2246

Urban, O., Klem, K., Ač, A., Havránková, K., Holišová, P., Navrátil, M., Zitová, M., Kozlová, K., Pokorný, R., Šprtová, M., Tomášková, I., Špunda, V., and *Grace, J.*, 2012: Impact of clear and cloudy sky conditions on the vertical distribution of photosynthetic CO_2 uptake within a spruce canopy. *Funct. Ecol. 26*, 46–55. https://doi.org/10.1111/j.1365-2435.2011.01934.x

Van Heerwaarden, C.C., and *Teuling, A.J.*, 2014: Disentangling the response of forest and grassland energy exchange to heatwaves under idealized land-atmosphere coupling. *Biogeosciences, 11*, 6159–6171. https://doi.org/10.5194/bg-11-6159-2014

Várallyay, G., 1993: *Soils in the region between the rivers Danube and Tisza (Hungary)*. In (Eds. *Szujkó-Lacza, J.* and *Kováts, D.*), The flora of the Kiskunság National Park I. Hungarian Natural History Museum. 21–42.

von Arx, G., Dobbertin, M. and *Rebetez, M.*, 2012: Spatio-temporal effects of forest canopy on understory microclimate in a long-term experiment in Switzerland. *Agric. For. Meteorol. 166–167*, 144–155. https://doi.org/10.1016/j.agrformet.2012.07.018

von Arx, G., Graf Pannatier, E., Thimonier, A., and *Rebetez, M.*, 2013: Microclimate in forests with varying leaf area index and soil moisture: potential implications for seedling establishment in a changing climate. J. Ecol. 101: 1201–1213. https://doi.org/10.1111/1365-2745.12121

Walther, G., Post, E., Convey, P., Menzel, A., Parmesan, C., Beebee, T.J.C., Fromentin, J.M., Hoegh-Guldberg, O., and *Bairlein, F.*, 2002: Ecological responses to recent climate change. *Nature 416*, 389–437. https://doi.org/10.1038/416389a

Will, R. E., Wilson, S. M., Zou, C. B., and *Hennessey, T. C.,* 2013: Increased vapor pressure deficit due to higher temperature leads to greater transpiration and faster mortality during drought for tree seedlings common to the forest–grassland ecotone. *New Phytol. 200,* 366–374. https://doi.org/10.1111/nph.12321

Williams, A. P., Allen, C. D., Macalady, A. K., Griffin, D., Woodhouse, C. A., Meko, D. M., Swetnam, T. W., Rauscher, S. A., Seager, R., Grissino-Mayer, H. D., Dean, J. S., Cook, E. R., Gangodagamage, C., Cai, M., and *Mcdowell, N. G.,* 2013: Temperature as a potent driver of regional forest drought stress and tree mortality. *Nat. Clim. Change. 3,* 292–297. https://doi.org/10.1038/nclimate1693

Wright, T. E., Kasel, S., Tausz, M., and *Bennett, L. T.,* 2010: Edge microclimate of temperate woodlands as affected by adjoining land use. *Agric. For. Meteorol. 150,* 1138–1146. https://doi.org/10.1016/j.agrformet.2010.04.016

Young, A. and Mitchell, N., 1994: Microclimate and vegetation edge effects in a fragmented podocarp-broadleaf forest in New Zealand. *Biol. Conserv. 67,* 63–72. https://doi.org/10.1016/0006-3207(94)90010-8

Yuan, W., Zheng, Y., Piao, S., Ciais, P., Lombardozzi, D., Wang, Y., Ryu, Y., Chen, G., Dong, W., Hu, Z., Jain, A. K., Jiang, C., Kato, E., Li, S., Lienert, S., Liu, S., Nabel, J.E.M.S., Qin, Z., Quine, T., … and *Yang, S.,* 2019: Increased atmospheric vapor pressure deficit reduces global vegetation growth. *Sci. Adv. 5,* 1–13. https://doi.org/10.1126/sciadv.aax1396

Zellweger, F., De Frenne, P., Lenoir, J., Rocchini, D., and *Coomes, D.,* 2019: Advances in Microclimate Ecology Arising from Remote Sensing. *Trends Ecol. Evol. 34,* 327–341. https://doi.org/10.1016/j.tree.2018.12.012

Zhan, C., Liang, C., Zhao, L., Jiang, S., Niu, K., Zhang, Y., and *Cheng, L.,* 2022: Vegetation Dynamics and its Response to Climate Change in the Yellow River Basin, China. *Front. Environ. Sci. 10,* 1–18. https://doi.org/10.3389/fenvs.2022.892747

DOI:10.28974/idojaras.2024.1.2

IDŐJÁRÁS

Quarterly Journal of the HungaroMet Hungarian Meteorological Service
Vol. 128, No. 1, January – March, 2024, pp. 27–39

Effect of teleconnection patterns on cloudiness in winter in Poland

Filip Miś

Adam Mickiewicz University
Faculty of Geographical and Geological Sciences
Bogumiła Krygowskiego 10,
61-680 Poznań, Poland

Author E-mail: filmis@st.amu.edu.pl

(Manuscript received in final form December 5, 2022)

Abstract—The subject of the study was the effect of teleconnection patterns on cloudiness in Poland in the period 1990–2020. The analysis was conducted based on daily cloudiness values from 34 measurement stations of Institute of Meteorology and Water Management - National Research Institute and monthly North Atlantic Oscillation (NAO) and Scandinavia (SCAND) indices from the collection of Climate Prediction Center (CPC). The course of cloudiness values in winter in the multiannual period was analyzed together with its averaged spatial distrubution for the entire winter and for particular winter months. Next, the coefficient of correlation of cloudiness with a given teleconnection pattern index was calculated. The analysis also covered cloudiness in the positive and negative teleconnection phases. The results confirm a variable course and increasing trend of winter cloudiness in Poland. The average cloudiness reached 76% in the studied multiannual period. The correlation coefficient for the North Atlantic Oscillation primarily adopted negative values, and positive for the Scandinavian circulation. The strongest correlation between the teleconnection pattern and cloudiness was observed in February for NAO and in December for SCAND. Cloudiness showed no considerable differences between the positive and negative teleconnection phases.

*Key-words:*cloudiness, teleconnection patterns, climate change, Poland, NAO, SCAND

1. Introduction

Cloudiness is the degree of cover of the sky with clouds. It is determined based on the assessment of the ratio of the area covered by clouds to the space covered by the observation (*Piotrowski*, 2017). Cloudiness depends on the content of water vapor in the air and on condensation conditions, primarily determined by

atmospheric teleconnection processes (*Kożuchowski et al.,* 2012). This atmospheric teleconnection processes are spatial patterns in the atmosphere that link weather and climate anomalies over large scale across the globe (*Feldstein* and *Franzke*, 2017). Cloudiness can also be modified due to the effect of local factors such as land relief. Clouds fulfil an important function in the global water circulation, providing atmospheric precipitation on Earth. Moreover, they strongly reflect solar radiation and limit losses on radiation emitted by the Earth's surface (*Piotrowski*, 2017).

The issue of cloudiness and teleconnection patterns has been addressed by many studies. The magnitude and general characteristics of cloudiness in Poland have been described by *Filipiak* (2021), *Sypniewska* and *Szyga-Pluta* (2018), and *Filipiak* and *Miętus* (2009). Equally numerous studies regarding cloudiness have been conducted at local and regional scales. These papers particularly include those by *Żmudzka* (2007), *Matuszko* and *Wojkowski* (2007), and *Wibig* (2008). Moreover, the correlation of cloudiness with the optical thickness of aerosol and sometimes insolation has been investigated (*Bartoszek et al*., 2020), as well as the effect of cloudiness on precipitation and air temperature in Poland (*Żmudzka* 2008).

As shown in earlier studies, the most important teleconnection patterns affecting weather and climate in central Europe include the North Atlantic Oscillation (NAO) and Scandinavia (SCAND) patterns (*Tomczyk*, 2014; *Ptak et al.,* 2018). NAO is a bipolar teleconnection pattern resulting from the co-occurrence of the Azores High and Icelandic Low. It is one of the most evident and repeatable teleconnection patterns. It dictates the weather variability from the eastern coast of North America to Siberia (*Hurrell et al.,* 2003). The positive NAO phase is characterized by a gradient of atmospheric pressure higher than average between the baric centers of the Azores High and Icelandic Low. It results in an inflow of humid and warm air masses from the west over the northern part of Europe, including Poland. The negative phase is related to a lower pressure gradient between these baric centers (Icelandic Low – higher than average pressure, Azores High – lower than average pressure). Such a situation generates inflow of dry and cool air masses from the northeast (*Hurrell,* 1995, *Hurrell* and *Deser,* 2010).

SCAND is a teleconnection pattern characterized by the occurrence of a strong high over the Scandinavian Peninsula with a center over Finland. The area of lower than average pressure extends from western Europe to eastern Russia/western Mongolia. The positive SCAND phase is related to higher than average pressure, creating a situation of blockage over Scandinavia and western Russia. The negative phase is related to lower than average pressure over northern Europe (*Bueha* and *Nakamura*, 2007; *Liu et al.*, 2014; *Nojarov*, 2017; *Tomczyk et al.*, 2019). In the positive phase, dry and cool air is transported over central Europe and central Russia (https://www.cpc.ncep.noaa.gov/data/teledoc/scand.shtml).

The effect of teleconnection patterns on climate and weather in Poland has been evidenced among others in papers by *Adamczyk* (2007) regarding the effect

of the North Atlantic Oscillation on cloudiness in Poland in the period 1961–1990. The paper evidenced the dependency of total cloudiness on the intensity of the NAO zonal circulation. The author proved that the correlation is not strong over a predominant part of the country, although in the north, the corelations are stronger and statistically significant. The effect of teleconnection patterns on atmospheric conditions in Poland have also been evidenced in papers regarding thermal and nival conditions (*Bednorz,* 2002; *Tomczyk,* 2015; *Szwed et al.*, 2017). Moreover, research conducted in recent years covered the effect of teleconnection patterns on the value and seasonality of outflow in Polish rivers (*Wrzesiński,* 2010), as well as thermal and ice conditions in lakes in northern Poland (*Ptak et al.,* 2018, 2019).

The study objective was to investigate the characteristics of cloudiness in Poland in winter in the years 1990/91–2019/20, and the determination of the effect of teleconnection patterns on cloudiness.

2. Study area, source material, and study methods

The study employed data from 34 stations in Poland functioning in the scope of activity of the Institute of Meteorology and Water Management – National Research Institute (*Fig. 1*). The stations were selected based on the completeness of measurement data.

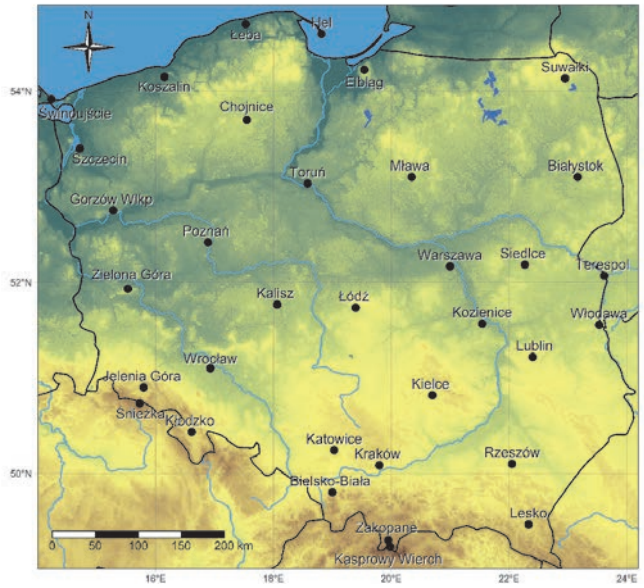

Fig. 1. Location of meteorological stations.

This paper employed mean daily data on cloudiness from 30 winter seasons from 1990/91 to 2019/20. The winter season was defined as the period from December to February. The assessment of cloudiness applies an 8-degree octane scale, where 0/8 means cloudless sky, and 8/8 means complete cloudiness. In the paper, the magnitude of cloudiness was converted from the octane scale to a percent scale. The aforementioned data provided the basis for the determination of the multiannual course of cloudiness in Poland in the winter season and in particular months of the season. Next, the trend and intensity of changes were determined, as well as the statistical significance of the recorded changes.

In the next step, the effect of teleconnection patterns on cloudiness in Poland was analyzed. The source material regarding the North Atlantic Oscillation (NAO) and Scandinavia (SCAND) indices was obtained from the data collection of the Climate Prediction Center (CPC). The teleconnection patterns included in the CPC database were designated by means of principal component analysis based on monthly values of anomalies of height of isobaric surface of 500 hPa (*Barnston* and *Livezey*, 1987). The monthly circulation indices were used for the calculation of the Pearson correlation coefficient between cloudiness and teleconnection patterns. The statistical significance of the correlations was verified by means of a t-student test. Moreover, the strength of correlations was determined according to the classification of correlation scale by Guillford (*Guillford*, 1947). Next, cloudiness was determined at low and high index values (1 and 3 quartiles of the set of index values). All maps and diagrams were prepared based on programming language R.

3. Results

Average cloudiness in winter in Poland in the years 1990/91–2019/20 reached 76%. The spatial distribution of cloudiness in winter and in each winter month showed the highest level in northern Poland, particularly in the central and eastern parts of it (*Fig. 4*). The lowest cloudiness was observed in the northwestern areas of Poland as well as in the south in mountainous areas. In individual stations, the average cloudiness ranged from 67% in Świnoujście to 80% in Suwałki (*Fig. 3*). The winter with the highest average cloudiness was season 2012/13 – 86% (*Fig. 2*). The lowest values were recorded in Świnoujście (76%), and the highest in Gorzów Wielkopolski (90%). In this period, in 85% of stations, the highest value in the analyzed multiannual period was observed. The season with the lowest cloudiness proved to be the season 1992/1993 – 67%. In that period, the lowest cloudiness was recorded in 47% of the stations. The averaged cloudiness for the entire Poland in the multiannual course shows an increasing, statistically significant trend. The analysis of changes in particular stations showed the greatest changes in the western part of the country. In seasons characterized by extreme values of the NAO index, an increase in cloudiness is observed. In the SCAND phase, such a trend is recorded only in the positive phase of the pattern (*Fig. 2*).

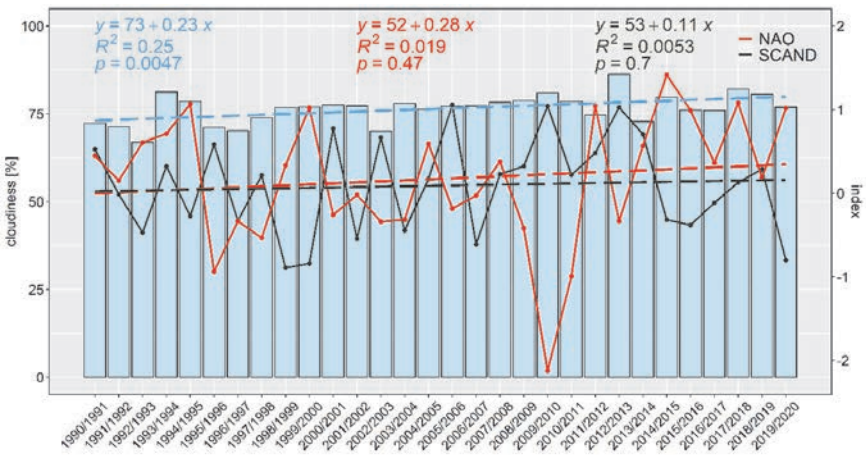

Fig. 2. Course of average cloudiness [%] together with the course of NAO and SCAND indices.

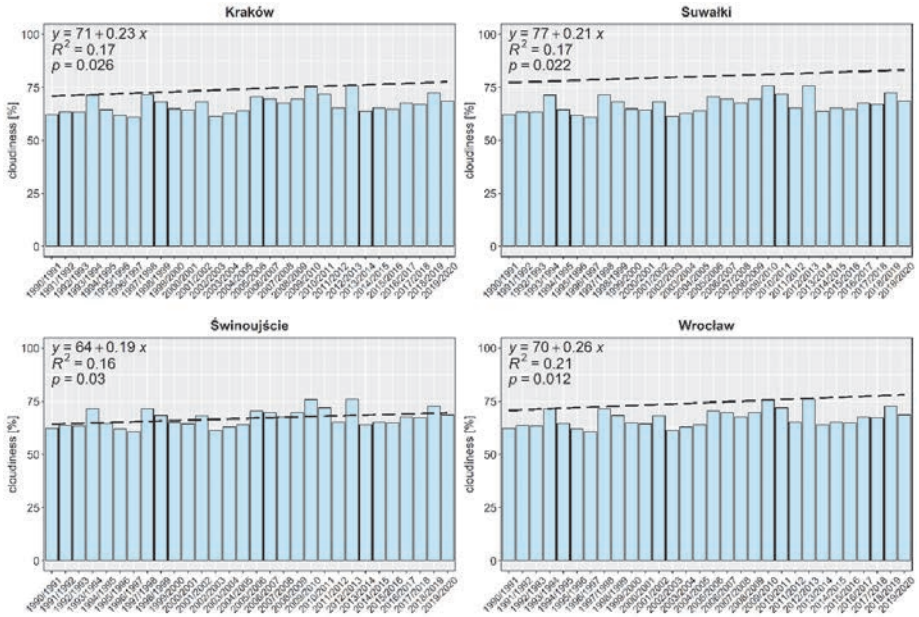

Fig. 3. Course of average seasonal cloudiness [%] in selected stations.

Average cloudiness throughout winter in the multiannual period 1990/91–2019/20 reached 76% (*Fig. 4*). An indentical value of cloudiness was recorded in January. December proved to be a month characterized by the highest cloudiness at the national scale – 78%, and the greatest spatial variability. In February, cloudiness adopted the lowest value of 73%, and showed the highest spatial stability – the variability between extreme cloudiness values was the lowest among all winter months. The maximum monthly cloudiness value was observed in January 2003 – 98%. A minimum was also recorded in January in 1993 – 11%. The level of cloudiness increased towards the north and northeast.

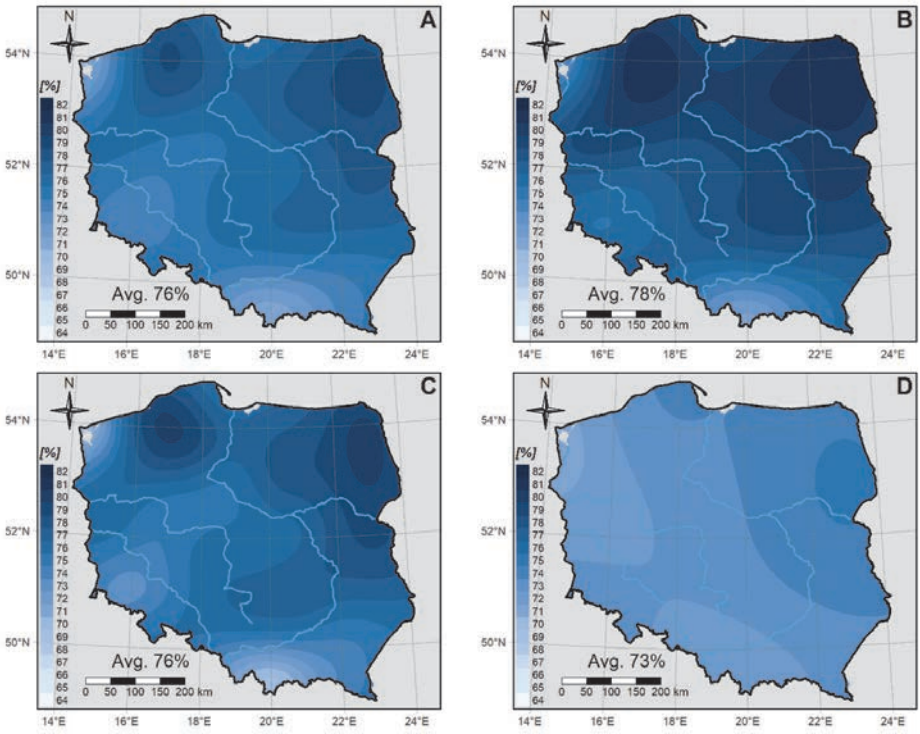

Fig. 4. Spatial distribution of the average cloudiness in winter (A), December (B), January (C), and February (D) in the years 1990/91–2019/20.

The average level of the North Atlantic Oscillation index for winter in the studied multiannual period reached 0.17. The maximum value of the NAO index was recorded in the season 2014/15 (1.41), and the minimum in the season 2009/10 (-2.12). In the studied multiannual period, a slight increase in the NAO index occurred, and it was not statistically significant.

At this stage of the study, the analysis covered the correlation between the cloudiness and the North Atlantic Oscillation index (*Fig. 5*). Over a prevalent area, the correlation was negative, suggesting that in the negative NAO phase, cloudiness increased, and decreased in the positive one. In the spatial distribution of the correlation coefficient for the entire winter period, the strongest correlations are observed in the northwestern part of the country, with a maximum in Świnoujście
(-0.35). Positive correlations are determined only in the north-east and in the mountain regions. The average correlation coefficient for the entire Poland reached -0.11. According to the Guillford's correlation scale classification, this suggests weak correlation. In Świnoujście, the correlation was average. In December in the studied multiannual period, the weakest correlation between cloudiness and NAO was recorded. The average correlation coefficient reached only -0.08. The entire northern Poland showed minimum positive values or those approximate to zero. The strongest negative correlations in that month were observed in the southeastern part of the country. Almost an identical situation concerns the spatial distribution of the correlation coefficient in January. Negative values are observed in southern and central Poland, and positive values in northeastern part of Poland with a maximum in Suwałki (0.26). The month most divergent from the average from the entire winter period was February. In that month, the average correlation coefficient for the entire Poland reached -0.42. The strongest correlation was observed in the northern part of the country, particularly in seaside stations such as: Hel (-0.58), Świnoujście (-0.55), or Łeba (-0.54). The only station showing statistical significance for the entire winter was Hel, and in February such significance is shown by as many as 73% of the analyzed stations.

In winter seasons with positive NAO index values (3 quartiles of the set of index values), the average cloudiness was 78%. It was 2% higher than in the negative phase (1 quartile of the set of index values) (*Fig. 6*). In the positive phase, the highest average cloudiness was observed in the north and northeastern parts of the country, as well as in the high mountain station on the Śnieżka Mountain – 83%. A similar situation is observed in the negative phase – the highest cloudiness occured near Koszalin, Łeba, and Suwałki. The exception are mountain areas, where the degree of cloudiness is considerably lower in the negative phase than in the positive one. The lowest cloudiness value was recorded in the northwestern part of Poland with a minimum in Świnoujście both in the positive (66%) and negative phases (68%).

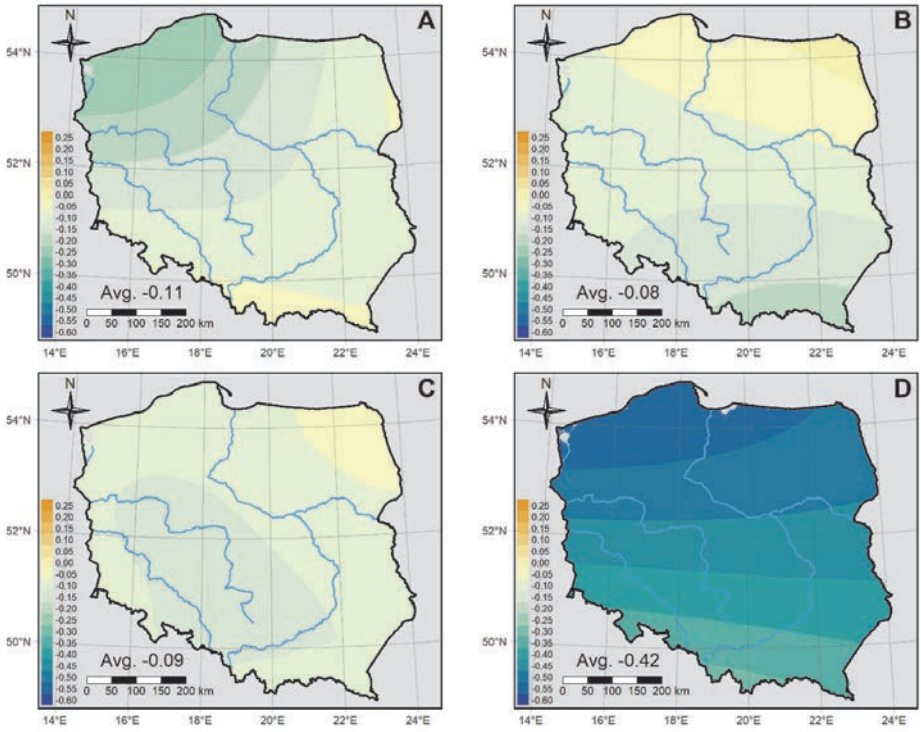

Fig. 5. Pearson correlation coefficient between the NAO index and the cloudiness in winter (A), December (B), January (C), and February (D) in the period 1990/91–2019/20

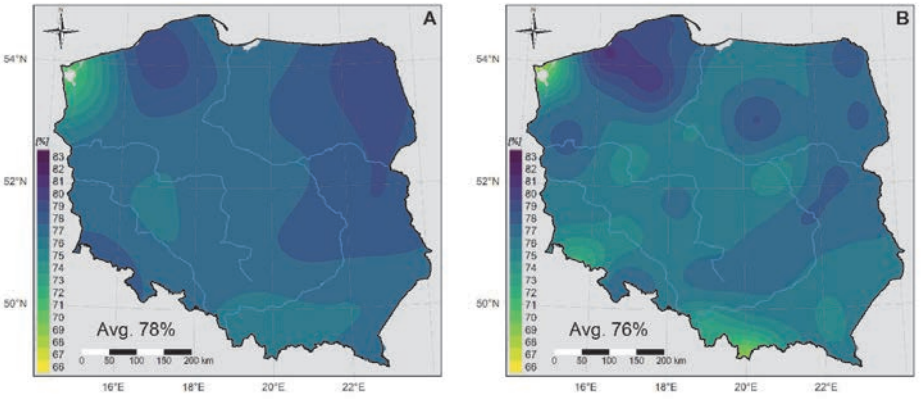

Fig. 6. Average cloudiness [%] in winter periods in which the NAO index was ≥75th percentile (A) and NAO≤ 25th percentile (B) in the years 1990/91–2019/20.

The average value of the Scandinavia index for winter reached 0.10. The highest SCAND index value was observed in season 2005/06 – 1.05. Equally high indices were recorded in seasons 2009/10 – 1.04 and 2012/13 – 1.02, and the lowest index value was observed in season 1998/99 (-0.89). In the studied multiannual period, a minimum increase in the SCAND index was determined. It was not statistically significant.

The Pearson correlation coefficient values between the SCAND index and the cloudiness primarily showed positive values, with the exception of January, when they adopted values below zero (-0.10) (*Fig. 7*). Positive values of the correlation coefficient suggest that the level of cloudiness increased with an increase in the circulation index. The average coefficient for the entire winter in the studied multiannual period reached 0.17, in February -0.06, and the highest correlation was recorded in December -0.39. The strongest correlation for the entire winter period was recorded in southwestern Poland, with a maximum in Wrocław and Kłodzko – 0.31. The only stations showing a negative correlation were high-mountain stations on Kasprowy Wierch and Śnieżka. The month with the strongest dependency between the teleconnection pattern and cloudiness was December. In 6 stations, a correlation higher than 0.50 was recorded. They were primarily stations in the eastern part of the country: Lublin, Terespol, Włodawa, and in the north: Świnoujście, Hel, Chojnice. January and February showed the lowest variability. Their average correlation coefficient values for the entire country were approximately zero. A positive correlation was observed in the west of the country in January and in the east of the country in February. In the multiannual course of winter periods, Hel was statistically significant, and in December as many as 59% of stations were significant.

The average cloudiness at extreme SCAND index values, both in the positive (3 quartiles of the set of index values) and negative phases (3 quartiles of the set of index values) reached equally 76% (*Fig. 8*). The spatial distribution of cloudiness is very similar in both phases. The highest cloudiness in the studied multiannual period was recorded in the north and northeastern part of the country in Koszalin in the negative phase – 80%, and in Chojnice in the positive phase – 80%. The lowest cloudiness values were observed in the northwestern part of the country and in the mountain areas. Minimum values were recorded in Świnoujście – 66% in the negative and 67% in the positive phase.

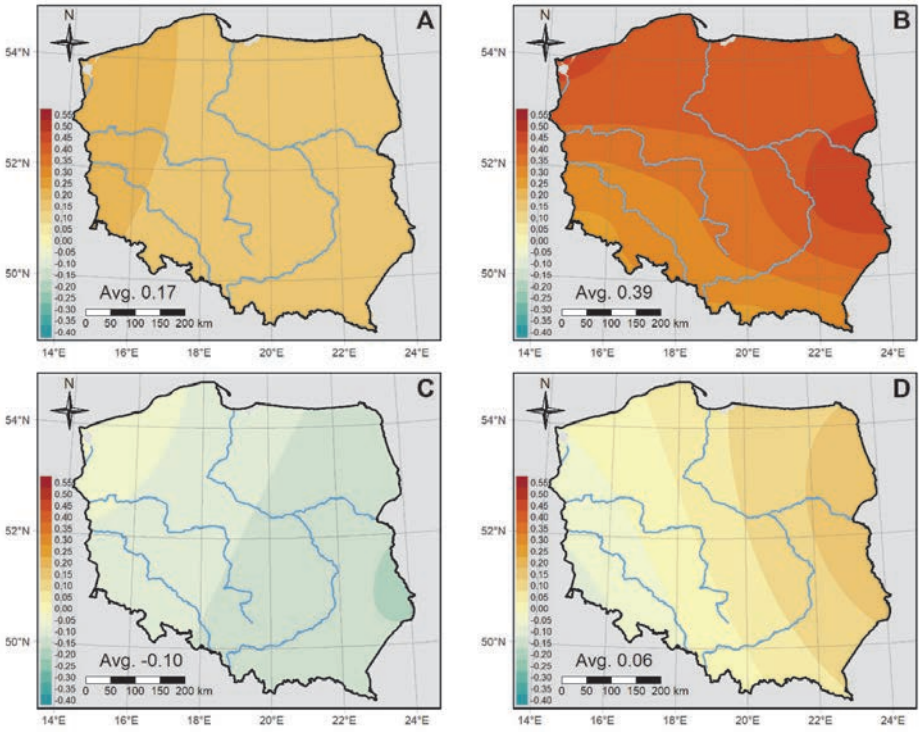

Fig. 7. Pearson correlation coefficient between the SCAND index and cloudiness in winter (A), December (B), January (C), and February (D) in the years 1990/91–2019/20.

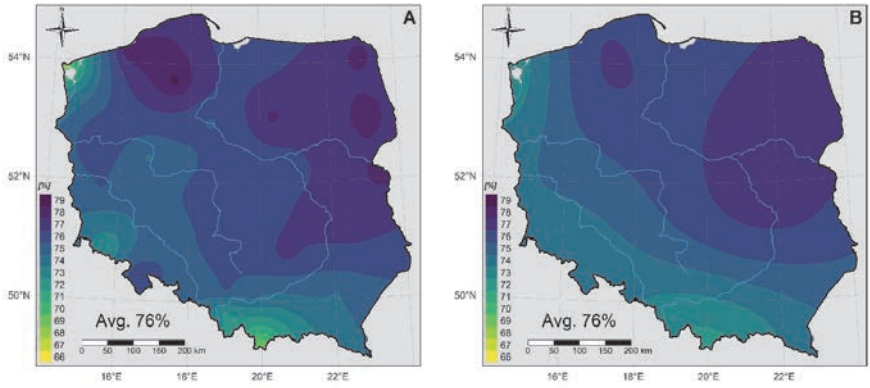

Fig. 8. Average cloudiness [%] in winter periods when the SCAND index was ≥ 75th percentile (A) and SCAND ≤ 25th percentile (B) in the years 1990/91–2019/20.

4. Summary and discussion

The paper shows the variable course of cloudiness in the studied multiannual period. Maximum cloudiness in winter for the entire Poland was recorded in the season 2012/13 – 86%, and the minimum in the season 1992/93 – 67%. The average cloudiness in the years 1990/91–2019/20 was 76%. The month with the highest cloudiness in winter was December – 78%. The increasing trend of cloudiness in Poland is statistically significant. The highest cloudiness in the spatial distribution of the country is observed in the north and northeastern parts of Poland, and stations that stand out including Koszalin, Suwałki, and Chojnice. The lowest cloudiness in the winter period was recorded in the northwest with a minimum in Świnoujście and in mountain areas. Approximate results were obtained in the papers by *Sypniewska* and *Szyga-Pluta* (2018) and *Okoniewska* (2016). Such a spatial distribution in Poland was largely determined by among others: vicinity of the Baltic Sea, more frequent occurrence of lows in northern Poland in winter, and inflow of polar-marine air from the northwest (*Okołowicz*, 1964; *Matuszko* and *Wojkowski*, 2007).

The obtained results confirm the dependency between cloudiness and teleconnection patterns. Averaged correlations in winter and in each individual winter month for the entire Poland are not high however, and in some regions of the country, the correlations are considerably stronger. Similar conclusions were drawn by *Adamczyk* (2007) in the paper regarding the dependency between the North Atlantic Oscillation and the cloudiness in Poland. Higher correlation coefficient values were obtained by among others *Bednorz* (2006) regarding snow cover in northwestern Poland, as well as *Ptak et al.* (2019) investigating ice conditions in Polish lakes. This paper primarily evidences a negative correlation in the dependency of NAO and cloudiness, and positive with SCAND. A negative correlation coefficient suggests that in the negative NAO phase, the level of cloudiness increases, and decreases in the positive phase. A positive correlation, respectively, presents the opposite dependency. The strongest correlation was recorded in the northwestern part of the country for the NAO pattern with a maximum in December, and for SCAND in the northeast with the strongest dependency in February. The correlation coefficient showed statistical significance only in Hel, both between cloudiness and NAO index and SCAND. Correlation coefficients were significant only in months characterized by a strong correlation, in a higher number of stations. Positive and negative teleconnection pattern phases show no particular variability of the average cloudiness for the entire country.

References

Adamczyk, R., 2007: Oscylacja Północnoatlantycka a wielkość zachmurzenia na obszarze Polski [w:] (*Piotrowicz K., Twardosz R.*), Wahania klimatu w różnych skalach przestrzennych i czasowych., Instytut Geografii i Gospodarki przestrzennej UJ., s. 85–91. (In Polish)

Barnston, A.G. and *Livezey, R.E.*, 1987: Classification, seasonality and persistence of low frequency atmospheric circulation patterns. *Month. Weather Rev. 115*, 1083–1126. https://doi.org/10.1175/1520-0493(1987)115<1083:CSAPOL>2.0.CO;2

Bartoszek, K., *Matuszko, D.*, and *Soroka, J*., 2020: Relationships between cloudiness, aerosol optical thickness, and sunshine duration in Poland. *Atmos. Res. 245*, 105097. https://doi.org/10.1016/j.atmosres.2020.105097

Bednorz, E., 2002: Snow cover in western Poland and macro-scale circulation conditions. *Int. J. Climatol. 22*, 533–541. https://doi.org/10.1002/joc.752

Bueha, C. and *Nakamuta, H*., 2007: Scandinavian pattern and its climatic impact. *Quart. J. Roy. Meteorol. Soc. 133*, 2117–2131. https://doi.org/10.1002/qj.173

Feldstein, S. and *Franzke, C.*, 2017: Atmospheric Teleconnection Patterns. In (Eds. *C. Franzke & T. O'Kane)* Nonlinear and Stochastic Climate Dynamics. Cambridge: Cambridge University Press. 54–104. https://doi.org/10.1017/9781316339251.004

Filipiak, J. and *Miętus, M.*, 2009: Spatial and temporal variability of cloudiness in Poland, 1971–2000. *Int. J. Climatol. 29*, 1294–1311. https://doi.org/10.1002/joc.1777

Filipiak, J., 2021: Change of cloudiness. In Climate Change in Poland. 217–274). Springer, Cham. https://doi.org/10.1007/978-3-030-70328-8_10

Hurrell, J.W., 1995: Decadal trends in the North Atlantic oscillation: regional temperatures and precipitation. *Science 269*, 676–679. https://doi.org/10.1126/science.269.5224.676

Hurrell, J.W. and *Deser C*., 2010: North Atlantic climate variability: the role of the North Atlantic Oscillation. *J. Marine Syst. 78*, 28–41. https://doi.org/10.1016/j.jmarsys.2008.11.026

Hurrell, J.W., *Kushnir, Y.*, *Ottersen, G.*, and *Visbeck, M*., 2003. An overview of the North Atlantic oscillation. *Geophysical Monograph-American Geophysical Union 134*, 1–36. https://doi.org/10.1029/134GM01

Kożuchowski, K., Wibig, J., and *Degirmendžić, J*., 2012. Meteorologia i klimatologia. Wydawnictwo Naukowe PWN. (In Polish)

Liu Y., Wang L., Zhou W., and *Chen W.*, 2014: Three Eurasian teleconnection patterns: spatial structures, temporal variability, and associated winter climate anomalies. *Climate Dynamics 42*, 2817–2839. https://doi.org/10.1007/s00382-014-2163-z

Matuszko, D. and *Wojkowski, J*., 2007. Zróżnicowanie przestrzenne wybranych cech klimatu Krakowa. Kraków: Instytut Geografii i Gospodarki Przestrzennej Uniwersytetu Jagiellońskiego. (In Polish)

Nojarov P., 2017: Circulation factors affecting precipitation over Bulgaria. *Theor. Appl Climatol. 27*, 87–101. https://doi.org/10.1007/s00704-015-1633-5

Okolowicz, W., 1964. Zachmurzenie Polski. Prace i Studia Instytutu Geograficznego Uniwersytetu Warszawskiego. *Katedra Klimatologii, 1*. (In Polish)

Okoniewska, M., 2016. Dobowy przebieg zachmurzenia w Polsce w kolejnych dekadach roku (na przykładzie lat 1990–2000). *J. Educat. Health Sport 6*, 730–740. (In Polish)

Piotrowski P., 2017: Atlas chmur i pogody. Wydawnictwo SBM. (In Polish)

Ptak, M., Tomczyk, A.M., and *Wrzesiński, D.*, 2018. Effect of teleconnection patterns on changes in water temperature in Polish lakes. *Atmosphere 9(2)*, p.66. https://doi.org/10.3390/atmos9020066

Ptak, M., Tomczyk, A.M., Wrzesiński, D., and *Bednorz, E.*, 2019: Effect of teleconnection patterns on ice conditions in lakes in lowland Poland. *Theor.Appl. Climatol. 138*, 1961–1969. https://doi.org/10.1007/s00704-019-02929-2

Sypniewska, L. and *Szyga–Pluta, K.*, 2018: Zmienność czasowa i zróżnicowanie przestrzenne zachmurzenia w Polsce w latach 2001–2016. *Badania Fizjograficzne Seria A-Geografia Fizyczna, 9 (69)*, 193–213. (In Polish) https://doi.org/10.14746/bfg.2018.9.15

Szwed, M., Pińskwar, I., Kundzewicz, Z.W., Graczyk, D., and *Mezghani, A.*, 2017: Changes of snow cover in Poland. *Acta Geophysica, 65(1)*, 65–76. https://doi.org/10.1007/s11600-017-0007-z

Tomczyk, A.M., 2014: Wpływ makroskalowych typów cyrkulacji na występowanie pokrywy śnieżnej w Europie. *Acta Geogr. Silesiana, 15*, 65–69. (In Polish)

Tomczyk, A.M., 2015: Impact of macro-scale circulation types on the occurrence of frosty days in Poland. *Bull. Geograph. Phys. Geogr. Ser. 9*, 55–65. https://doi.org/10.1515/bgeo-2015-0016

Tomczyk, A.M., *Szyga-Pluta, K.*, and *Bednorz, E.*, 2019: The effect of macro-scale circulation types on the length of the growing season in Poland. *Meteorol. Atmosph. Phys. 131*, 1315–1325. https://doi.org/10.1007/s00703-018-0639-9

Wibig, J., 2008. Cloudiness variations in Łódź in the second half of the 20th century. *Int. J. Climatol. 28*, 479–491. https://doi.org/10.1002/joc.1544

Wrzesiński, D., 2010: Odpływ rzek w Polsce w różnych fazach Oscylacji Północnoatlantyckiej. (In Polish) https://doi.org/10.2478/v10116-010-0007-z

Żmudzka, E., 2007: Cloudiness over the north-western Poland. *Quaestiones Geographicae 26*.

Żmudzka, E., 2008: The influence of cloudiness on air temperature and precipitation on the territory of Poland (1951-2000). *Miscellanea Geograph. Reg. Studies Develop. 13*, 89–103. https://doi.org/10.2478/mgrsd-2008-0009

DOI:10.28974/idojaras.2024.1.3

IDŐJÁRÁS

Quarterly Journal of the HungaroMet Hungarian Meteorological Service
Vol. 128, No. 1, January – March, 2024, pp. 41–57

An empirical and a dynamic-empirical model for the estimation of maize seedbed temperature

Gombos Béla [1,2,*] and **Nagy János** [2]

[1]*Department of Irrigation and Land Improvement*
Institute of Environmental Sciences
Hungarian University of Agriculture and Life Sciences
Szabadság út 1-3., Szarvas, H-5540, Hungary

[2]*Institute of Land Use, Engineering and Precision Farming Technology*
Faculty of Agricultural and Food Sciences and Environmental Management
University of Debrecen
Böszörményi út 138., Debrecen, H-4032, Hungary

**Corresponding author E-mail: gombos.bela@uni-mate.hu*

(Manuscript received in final form March 6, 2023)

Abstract— Soil temperature is the main factor in determining the germination of maize seeds and the emergence time of the crop. It controls the rate of phenological development while the meristem is underground, which is until the V6 (six leaf collar) stage of maize. The research performed by the authors aimed to model maize seedbed temperatures at sowing depth (soil temperature at 5 cm depth) during the sowing-emergence-early development period. The research is based on measurements in ploughed plots of the maize experiments at the Látókép Experiment Site of the University of Debrecen (Eastern Hungary) in two growing seasons of 2021–2022. Two types of empirical models were established, a multilinear regression model (M1) and a dynamic-empirical model (M2), where the daily increase and decrease of soil temperature are determined by multilinear regression. Candidates for input variables for both models were various, easily available daily meteorological parameters. M2 model performed better than M1 when applied to an independent database of 2022. This is particularly valid for the maximum and minimum soil temperatures. It was found that both M1 and M2 can be used to predict the soil temperature of the maize seedbed before shading by the plants. For daily mean temperature, M1 and M2 give a similarly good estimation, while the dynamic-empirical model has to be preferred for the maximum and minimum temperatures. M2, which is based on daily temperature, global radiation and wind speed data, predicts the daily mean (RMSE = 1.4 °C), maximum (RMSE = 2.2 °C), and minimum (RMSE = 1.6 °C) of seedbed temperature not worse than many earlier soil temperature models do, even hybrid or mechanistic ones with a large number of parameters.

Key-words: soil temperature, dynamic-empirical model, seedbed, maize, linear regression

1. Introduction

Soil temperature has an important role in crop production. It is the main factor in determining the germination of maize seeds and the emergence time of the crop (*Stone et al.*, 1998; *Santos et al*., 2019). Soil temperature controls the rate of phenological development while the meristem is underground, which is until six leaves fully expand (V6 stage) or the tip of the 10th leaf appears (*Stone et al.*, 1999). The results of field experiments with soil cover (nearly identical air temperatures and significantly different soil temperatures) demonstrate this effect (*Lu et al.*, 2020). At higher soil temperatures, the faster initial development results in a shorter growing season and significantly earlier flowering and physiological maturation (*Stone et al.*, 1998). In maize (*Bollero et al.*, 1996) and other crops (*Jamieson et al.*, 1995), it is often more effective to calculate the length of early developmental stages using soil temperature rather than air temperature. However, when there are no different soil temperature "treatments", soil temperature-based thermal unit models do not perform better than air temperature-based models as found out by *McMaster* and *Wilhelm* (1998). Soil temperature directly or indirectly affects various physical, chemical and biological processes in the soil. From the perspective of practical maize production, other important processes that are affected by soil temperature include root growth (*Xia et al*., 2021), phenological development of maize pests (*Streda et al.*, 2013), and water and nutrient uptake by roots (*Ni et al.*, 2019).

At weather stations, soil temperatures are typically measured under bare surface, sometimes under grass. According to WMO standards, a bare (uncovered) area of approximately 2 m × 2 m should be designated for measuring soil temperature at synoptic and climate stations (*WMO*, 2018). The Hungarian Meteorological Service recommends that measurements should be taken in an area of at least 1 m^2, kept permanently free of weeds. For agricultural weather stations, two types of standard cover are used – bare soil and short grass. Wherever possible, simultaneous readings should be made under both standards for comparison (*WMO*, 2012).

Under field conditions, the temperature conditions are different from both bare and grass covered soils. Significant differences can occur in the radiative balance of the soil surface and in the magnitude of sensible and latent heat fluxes. The soil structure due to tillage is also different from the basically undisturbed soil structure of the weather stations, causing differences in the soil thermal properties and in its temperature conditions. Tillage typically increases soil temperature in the upper layers, which can be observed even under strip tillage (*Cox et al.*, 1990; *Licht* and *Al-Kaisi*, 2005; *Ozpinar* and *Ozpinar*, 2015). Soil thermal properties are spatially highly variable, mainly due to heterogeneity in moisture content and compaction (*Usowicz et al.*, 1996). Heat capacity increases linearly with soil moisture and is significantly less sensitive to soil volumetric mass. Thermal conductivity also increases with soil moisture, although at a

decreasing rate. Soil thermal properties are sensitive to changes in soil compaction, especially in the less compacted range (*Abu-Hamdeh* and *Reeder*, 2000).

Soil temperature is determined by a combination of meteorological factors, soil thermal properties, and certain crop parameters. These (or a subset of them) can be used to calculate soil temperature, and mechanistic, empirical, and hybrid models combining the two can be used in practice. Mechanistic models describe the physical processes that determine soil temperature, whose main elements are the surface energy balance, with components such as the radiative balance, latent and sensible heat fluxes in the air, and molecular heat conduction in the soil. These models should be run preferably with site-specific input data combined with hydrological or plant simulation models to maximize the potential of the sophisticated method. Complex simulation models including soil temperature modules such as APSIM (*Keating et al.*, 2003; *Chauhan et al.*, 2007; *Archontoulis et al.*, 2014), DSSAT (*Jones et al.*, 2003) can be used effectively for calculating soil temperature of arable crops. Soil thermal and water retention conditions including plant cover are modeled by the CoupModel (*Liu et al.*, 2022), AGRISOTES (*Grabenweger et al.*, 2021), SiSPAT (*Brauda et al.*, 1995; *Ji et al.*, 2009), and HYDRUS-1D models (*Simunek et al.*, 2008).

Empirical models are based on statistical relationships between soil temperature and various meteorological and soil parameters. In many cases, they provide a reasonable accuracy for practical applications using only a few basic meteorological variables. The surface energy balance is the main determinant of both air and soil temperatures, so they are closely related. *Günes et al.* (2014) modeled daily air temperature data for different soil types at a depth of 5 cm below the grass surface using non-linear empirical relationships depending on the saturated/unsaturated state of the soil. *Barman et al.*, (2017) estimated soil temperature values at 5, 15, and 30 cm below bare soil surface using regression analysis. For morning soil temperature, the best prediction was obtained using the nonlinear functions of daily mean temperature and for afternoon soil temperature (in the upper layers) with daily maximum air temperature. Examining many years of soil temperature data obtained by the weather stations, it was found that the correlation with air temperature decreases with depth, with the highest correlation for 5 and 10 cm (*Islam et al.*, 2015). Backward reconstruction of soil temperature below forest canopy was successfully achieved using regression equations based on air temperature data (*Brown et al*., 2000). On a continental scale, a sufficiently accurate estimate of soil temperature can be obtained using a shifting average of daily precipitation sum and air temperature (*Zheng et al*., 1993). The base model is valid for bare soil, while the effect of plant cover was described in the model using the leaf area index. *Perreault et al.* (2013) modeled soil temperature under maize stands at depths of 10, 25, and 50 cm with soil texture, daily maximum and minimum temperatures, and daily precipitation data as inputs. Their results were used to study weed germination and emergence. In estimating daily soil

temperature, *Delbari et al.* (2019) found the performance of a support vector regression (SVR) based model and the more classical multilinear regression models (MLR) similarly favorable for the 10-cm layer. In estimating soil temperature at deeper layers, SVR performed better than MLR. The empirical soil temperature models are essentially site-specific (*Langat*, 2021) and valid under the given climatic and soil conditions and agrotechnology.

The base temperature of maize is typically between 7–10 °C (*Gilmore* and *Rogers*, 1958; *Narwal et al.*, 1986; *Birch et al.*, 1998; *Tsimba et al.*, 2013). According to practical recommendations, maize should be sown when soil temperature is permanently above the base temperature. The course of spring soil temperatures, the actual and forecast values, is very important agrometeorological information needed by growers because of its direct practical use. Although measured and predicted soil temperature data are available, they are not sufficiently specific and do not characterize seedbed temperature conditions properly.

This research aimed to develop a soil temperature model that calculates maize seedbed temperatures at sowing depth (soil temperature at 5 cm depth) during the sowing-emergence-early development period. It was important to use only easily available daily meteorological data and to reach an accuracy suitable for practice.

2. Material and methods

The performed research is based on measurements taken in Eastern Hungary at the Látókép Experiment Site of the University of Debrecen (N 47°33', E 21°27', 120 m asl). The soil of the area is mid-heavy calcareous chernozem with a physical type of loam, and Arany's plasticity index of 39. The soil is characterized by excellent hydrophysical properties and high yield potential. The soil temperature measurements were set up in ploughed plots of the maize experiments (multifactoral long-term field experiment and sowing time experiment) in two growing seasons of 2021-2022. Following the typical soil cultivation practice, the experimental plots were ploughed in the months of October-November prior to the growing season at a depth of 30 cm. Basal fertilizer was applied at the rates of 80 kg N ha^{-1}, 60 kg P_2O_5 ha^{-1}, and 90 kg K_2O ha^{-1}. After winter, the first soil cultivation (field rolling) was performed in March, when soil moisture conditions became favorable. Seedbed preparation was done within a few days before sowing. Maize (Merida FAO 380) was sown at a density of 80,000 plants ha^{-1}, with 0.76 m row spacing. Sowing depth was 5-6 cm. Interrow cultivation was performed only after the trial period.

2.1. Soil temperature measurements

Soil temperature measurements were carried out using HOBO UA-002 temperature data loggers. All thermologgers were preliminary tested with parallel measurements in stable, homogeneous indoor circumstances. The average temperature of the 24-hour period was calculated from 10-minute measurements for each device. These values showed very small differences (maximal difference from the total mean did not exceed 0.3 °C). However, a correction value was determined and applied for each device according to the obtained test results. The thermometers were installed in each parcel within a few days after sowing. Measurements covered most of the growing season, but only data of up to 30 days after sowing was used according to the purpose of the research, when the shading effect of the emerged maize was still negligible (*Table 1*). Two plots with different sowing date were used in the research in order to have a longer measurement period for modeling. For both years, the first part of the soil temperature dataset used in modeling originates from the first sown plot of the sowing date experiment performed in maize. The second part of the dataset is based on the measurements in the multifactorial long-term experiment, where maize was sown 3–4 weeks later.

Table 1. Timing of the soil temperature measurement program in 2021–2022 and the related crop data

year	examination period	date			
		sowing	installation of thermologgers	emergence	V6
2021	April 1–27	March 31	March 31	April 27	May 25
	April 28 – May 22	April 22	April 27	May 6	June 3
2022	April 8 – May 3	April 6	April 7	April 28	May 23
	May 4 – June 1	May 2	May 3	May 9	May 31

The thermometers were placed exactly in the rows at a depth of 5 cm, in four replicates in 2021. In 2022, there was a possibility for only three replicates, because of the changes in the complex soil temperature research program (aiming at the effect of depth and tillage). While installing the thermologgers, we focused to regenerate the original soil surface and compaction conditions of the seedbed.

The daily mean, minimum, and maximum temperature values were determined from data recorded at 10-minute intervals. Using 0–24 hour observing

window in search for minimum/maximum temperature often omits the true temperature extrema, and instead identifies endpoint temperatures. The capturing of true "peaks and lows" of diurnal temperature cycle can be improved by recording maximum and minimum values at the coldest and warmest time of day, respectively (*Rischard et al.*, 2018). Another possibility is the identification of temperature extrema within continuous nighttime and daytime intervals (*Zaknic-Catovic* and *Gough*, 2022). Adapting this night-and-day climatological observing window for our soil temperature model, the daily minimum values were calculated on the 0–14 CET time intervals and the maximum values on the 12–02 CET time intervals.

2.2. Meteorological measurements

Air temperature and humidity measurements were taken at 2 m height, at 10-minute intervals, in a distance of 500 m from the experimental area, above a short-cut grass surface. Microsoft Excel was used to determine the daily data for statistical analyses. Precipitation was measured using a conventional Hellmann rain gauge and an automatic weighing gauge in parallel. The data from the latter were used to characterize the rainfall patterns of the study periods.

The wind speed (10 m) and global radiation data measured at the Debrecen-Kismacs station of the Hungarian Meteorological Service (OMSZ, 2022) were used for the analysis. Considering the number of factors (distance of 10 km, similar agricultural area, high accuracy measurements, spatial heterogeneity), this solution is acceptable.

2.3. Soil temperature model

The aim of this research was to create an empirical model for estimating daily soil temperature values. According to the data requirements of the different thermal time methods, the determination of daily minimum and maximum values in addition to the daily mean temperature was part of the calculations. The research focused only on the period of sowing-emergence-early development, when the soil temperature information is especially needed by maize growers in practice. The two model versions were not aimed to be extended to the later phenological phases, therefore, the shading effect of the vegetation was not included. Data from 2021 was used for model calibration, while validation was based on 2022 data.

In Model 1 (M1), the following meteorological parameters were included in the multilinear regression analysis (stepwise regression, SPSS Statistics 27.0): daily average temperature (TA_{ave}, °C), daily minimum temperature (TA_{min}, °C), daily maximum temperature (TA_{max}, °C), daily global radiation (G, MJ m^{-1}), daily average wind speed (w, ms^{-1}), and mean temperature of the preceding 1-, 2-, 3-, 4-, 5-, 6-, and 7-day-period.

The study also included a specific dynamic-empirical model (Model 2, M2), which has the same base as a previous model describing the temperature of the rice floodplain (*Gombos*, 2008). The model treats the warming and cooling phases of the daily soil temperature cycle separately, and determines the nighttime temperature decrease ($\Delta T1$) and daytime temperature increase ($\Delta T2$) of the soil for each day (n is the day of the simulation) based on empirical relationships. Steps:

1. Setting the maximum soil temperature for the previous day of the study period, with estimated or measured initial value ($TS_{max,0}$);
2. Determination of the night-time decrease in soil temperature based on meteorological data (and soil temperature) using an empirical formula ($\Delta T1_n$)
3. Calculation of the minimum soil temperature: $TS_{min,n} = TS_{max,n-1} - \Delta T1_n$;
4. Calculation of the daytime increase in soil temperature using an empirical formula: ($\Delta T2_n$);
5. Calculation of daily maximum soil temperature by adding the increase to the minimum: $TS_{max,n} = TS_{min,n} + \Delta T2_n$.

Repeating steps 2 to 5 N times, the minimum and maximum soil temperature is obtained for each day of the period under study (N is the number of days).

The empirical formulas estimating $\Delta T1$ and $\Delta T2$ were determined also in this case using multivariate linear regression analysis. Compared to the M1 model, the set of initial parameters differed:

- the mean temperature of the preceding 1, 2, ..., 7-day periods was omitted,
- the parameter CF representing the cooling effect of air was included: $CF_n = TS_{max,n-1} - TA_{min,n}$,
- and WF representing the heating effect of air was calculated $WF_n = TA_{max,n} - TS_{min,n}$.

The idea for the introduction of the new parameters is based on the assumption that the greater the values of CF (the difference of the minimum air temperature and the previous day's soil temperature maximum) are, the higher the decrease in soil temperature is. The introduction of the WF variable can be explained similarly. An increase in model stability is also expected by defining new variables in this way, as it provides negative feedback.

2.4. Model validation

Model calibration and regression coefficients were determined using data from 2021 (52 days) and validated with data from 2022 (55 days). The comparison of the estimated (P_i) and actual (O_i) daily minimum, maximum, and mean soil

temperature values was compared graphically first. As a next step, to objectively evaluate the performance of the model, the commonly used statistical indices were applied (*n* is the number of days). These statistics focus on different aspects of model performance:

- The coefficient of determination (*CD*) shows how closely the estimated data follow the trend of the measured values. Values close to 1 indicate that the model is optimal in this aspect.
- Root mean square error (*RMSE*) quantifies the deviation between estimates and observations according to this formula:

$$RMSE = \sqrt{\frac{\sum(P_i - O_i)^2}{n}}. \quad (1)$$

- Model efficiency (*EF*), the optimum of this coefficient is 1, if positive, the model is a better predictor than the average of measured values:

$$EF = 1 - \frac{\sum(P_i - O_i)^2}{\sum(O_i - \bar{O})^2}. \quad (2)$$

- Mean absolute error (*MAE*) provides a measure of error based on the absolute value of the deviations:

$$MAE = \frac{|P_i - O_i|}{n}. \quad (3)$$

- Mean error (*ME*) or bias shows whether and to what extent the model over or underestimates the measured values in average:

$$ME = \frac{P_i - O_i}{n}. \quad (4)$$

In addition to the real daily mean temperature, a value calculated from the average of the maximum and minimum can also be important (many models calculate daily thermal units based on the latter). The M1 model gives a separate estimate for both, while for M2, both parameters can be estimated with the same value ($TS_{nx/2}$).

3. Results

3.1. Weather conditions

Both the calibration (2021) and validation (2022) periods greatly overlapped with the time period April-May.

The weather in April 2021 was poor in sunshine and significantly cooler than the long-term average. There were several occasions of light precipitation, but the total monthly rainfall was only half the long-term average (*Fig. 1*). In May, the weather was cooler than normal for this time of year, with near average rainfall and sunshine duration. April 2022 was also cool with less hours than average, but with more rainfall than in the previous year. The weather in May was the opposite as in 2021, with above-average temperature, more sunshine, and small amount of precipitation. It can be concluded that the weather conditions in the calibration and validation periods differed significantly, especially in May.

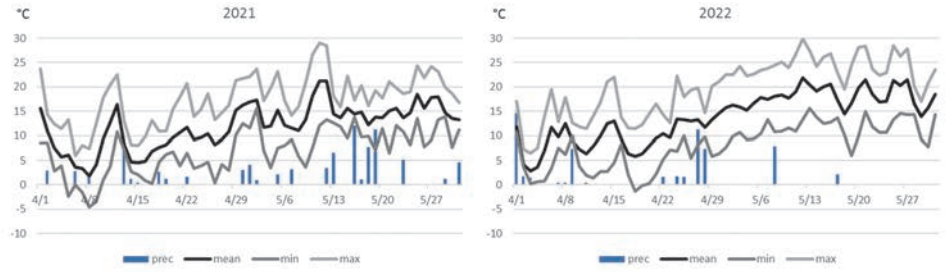

Fig. 1. Daily values of precipitation and mean, minimum, and maximum temperatures in the period of April to May in 2021 and 2022.

3.2. Calibration

3.2.1. Model 1

In our multilinear regression model (M1) for estimating the daily mean soil temperature (TS_{ave}), the final formula obtained using the stepwise method includes the daily mean air temperature (TA_{ave}), mean temperature of the previous 7 days (TA_7), and global radiation (G) as independent variables. The model was not significantly improved by wind speed, relative humidity, daily minimum and maximum temperatures.

$$TS_{ave} = 0.660 \cdot TA_{ave} + 0.329 \cdot TA_7 + 0.102 \cdot G + 0.74\,. \qquad (5)$$

For daily minimum soil temperature (TS_{min}), the parameter of greatest weight is the minimum air temperature (TA_{min}), the other important parameter is the mean temperature of the previous day (TA_1). Logically, the daily global radiation has no

effect due to the time lag. This explains why no daily mean value of any meteorological element appears in the formula.

$$TS_{min} = 0.455 \cdot TA_{min} + 0.346 \cdot TA_{1} + 2.82 \, . \quad (6)$$

The regression calculation for the daily maximum of soil temperature (TS_{max}) also confirmed the preliminary expectations. The daily maximum (TA_{max}), mean and global radiation (G) of air temperature are included in the formula. Temperature averages on previous days are also correlated with the soil temperature maximum, with significant improvements in the model obtained by including the 4-day mean temperature (TA_4) as an independent variable. The regression equation is as follows:

$$TS_{max} = 0.397 \cdot G - 0.147 \cdot TA_{max} + 0.808 \cdot TA_{ave} + 0.172 \cdot TA_{4} + 2.82 \, . \quad (7)$$

For the calibration period, the following were found (*Table 2*):

- The coefficient of determination and the model efficiency have high values (R^2 = 0.95 – 0.96, EF = 0.94 – 0.96), almost equal for all variables.
- The average error, which refers to the systematic error, is very small, with an underestimation of 0.2°C only for the minima.
- The root mean square error and the mean absolute error are the largest for daily maxima and the smallest for daily mean temperature.

There is no significant difference in the estimates of the two different daily means.

Table 2. M1 model performance on the calibration (2021) data set

M1	*RMSE*	*MAE*	*ME*	R^2	*EF*
minimum	0.9	0.7	-0.2	0.95	0.94
maximum	1.2	1.0	0.0	0.95	0.95
average	0.9	0.7	0.0	0.95	0.95
(max+min)/2	0.8	0.7	-0.1	0.96	0.96

3.2.2. Model 2

In the dynamic-empirical model (M2), multivariate linear regression was used to describe the daily cooling and warming phases of the soil and its temperature changes. The nighttime soil temperature decrease ($\Delta T1$) showed the strongest correlation with the variable *CF*, which can be interpreted as the cooling effect of air.

The inclusion of the air temperature minimum significantly improved the prediction. The regression equation is as follows:

$$\Delta T1 = 0.725 \cdot CF + 0.190 \cdot AT_{min} - 1.37 \, . \quad (8)$$

The increase in soil temperature during the day ($\Delta T1$) is estimated using a regression equation with daily global irradiance, daily mean wind speed, and the warming effect of air (WF) as independent variables:

$$\Delta T2 = 0.392 \cdot G - 0.844 \cdot w + 0.229 \cdot WF + 2.69 \, . \quad (9)$$

From the values of $\Delta T1$ and $\Delta T2$ calculated for each day, the daily minimum and maximum of the soil temperature for the whole calibration period are obtained by successive subtraction and addition, respectively. By taking the simple arithmetic mean of these extremes, the daily mean temperature can be calculated.

While the M1 model is based on a direct empirical estimation of daily soil temperature values (min, max, mean), in the dynamic-empirical model, the soil temperature data are obtained indirectly after a multi-step calculation. Therefore, as expected, the estimation error of the M2 model on the calibration database is larger than that of the M1 model (*Table 3*). Further findings on the performance of the M2 model are:

- The largest error, as for M1, is in the predictions of daily maximum soil temperature (*RMSE* = 1.7 °C, *MAE* = 1.4 °C).
- The *RMSE* and *MAE* for minimum temperature are slightly smaller than for mean temperature.
- The values of the coefficient of determination (R^2 = 0.94 – 0.97) show no difference compared to M1, but the model efficiency is lower (*EF* = 0.86 – 0.90).
- The systematic error is negligible for the maxima and minima and, as a result, also for their mean. The actual daily mean differs from the latter (it is lower), resulting in an average overestimation of 0.4 °C.

Table 3. M2 model performance on calibration (2021) data set

M1	*RMSE*	*MAE*	*ME*	R^2	*EF*
minimum	1.4	1.1	0.0	0.97	0.87
maximum	1.7	1.4	0.0	0.94	0.90
average	1.6	1.3	0.4	0.95	0.86
(max+min)/2	1.5	1.2	0.0	0.96	0.87

3.3. Validation

Indices for the evaluation of the models were calculated using the independent validation data of 2022. It is normal that the performance of empirical models is weaker for a new independent data set than for the calibration period. This is clearly the case for the M1 model (*Table 4*):

- Especially in the estimation of the temperature extremes, there is a large loss in accuracy.
- The M1 model is the most inaccurate in predicting the maximum soil temperature, followed by minimum temperature. The regressed maxima (2.0 °C) and minima (1.4 °C) are lower than the measured values averaged over the 52 days.
- These errors for mean temperature are significantly smaller (*RMSE* = 1.5 °C, *MAE* = 1.2 °C, *ME* = -0.9 °C).
- The model efficiency is below 0.8 for the extreme value estimate, but above 0.9 for the daily average.
- The mean calculated by averaging the estimated extremes is significantly less suitable to estimate the real daily mean than the direct (applied to the daily mean) empirical relationship.

The majority of the indices show an advantage of the M2 model over the M1 (except for the coefficient of determination for the daily mean temperature), (*Table 4*):

- Its advantage over M1 is the largest for the minimum temperature, but also significant for daily maximum values and for the mean temperature calculated from extreme values.
- The performance of M2 is also the weakest (in all indices) in prediction of the daily maximum soil temperature and the best for daily mean temperature.
- It should be noted that the dynamic-empirical model estimates the daily mean temperature on the validation dataset with smaller errors (*RMSE, MAE, ME*) compared to the calibration dataset.

Table 4. M1 and M2 model performance on the validation (2022) data set

M1	*RMSE*	*MAE*	*ME*	R^2	*EF*
minimum	2.6	2.2	-1.4	0.91	0.76
maximum	2.7	2.3	-2.0	0.89	0.76
average	1.5	1.2	-0.9	0.96	0.92
(max+min)/2	2.3	2.0	-1.7	0.94	0.80
M2	*RMSE*	*MAE*	*ME*	*R2*	*EF*
minimum	1.6	1.2	-0.4	0.92	0.91
maximum	2.2	1.7	-1.3	0.92	0.84
average	1.4	1.0	-0.3	0.93	0.93
(max+min)/2	1.5	1.1	-0.8	0.95	0.91

Fig. 2 shows the measured daily mean soil temperature and the values calculated by the two model versions. M1 reproduces the real values very well over the whole calibration period. The M2 model showed an underestimation of more than 2°C for the period April 6-8, 2021 (*Fig. 2*). During the last days of major warming events, M2 tends to overestimate the soil temperature (above 2 °C: April 12, April 29 – May 2). In the 2022 validation period, M1 prediction is below the daily mean from the measured data on most days. However, the deviations exceed 2 °C only on a few days at the end of May. The M2 model gives a very accurate prediction for most of the period, but there are some critical periods when the error is larger than that of the M1 model. On 7 days, which is 13% of the total number of days in the study period, the prediction error (absolute value) is larger than 2 °C, which is reasonable compared to the results of other studies. *Zheng et al*. (1993) found in average 40% of days with larger than 2 °C error in their empirical model for soil temperature at 10 cm.

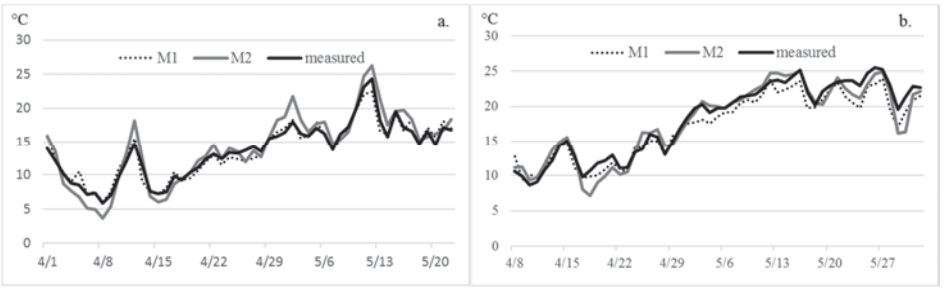

Fig. 2. Daily mean soil temperature values estimated by M1 and M2 models and the daily average of the measured (in every 10 minutes) soil temperature data. (a) Calibration period (April 1 -May 22, 2021), (b) validation period (April 28 -June 1, 2022).

4. Conclusions

The research described in this paper has shown that maize seedbed temperature can be estimated using multilinear regression with high accuracy over the calibration period. For the minimum temperature, it is sufficient to use various air temperature data as input, while the addition of global radiation in the regression estimation of the daily mean and maximum leads to a significant improvement. For the daily mean soil temperature, the classical empirical model (M1) fits very well (*RMSE* = 0.9 °C, *MAE* = 0.7 °C, *ME* = 0.0 °C, *R2* = 0.95, *EF* = 0.95).

However, validation on an independent database gives a more realistic indication of model applicability. A common way is to divide the test period into two parts to define the calibration and validation databases. The outlined research followed this approach, and it was found that the model performance had become weaker. The mean temperature estimate still remained favorable when compared with literature data. The *RMSE* of 1.5 °C is acceptable, because the maize seedbed at 5 cm depth is more directly exposed to weather than the soil at greater depths and under vegetated surface.

The dynamic-empirical (M2) model performed well on the calibration database, but underperformed the classical empirical model. The explanation for this difference is that M2 calculates the daily maximum and minimum values indirectly, with daily steps up and down in the soil temperature. However, as in a previous similar study on rice flooding water (*Gombos*, 2008), the M2 model performed better than M1 when applied to an independent database. This is particularly valid for the maximum and minimum soil temperatures. In the prediction of daily mean temperature, M2 even improved slightly compared to the calibration period. Overall, M2, which is based on daily temperature, global radiation and wind speed data, calculates the daily mean (*RMSE* = 1.4 °C), maximum (*RMSE* = 2.2 °C) and minimum (*RMSE* = 1.6 °C) of seedbed

temperature with the accuracy expected. These values of *RMSE* and also the coefficients of determination (0.92–0.93) are in the same range as or better than in the case of many earlier soil temperature models, even hybrid or mechanistic ones with a large number of parameters (*Roloff et al.,* 1998; *Kang et al.,* 2000; *Sándor* and *Fodor,* 2012; *Liu et al.,* 2013; *Perreault et al.,* 2013). It can be concluded that both M1 and M2 can be used to predict the soil temperature of the maize seedbed before shading of the plants. For daily mean temperature, M1 and M2 provide a similarly good estimation, while the dynamic-empirical model has to be preferred for the maximum and minimum temperatures. However, the results must be used with appropriate care because of the small number of experimental years. Further measurements are needed to increase the validity of the results.

Acknowledgments: Project no. TKP2021-NKTA-32 has been implemented with the support provided from the National Research, Development and Innovation Fund of Hungary, financed under the TKP2021-NKTA funding scheme.

References

Abu-Hamdeh, N.H. and *Reeder R.C.*, 2000: Soil thermal conductivity: effects of density, moisture, salt concentration and organic matter. *Soil Sci. Soc. America J. 64*, 1285–1290. https://doi.org/10.2136/sssaj2000.6441285x

Archontoulis, S.V., Miguez, F.E. and *Moore, K.J.*, 2014: Evaluating APSIM Maize, Soil Water, Soil Nitrogen, Manure, and Soil Temperature Modules in the Midwestern United States. *Agron. J. 106*, 1025–1040. https://doi.org/10.2134/agronj2013.0421

Barman, D., Kundu, D.K., Pal, Soumen,- Pl Susanto, Chakraborty, A.K., Jha, A.K., Mazumdar, S.P., Saha, R., and *Bhattacharyya, P.*, 2017: Soil temperature prediction from air temperature for alluvial soils in lower Indo-Gangetic plain. *Int. Agrophysics 31*, 9–22. https://doi.org/10.1515/intag-2016-0034

Birch, C. J., Hammer, G.L., and *Rickert, K.G.*, 1998: Temperature and photoperiod sensitivity in five cultivars of maize (Zea mays) until tassel initiation. *Field Crops Res. 55*, 93–107. https://doi.org/10.1016/S0378-4290(97)00062-2

Bollero, G.A., Bullock, D.G., and *Hollinger, S.E.*, 1996: Soil Temperature and Planting Date Effects on Corn Yield, Leaf Area, and Plant Development. *Agron. J. 88*, 385–390. https://doi.org/10.2134/agronj1996.00021962008800030005x

Brauda, I., Dantas-Antonino, A.C., Vauclin, M., Thony, J.L., and *Ruelle, P.*, 1995: A simple soil-plant-atmosphere transfer model (SiSPAT) development and field verification. *J. Hydrol. 166*, 213–250. https://doi.org/10.1016/0022-1694(94)05085-C

Brown, S.E., Pregitzer, K.S., Reed, D.D., and *Burton, A.J.*, 2000: Predicting Daily Mean Soil Temperature from Daily Mean Air Temperature in Four Northern Hardwood Forest Stands. *Forest Sci. 46*, 297–301. https://doi.org/10.1093/forestscience/46.2.297

Chauhan, Y., Wright, G., Rachaputi, N.R., Krosch, S., Robertson, M., Hargreaves, J., and *Broome, A.*, 2007: Using APSIM-soiltemp to simulate soil temperature in the podding zone of peanut. *Australian J. Experiment. Agricult. 47*, 992–999.http://dx.doi.org/10.1071/EA06137

Cox, W.J., Zobel, R.W., Es, H.M., and *Otis, D.J.*, 1990: Growth development and yield of maize under three tillage systems in the northeastern USA. *Soil Tillage Res. 18*, 295–310. https://doi.org/10.1016/0167-1987(90)90067-N

Delbari, M., Sharifazari, S., and *Mohammadi, E.*, 2019: Modeling daily soil temperature over diverse climate conditions in Iran—a comparison of multiple linear regression and support vector regression techniques. *Theor. Appl. Climatol. 135*, 991–1001. https://doi.org/10.1007/s00704-018-2370-3

Gilmore, E. and *Rogers, J.*, 1958: Heat units as a method of measuring maturity in corn. *Agronomy J. 50*, 611–615. https://doi.org/10.2134/agronj1958.00021962005000100014x
Gombos, B., 2008: Modeling water temperature of Hungarian rice fields. *Időjárás 112*, 33–43.
Grabenweger, P., Lalic, B., Trnka, M., Balek, J., Murer, E., Krammer, C., Mozny, M., Gobin, A., Saylan, L. and *Eitzinger, J.*, 2021: Simulation of Daily Mean Soil Temperatures for Agricultural Land Use Considering Limited Input Data. *Atmosphere 12*, 441. https://doi.org/10.3390/atmos12040441
Günes A., Özgül M., Bilgili A.V., and *Turan M.*, 2014: Basic prediction approach for determination of soil temperature using air temperature in some selected soil orders of Eastern Turkey. *J. Food, Agricult. Environ. 12*, 424–429.
Islam, K.I., Khan, A. and *Islam, T.*, 2015: Correlation between Atmospheric Temperature and Soil Temperature: A Case Study for Dhaka, Bangladesh. *Atmosph. Climate Sci 5*, 200–208. http://dx.doi.org/10.4236/acs.2015.53014
Jamieson, P.D., Brooking, I.R., Porter, J.R., and *Wilson, D.R.*, 1995: Prediction of leaf appearance in wheat: A question of temperature. *Field Crops Res. 41*, 35–44. https://doi.org/10.1016/0378-4290(94)00102-I
Ji, X.B., Kang, E.S., Zhao, W.Z., Zhang, Z.H., and *Jin, B.W.*, 2009: Simulation of heat and water transfer in a surface irrigated, cropped sandy soil. *Agric. Water Manag. 96*, 1010–1020. https://doi.org/10.1016/j.agwat.2009.02.008
Jones, J.W., Hoogenboom, G., Porter, C.H., Boote, K.J., Batchelor, W.D., Hunt, L.A., Wilkens, P.W., Singh, U., Gijsman, A.J., and *Ritchie, J.T.*, 2003: The DSSAT cropping system model. *European Journal of Agronomy 18*, 235–265.https://doi.org/10.1016/S1161-0301(02)00107-7
Kang, S., Kim, S., Oh, S. and *Lee, D.*, 2000: Predicting spatial and temporal patterns of soil temperature based on topography, surface cover and air temperature. *Forest Ecol. Manage. 136*, 173–184. http://dx.doi.org/10.1016/S0378-1127(99)00290-X
Keating, B.A., Carberry, P.S., Hammer, G.L., Probert, M.E., and *Robertson, M.J.*, 2003: An overview of APSIM, a model designed for farming systems simulation. *Eur. J. Agronomy 18*, 267–288. https://doi.org/10.1016/S1161-0301(02)00108-9
Langat, J.K., 2021: Soil temperature prediction using measured atmospheric temperature in two high altitude regions of Kenya. *Int. J. Forest Soil Erosion 11*, 75–86.
Licht, M.A. and *Al-Kaisi, M.*, 2005: Strip-tillage effect on seedbed soil temperature and other soil physical properties. *Soil Tillage Res. 80*, 233–249. https://doi.org/10.1016/j.still.2004.03.017
Liu, S., Li, J. and *Zhang, X.:* 2022: Simulations of SoilWater and Heat Processes for No Tillage and Conventional Tillage Systems in Mollisols of China. *Land 11*, 417. https://doi.org/10.3390/land11030417
Liu, S., Yang, J.Y., Zhamg, X.Y,m Drury, C.F., Reynolds, W.D., and *Hoogenboom, G.*, 2013: Modelling crop yield, soil water content and soil temperature for a soybean–maize rotation under conventional and conservation tillage systems in Northeast China. *Agric. Water Manage. 123*, 32-44. https://doi.org/10.1016/j.agwat.2013.03.001
Lu, H., Xia, Z., Fu, Y., Wang, Q., Xue, J., and *Chu, J.*, 2020: Response of Soil Temperature, Moisture, and Spring Maize (Zea mays L.) Root/Shoot Growth to Different Mulching Materials in Semi-Arid Areas of Northwest China. *Agronomy 10*, 453. https://doi.org/10.3390/agronomy10040453
McMaster, G.S. and *Wilhelm, W.*, 1998: Is Soil Temperature Better than Air Temperature for Predicting Winter Wheat Phenology? *Agronomy J. 90*, 602–607. https://doi.org/10.2134/agronj1998.00021962009000050006x
Narwal, S.S., Poonia, S., Singh, G., and *Malik, D.S.*, 1986: Influence of sowing dates on the growing degree days and phenology of winter maize (*Zea mays* L.). *Agricult. Forest Meteorol38*, 47–57. https://doi.org/10.1016/0168-1923(86)90049-3
Ni J., Cheng Y., Wang Q., Ng C.W.W., and *Garg A.*, 2019: Effects of vegetation on soil temperature and water content: Field monitoring and numerical modelling. *J. Hydrol. 571*, 494–502. https://doi.org/10.1016/j.jhydrol.2019.02.009
OMSZ, 2022: Hungarian Meteorological Service: Meteorological Data Bank. https://odp.met.hu/
Ozpinar, S. and *Ozpinar, A.*, 2015: Tillage effects on soil properties and maize productivity in western Turkey. *Arch. Agronomy Soil Sci. 61*, 1029–1040. https://doi.org/10.1080/03650340.2014.978302

Perreault S., Chokmani K., Nolin M.C. and *Bourgeois G.*, 2013: Validation of a Soil Temperature and Moisture Model in Southern Quebec, Canada. *Soil Sci. Soc. Amer. J. 77*, 606–617. http://dx.doi.org/10.2136/sssaj2012.0311

Rischard M., Pillai, N. and *McKinnon K.A.*, 2018: Bias correction in daily maximum and minimum temperature measurements through Gaussian process modeling. *arXiv preprint arXiv 1805*.10214. https://doi.org/10.48550/arXiv.1805.10214

Roloff, G., DeJong, R. and *Nolin, M.C.*, 1998: Crop yield, soil temperature and sensitivity of EPIC under central-eastern Canadian conditions. *Canadian Journal of Soil Science 78*, 431–439. https://doi.org/10.4141/S97-087

Sándor R. and *Fodor N.*, 2012: Simulation of Soil Temperature Dynamics with Models Using Different Concepts. *Sci. World J. 2012*, Article ID 590287. https://doi.org/10.1100/2012/590287

Santos, H., Vasconcellos, R., Pauli, B., Pires, R., Pereira, E., Tirelli, G., and *Pinho, R.*, 2019: Effect of Soil Temperature in the Emergence of Maize Seeds. *J. Agricult. Sci. 11*, 479–484. http://dx.doi.org/10.5539/jas.v11n1p479

Simunek, J., Van Genuchten, M.T., and *Sejna, M.*, 2008: Development and applications of the HYDRUS and STANMOD software packages and related codes. *Vadose Zone J. 7*, 587–600. http://dx.doi.org/10.2136/vzj2007.0077

Stone, P.J., Sorensen, I.B., and *Jamieson, P.D.*, 1998: Soil temperature affects growth and development of maize. *Proc. Agronomy Soc. N.Z 28*, 7–8.

Stone, P.J., Sorensen, I.B. and *Jamieson, P.D.*, 1999: Effect of soil temperature on phenology, canopy development, biomass and yield of maize in a cool-temperate climate. *Field Crops Res. 63*, 169–178. https://doi.org/10.1016/S0378-4290(99)00033-7

Streda T., Vahala O., and *Stredova H.*, 2013: Prediction of Adult Western Corn Rootworm (*Diabrotica virgifera virgifera* LeConte) Emergence. *Plant Protect. Sci. 49*, 89–97. https://doi.org/10.17221/28/2012-pps

Tsimba, R., Edmeades, G.O., Millner, J.P. and *Kemp, P.D.*, 2013: The effect of planting date on maize: Phenology, thermal time durations and growth rates in a cool temperate climate. *Field Crops Research 150*, 145–155. https://doi.org/10.1016/j.fcr.2013.05.021

Usowicz, B., Kossowski, J., and *Baranowski, P.*, 1996: Spatial variability of soil thermal properties in cultivated fields. *Soil Till. Res. 39*, 85–100. https://doi.org/10.1016/S0167-1987(96)01038-0

WMO World Meteorological Organization., 2012: Guide to Agricultural Meteorological Practices. WMO-No.134.

WMO World Meteorological Organization., 2018: Guide to Instruments and Methods of Observation. Volume I. Measurement of Meteorological Variables. WMO-No.8.

Xia Z., Zhang G., Zhang S., Wang Q., Fu Y., and *Lu H.*, 2021: Efficacy of Root Zone Temperature Increase in Root and Shoot Development and Hormone Changes in Different Maize Genotypes. *Agriculture 11*, 477. https://doi.org/10.3390/agriculture11060477

Zaknic-Catovic, A. and *Gough, W.A.*, 2022: Diurnal Extrema Timing - A New Climatological Parameter? *Climate 10*, https://doi.org/10.3390/cli10010005

Zheng, D., Hunt Jr., E.R., and *Running, S.W.*, 1993: A daily soil temperature model based on air temperature and precipitation for continental applications. *Climate Res. 2*, 183–191.

DOI:10.28974/idojaras.2024.1.4

IDŐJÁRÁS

Quarterly Journal of the HungaroMet Hungarian Meteorological Service
Vol. 128, No. 1, January – March, 2024, pp. 59–75

Assessment and efficiency of CMIP6 models in simulation and prediction of climatic parameters of precipitation and temperature in the Samalghan basin, Iran

Zahra Zeraatkar[1], **Ali Shahidi**[2,*], and **Hadi Memarian**[3]

[1] *Department of Water Science Engineering*
University of Birjand, Birjand, Iran

[2] *Department of Water Science Engineering*
University of Birjand, Birjand, Iran

[3]*Department of Watershed Management*
Faculty of Natural Resources and Environment
University of Birjand, Birjand, Iran

**Corresponding Author e-mail: ashahidi@birjand.ac.ir*

(Manuscript received in final form December 12, 2022)

Abstract— In the present study, four global climate models MRI-ESM2-0, IPSL-CM6A-LR, CanESM5, and GFDL-ESM4 from the set of CMIP6 models are assessed to select the best model and determine the effects of climate change on temperature and precipitation parameters under three shared socioeconomic pathway scenarios (SSP1-2.6, SSP2-4.5, and SSP5-8.5) for the base period (1988–2017) and a future period (2020–2049) in the Samalghan basin. Statistical measures such as mean absolute error, root mean square error, mean bias error are applied to test the models, and the correlation coefficient is used to compare the results of the historical period of the models with the observational data of the selected stations. Taking the obtained results into account, the global climatic model IPSL-CM6A-LR is chosen to study the trend of temperature and precipitation changes in the future period under scenarios. The results of this study indicate an increasing trend of the average annual precipitation in the desied period compared to the base period for the SSP1-2.6 and SSP2-4.5 scenarios at all stations. Also, it increases in the SSP5-8.5 scenario for all stations except Besh Ghardash, Hesegah and Darkesh stations. The predictions of temperature show an increase in the minimum and maximum temperature values under all scenarios compared to the base period.

Key-words: climate change, CMIP6, SSP senarios, Samalghan basin

1. Introduction

The growth of industrial societies and increasing use of fossil fuels in recent years have led to an increase in the greenhouse gases, global warming, and melting of polar glaciers (IPCC, 2013). Climate change is one of the major threats of the 21st century. Long-term change in global average annual temperature indicates that global warming has significant effects on terrestrial ecosystems. They have lasting impacts on hydrological, agricultural, and drought cycles (*Dai*, 2011). Therefore, the assessment of the average temperature changes at the regional level as well as understanding how this parameter and its related indicators such as heat stress change at different time scales are important to implement informed decisions on economic development and climate action plans (CAP). The phenomenon of global warming is occurring according to numerous conducted studies of climate researchers around the world. Various climatic parameters such as temperature and precipitation are significantly changing in different parts of the world (*Azari et al.*, 2016). Climate change is a well-documented phenomenon that is characterized by changes in climate patterns and is likely to persist (*de Oliveira et al.*, 2019). These changes, as mentioned, can have significant impacts on climatic parameters, and ultimately these changes can affect other components of a system, such as water and soil resources. This issue, therefore, highlights the importance of assessing the trend of changes in parameters such as temperature and precipitation to make well-educated management decisions for the future. One of the major sources for studying the future climate is mainly the output of atmospheric circulation models. These models are widely used to monitor and predict past and future climate changes (*He et al.*, 2019) and assess regional risk (*Khan et al*., 2020), and they can be downscaled by climate-regional techniques and models for a specific area. The output data of the Coupled Model Intercomparison Project Phase 6 (CMIP6) have recently been released (*Eyring et al.*, 2016). Previous models (e.g., CMIP3 and CMIP5) have been extensively evaluated and applied in several studies (*Maxino et al*., 2008; *McAfee et al*., 2011; *Rupp et al*., 2013; *Jiang et al.*, 2015; *Bozkurt et al.*, 2018; *Almagro et al*., 2020).

The results of precipitation evaluation of previous models have indicated that the GCM outputs may significantly overestimate or underestimate the observed precipitation in different seasons (*Johnson et al*., 2011; *Gouda et al*., 2018; *Liu et al*., 2014). Several researchers (*Jia et al*., 2019; *Li et al*., 2013; *Su et al.*, 2013) analyzed a couple of CMIP5 models and obtained the same result regarding the overestimation of precipitation. *Jia et al* (2019) evaluated 33 atmospheric circulation models from the fifth report series at the Tibetan Plateau, and found that all models overestimate the precipitation, especially in spring and summer.

Also, the performance of the models may also be significantly affected by the topographic features (*Ashiq et al*., 2010). For instance, *Lv et al*. (2020) revealed that CMIP5 model simulations overestimate and underestimate precipitation in northern and southern China, respectively.

The output of the Coupled Model Intercomparison Project Phase 6 (CMIP6) are a new phase of climate models. Indeed, these models are GCMs, which have been using new scenarios (SSPs) since 2015, with a new set of concentration, emission specifications, and land cover scenarios (*Gidden et al*., 2019) to simulate the future climate of the Earth. In this phase, the combination of greenhouse gas forcing and socioeconomic trajectories has been employed for the scenarios (*Riahi et al.*, 2017). The results of recent regional evaluation studies have shown that CMIP6 models have improved and perform better than the previous models (*Rivera* and *Arnould*, 2020; *Gusain et al*., 2020). The objectives of this study are as follows:

(i) Investigating the future changes in temperature and precipitation in the Samalghan basin located in North Khorasan province by using CMIP6 models.

(ii) Evaluating the impact of climate change on these variables in three emission scenarios SSP1-2.6, SSP2-4.5, and SSP5-8.5.

The prediction of precipitation and temperature changes in future gives a proper understanding of the status of water resources in this basin and the effects of climate change on these resources in the future. Moreover, the right decisions can be made in this basin for optimal management of water resources according to these changes.

2. Material and methods

2.1. Study area

The Samalghan basin is located in the Atrak catchment in North Khorasan province with an area of 1120 km^2. This basin includes 321 km^2 mountainous area, and the rest are plains and aquifers. Its geographical coordinates are 37°24'– 37°29' E and 56°37'– 56°59' N. The highest and lowest points from the sea level are 2511 and 511 m, respectively. The geographical location of the Samalghan basin in the Atrak catchment area in North Khorasan province is shown in *Fig. 1*.

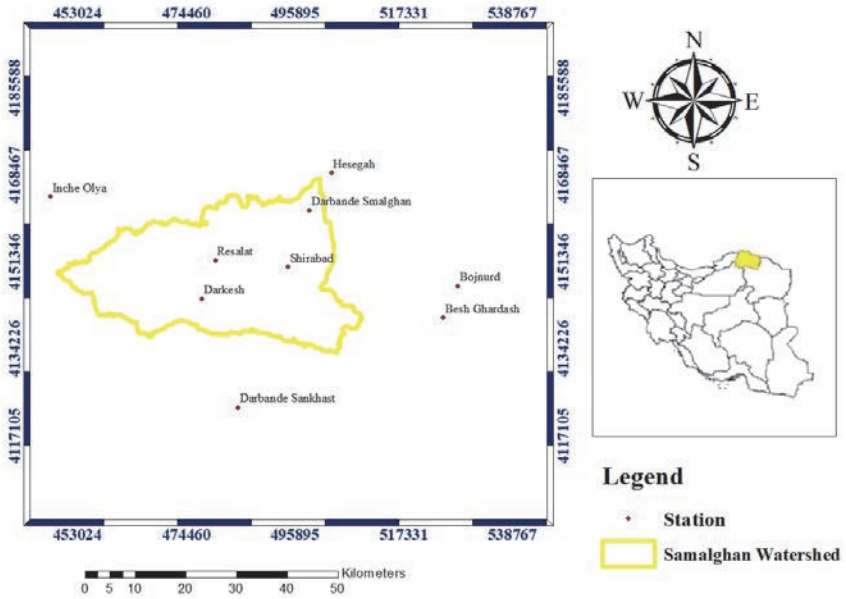

Fig. 1. Geographical location and meteorological stations of the study area.

2.2. Method

In the present study, daily data are gathered from nine stations including eight precipitation and evaporation stations (Darkesh, Shirabad, Inche Olya, Darbande Samalghan, Besh Ghardash, Darbande Sankhast, Hesegah, and Resalat) and one synoptic station (Bojnourd) during the statistical period 1988–2017. *Fig. 1* shows the location of the studied stations. The existing models and conducted research on the climate of the region are assessed to determine the trend of climate change (*Yazdandoost et al*., 2021). After a comprehensive assessment, four global climatic models including MRI-ESM2-0, IPSL-CM6A-LR, CanESM5, and GFDL-ESM4 were selected from the set of CMIP6 models. Their specifications are presented in *Table 1*. Then, historical temperature and precipitation data of these models for the base period of 30 years (1988–2017) were prepared to test the accuracy of these models for the study area. For this purpose, the average monthly values of 30-year data of the models are compared with the average monthly values of observational data. Mean absolute error (*MAE*), root mean square error (*RMSE*), mean bias error (*MBE*), and correlation coefficient (r) are applied for comparative analysis. These statistics are computed using Eqs. (1) to (4).

$$MAE = \frac{\sum_{i=1}^{n}|O_i - P_i|}{n}, \quad (1)$$

$$RMSE = \sqrt{\frac{\sum_{i=1}^{n}(O_i - P_i)^2}{n}}, \quad (2)$$

$$MBE = \frac{\sum_{i=1}^{n} O_i - P_i}{n}, \quad (3)$$

$$r = \frac{\sum_{i=1}^{n}(O_i - \bar{O})(P_i - \bar{P})}{\sqrt{\sum_{i=1}^{n}(O_i - \bar{O})^2 \sum_{i=1}^{n}(P_i - \bar{P})^2}}, \quad (4)$$

where O_i represents the observational data values, P_i represents the predicted values by the model, i and n represent the month, and the number of months, respectively.

Table 1. List of the four CMIP6 models, utilized in the present study

Model	Institute	Country	Horizontal resolution	
			Longtitude	Latitude
CanESM5	Canadian Centre for Climate Modeling and Analysis	Canada	2.81°	2.81°
GFDL-ESM4	NOAA Geophysical Fluid Dynamics Laboratory	USA	1.25°	1°
IPSL-CM6A-LR	Institute Pierre Simon Laplace	France	2.5°	1.25°
MRI-ESM2-0	Meteorological Research Institute	Japan	1.125°	1.125°

The shared socioeconomic pathways (SSPs) scenarios are parts of a new framework for global change to provide integrated analyses of climate impacts, vulnerabilities, and adaptation policies (*Frame et al*., 2018). These scenarios enable the users organize assessments of the challenges associated with adaptation policies and possible future adjustment (*Riahi et al*., 2017). The SSP scenarios are defined based on the five fundamental approaches of sustainable development, regional competition, inequality, growth in fossil fuels, and development based on intermediate policies (*O'Neill et al*., 2017; *Rogelj et al.*, 2018; *Estoque et al.*, 2020). These scenarios were placed in 5 categories which are known as SSP1 to SSP5. The assumptions of SSP1 include sustainable consumption, low population growth, increased energy efficiency, faster replacement of renewable energies, and more global cooperation. SSP2 assumptions represent intermediate

conditions, where the socioeconomic development is in sync with the usual conditions. The world of SSP5 is an advanced yet fossil-fueled world, where energy-intensive lifestyles are used.

The SSP1-2.6, SSP2-4.5, and SSP5-8.5 scenarios were selected from the available scenarios for two reasons:

1. Optimistic, intermediate, and pessimistic scenarios are used in the context of climate change vulnerabilities and their subsequent responses (*Warnatzsch* and *Reay*, 2019).
2. Scenario assumptions of SSP1-2.6 are very close to RCP2.6, SSP2-4.5 to RCP4.5, and SSP5-8.5 to RCP8.5, which comparison is possible with CMIP5 studies based on the results of this model.

2.3. Downscaling

Having large-scale computational cells is the main limitations of using the output of atmosphere-ocean general circulation models (AOGCM) as these cells are incompatible with hydrological models in terms of temporal and spatial accuracy. There are various methods to increase the temporal and spatial accuracy of the output of these models, which are termed downscaling. In the present study, the proportional downscaling method has been used to eliminate this limitation. In this method, monthly ratios are usually obtained for historical data series. Therefore, climate change scenarios are first created for temperature and precipitation. Then, the values of "difference" for temperature (Eq.(5)) and "ratio" for precipitation (Eq.(6)) are computed for the long-term average values of each month in the next period 2020–2049 to determine the climate change scenario in each model. The base simulation period is determined by the same model (base period 1988–2017) for each cell of the computational network (*Jones* and *Hulme*, 1996).

$$\Delta T_{\mathrm{i}} = \left(\bar{T}_{GCM,FUT,i} - \bar{T}_{GCM,base,i}\right), \tag{5}$$

$$\Delta P_i = \left(\bar{P}_{GCM,FUT,i} \Big/ \bar{P}_{GCM,base,i}\right), \tag{6}$$

which ΔT_i and ΔP_i indicate the climate change scenario associated with temperature and precipitation, respectively, for the long-term average values of 30 years per month, and $\bar{T}_{GCM,FUT,i}$ denotes the 30-year average of temperature simulated by AOGCM in the future period for each month, $\bar{T}_{GCM,base,i}$ is the 30-year average temperature simulated by AOGCM in the same period as the observational period for each month. Similarly, precipitation follows the same equation and definition of indices. After determining the climate change scenarios, the change factor method is used to apply proportional downscaling of

the data (*Tabor* and *Williams*, 2010; *Minville et al*., 2008). In the change factor method, the climate change scenarios are added to the observational values to determine the time series of the climate scenario in the future.

3. Results and discussion

3.1. Performance assessment of global climate models

To evaluate the performance of global climate models of MRI-ESM2-0, IPSL-CM6A-LR, CanESM5, and GFDL-ESM4 in generating temperature and precipitation data, the historical data series of these models are monthly compared with observational data of the base period for selected stations in the basin, and then statistical measures are determined. The results obtained from the performance of the models at these nine stations are presented in *Tables 2* and *3*. In general, the results obtained from the statistical measures indicate a relatively good performance of these models in the study area. Selecting the optimal models is based on their performance in the basin, therefore, the global climate model of the IPSL-CM6A-LR is used to assess the trend of temperature and precipitation changes in the future period under scenarios SSP1-2.6, SSP2-4.5, and SSP5-8.5 according to results.

Table 2. Values of the statistical measures in the base period for the precipitation variable at the selected stations

Station	Model	*MAE*	*RMSE*	*MBE*	*r*
Inche Olya	MRI-ESM2-0	0.57	0.66	-0.48	0.89
	IPSL-CM6A-LR	0.34	0.43	-0.27	0.94
	CanESM5	0.47	0.54	0.47	0.86
	GFDL-ESM4	0.61	0.73	-0.42	0.84
Resalat	MRI-ESM2-0	0.42	0.48	-0.32	0.91
	IPSL-CM6A-LR	0.20	0.24	-0.11	0.96
	CanESM5	0.63	0.75	0.63	0.82
	GFDL-ESM4	0.57	0.65	-0.26	0.75
Besh Ghardash	MRI-ESM2-0	0.58	0.65	-0.49	0.90
	IPSL-CM6A-LR	0.35	0.41	-0.27	0.94
	CanESM5	0.46	0.56	0.46	0.75
	GFDL-ESM4	0.64	0.79	-0.42	0.70
Bojnourd Synoptic	MRI-ESM2-0	0.59	0.69	-0.56	0.93
	IPSL-CM6A-LR	0.36	0.45	-0.34	0.95
	CanESM5	0.39	0.50	0.39	0.78
	GFDL-ESM4	0.66	0.81	-0.49	0.74

Table 2. Continued

Station	Model	*MAE*	*RMSE*	*MBE*	*r*
Hesegah	MRI-ESM2-0	0.38	0.46	-0.25	0.86
	IPSL-CM6A-LR	0.20	0.26	-0.03	0.92
	CanESM5	0.71	0.84	0.71	0.81
	GFDL-ESM4	0.48	0.56	-0.18	0.82
Darbande Samalghan	MRI-ESM2-0	0.48	0.54	-0.38	0.90
	IPSL-CM6A-LR	0.25	0.31	-0.16	0.95
	CanESM5	0.58	0.68	0.58	0.79
	GFDL-ESM4	0.56	0.68	-0.31	0.77
Darbande Sankhast	MRI-ESM2-0	0.61	0.72	-0.59	0.88
	IPSL-CM6A-LR	0.39	0.46	-0.37	0.95
	CanESM5	0.38	0.50	0.36	0.81
	GFDL-ESM4	0.63	0.81	-0.52	0.75
Shirabad	MRI-ESM2-0	0.31	0.37	-0.19	0.93
	IPSL-CM6A-LR	0.16	0.18	0.02	0.97
	CanESM5	0.76	0.89	0.76	0.83
	GFDL-ESM4	0.51	0.58	-0.13	0.78
Darkesh	MRI-ESM2-0	0.31	0.34	0.05	0.89
	IPSL-CM6A-LR	0.27	0.35	0.27	0.95
	CanESM5	1.00	1.19	1.00	0.80
	GFDL-ESM4	0.50	0.60	0.12	0.75

Table 3. Values of the statistical measures in the base period for the minimum and maximum temperature variables

	Station	Model	*MAE*	*RMSE*	*MBE*	*r*
Minimum temperature	Resalat	MRI-ESM2-0	3.09	3.79	-3.09	0.99
		IPSL-CM6A-LR	1.79	2.34	-1.49	0.99
		CanESM5	5.27	5.86	-1.36	0.77
		GFDL-ESM4	4.25	4.94	-2.79	0.84
	Bojnourd Synoptic	MRI-ESM2-0	2.69	3.12	-2.69	0.99
		IPSL-CM6A-LR	1.68	1.92	-1.09	0.99
		CanESM5	5.08	5.57	-0.96	0.79
		GFDL-ESM4	4.22	4.73	-2.40	0.85

Table 3. Continued

	Station	Model	*MAE*	*RMSE*	*MBE*	*r*
Maximum temperature	Resalat	MRI-ESM2-0	5.31	5.54	5.31	0.99
		IPSL-CM6A-LR	3.84	4.28	1.50	0.99
		CanESM5	8.62	10.19	-5.96	0.73
		GFDL-ESM4	5.15	5.65	-0.21	0.83
	Bojnourd Synoptic	MRI-ESM2-0	3.42	5.57	-1.12	0.99
		IPSL-CM6A-LR	2.71	3.15	2.69	0.99
		CanESM5	9.82	11.74	-8.58	0.75
		GFDL-ESM4	5.56	6.16	-2.83	0.84

3.2. The assessment of LARS-WG6 model performance in simulating basin temperature and precipitation

LARS-WG model is one of the most famous models for generating random weather data and is used to generate minimum and maximum temperature, precipitation and radiation daily in current and future climate conditions. This model is more useful than other programs due to the repetition of calculations, less need for input data and simplicity and efficiency (Kilsby et al., 2007). Also, despite the less complexity of the simulation process and input and output data, has a high ability to predict climate change (Semenov and Stratonovich, 2010). Additionally, the Long Ashton Research Station Weather Generator, version 6 (LARS-WG6) was used to dawnscale the precipitation and temperature data of the AOGCMs. Data generation by the LARS-WG6 model is performed in three stages: calibration, assessment, and meteorological data generation for the future period. The results of statistical analysis and assessment criteria show that the highest error is associated with precipitation modeling. However, the minimum and maximum temperature parameters have been modeled with high accuracy, which is consistent with the results of other studies (*Hassan et al*., 2014; *Huang et al.,* 2011; *Liu et al.*, 2011). Also, the results indicate that the LARS-WG6 model is perfectly capable of simulating the parameters of precipitation, minimum temperature and maximum temperature of the studied stations (*Table 4*). Validation of the efficiency of the model by root mean square error, mean absolute error, mean bias error, and correlation coefficient between observational data and model output in the period (1988–2017) displays that the LARS-WG6 model has the ability to model the climate of the previous period of the study basin.

Table 4. The assessment results of LARS-WG6 downscaling model in 1988–2017

Parameter	Station	*MAE*	*RMSE*	*MBE*	*r*
Precipitation	Inche Olya	2.51	3.18	-0.32	0.96
	Resalat	2.00	2.86	1.09	0.99
	Besh Ghardash	1.68	2.37	0.61	0.98
	Bojnourd Synoptic	2.09	2.52	-1.79	1.00
	Hesegah	2.29	2.89	-1.63	0.99
	Darbande Samalghan	2.97	3.63	0.63	0.97
	Darbande Sankhast	2.21	3.03	0.30	0.98
	Shirabad	2.81	3.51	-2.73	0.99
	Darkesh	2.72	3.51	-0.48	0.99
Minimum temperature	Resalat	0.17	0.19	0.00	1.00
	Bojnourd Synoptic	0.16	0.20	0.13	1.00
Maximum temperature	Resalat	0.21	0.26	0.03	1.00
	Bojnourd Synoptic	0.17	0.22	0.03	1.00

3.3. Basin climate change assessment for the 2020–2049 period in the LARS-WG6 model

The global climatic model IPSL-CM6A-LR under three scenarios (the optimistic SSP1-2.6, intermediate SSP2-4.5, and very pessimistic SSP5-8.5) are considered for the period 2020–2049 in the study area based on the results obtained from the performance of global climatic models in simulating climatic variables of temperature and precipitation on the Samalghan basin and the studied stations. Taking the capability of the LARS-WG6 model into account, the output of the IPSL-CM6A-LR model is downscaled under the relevant scenarios, and the desired parameters are predicted and compared with their values in the period 1988–2017 (*Figs. 2* and *3*).

The assessment of *Fig. 2* indicates that the average monthly precipitation in all scenarios increases in July, August, and September in all stations, whereas different results are observed in other months under these scenarios. The average annual precipitation in the desired period is increased compared to the base period for the two scenarios SSP1-2.6 and SSP2-4.5. Nonetheless, the average annual precipitation has a decreasing trend in the SSP5-8.5 scenario for Besh Ghardash, Hesegah, and Darakesh, and it has an increasing trend in other stations (*Table 5*). It should be noted, that the increase in precipitation under the three scenarios SSP1-2.6, SSP2-4.5, and SSP5-8.5 in the future period in some stations can be mainly due to different assumptions. In general, the increase in temperature in mountainous areas is mainly due to the rise in humidity which increases precipitation, therefore, it is likely that increased temperature has caused precipitation growth in the mountainous area of the Samalghan basin.

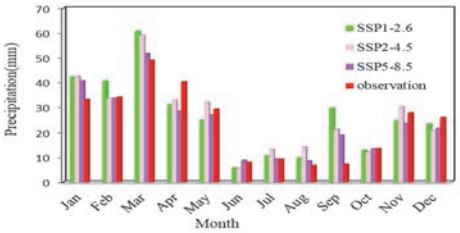

Darbande Samalghan station

Besh Ghardash station

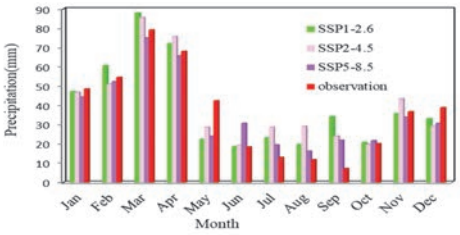

Darkesh station

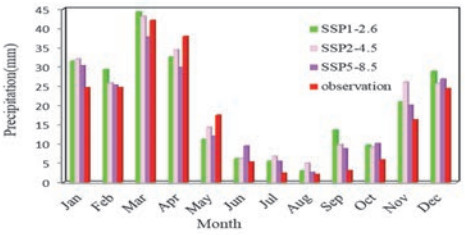

Darbande Sankhast station

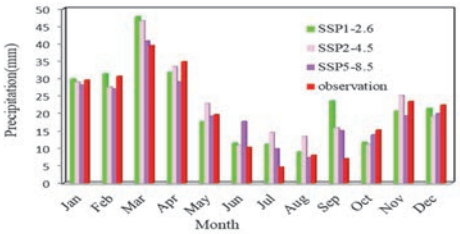

Inche Olya station

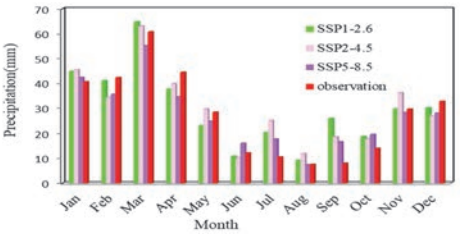

Hesegah station

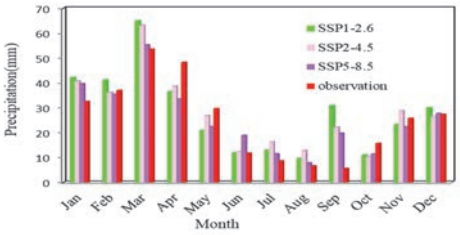

Resalat station

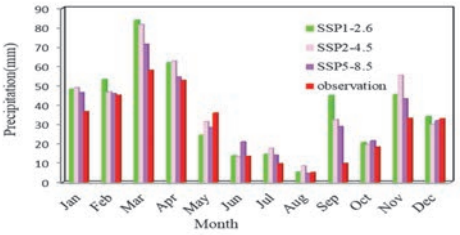

Shirabad station

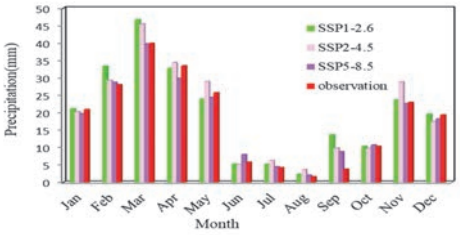

Bojnourd Synoptic station

Fig. 2. Changes in the average monthly precipitation under different scenarios for the 2020–2049 and the base period

Table 5. The average annual precipitation in the base period and under different scenarios (mm)

Station / Scenario	SSP1-2.6	SSP2-4.5	SSP5-8.5	Historical
Inche Olya	266.97	269.35	246.56	244.52
Resalat	335.38	335.38	306.29	241.98
Besh Ghardash	253.73	257.81	236.65	241.98
Bojnourd Synoptic	237.62	239.62	217.20	215.89
Hesegah	356.29	359.73	326.54	331.24
Darbande Samalghan	316.59	317.90	285.96	284.12
Darbande Sankhast	236.36	238.46	218.27	205.79
Shirabad	449.56	448.01	411.18	349.85
Darkesh	474.97	481.76	435.89	438.45

The average minimum temperature of different months in the period 2020–2049 has increased compared to the base period, however, this increase varies in different months and under various scenarios (*Fig. 3*). The highest increase occurs in September under the SSP5-8.5 scenario which are 1.69 °C and 1.62 °C for Bojnourd synoptic and Resalat stations, respectively. The lowest increase values, however, are 0.07 °C and 0.23 °C in February under the SSP1-2.6 and SSP2-4.5 scenarios, respectively for Resalat station. The lowest increase values are 0° C and 0.33 °C in January under two scenarios (SSP1-2.6 and SSP2-4.5), respectively, for Bojnourd synoptic station (*Table 6*). During this period, the values of average annual minimum temperature are 6.91 °C and 6.51 °C for Bojnourd synoptic and Resalat stations in the base period, respectively. Moreover, the average annual minimum temperature in Resalat station will increase by 10%, 12%, and 13% under scenarios SSP1-2.6, SSP2-4.5, and SSP5-8.5, respectively. Similarly, the average annual minimum temperature in Bojnourd synoptic station will increase by 11%, 14%, and 15% under scenarios SSP1-2.6, SSP2-4.5, and SSP5-8.5, respectively.

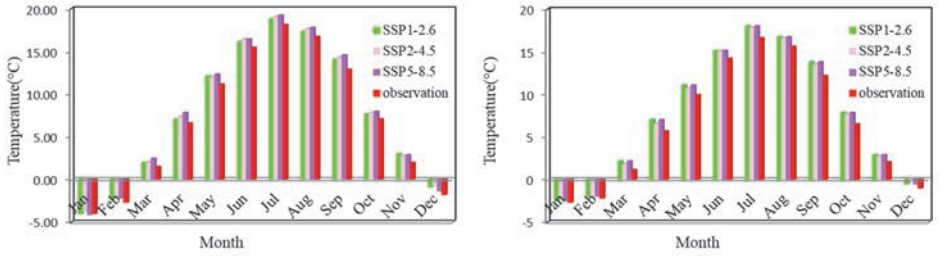

Bojnourd synoptic station Resalat station

Fig. 3. The average minimum temperature changes under different scenarios (2020-2049) and the base period.

Table 6. The minimum monthly temperature changes in the period 2020–2049 compared to the base period in °C

Station	Scenario	Jan	Feb	Mar	Apr	May	Jun	Jul	Aug	Sep	Oct	Nov	Dec
Bojnourd Synoptic	SSP1-2.6	0.00	0.38	0.50	0.47	0.94	0.69	0.70	0.62	1.18	0.60	1.04	0.91
	SSP2-4.5	0.33	0.52	0.61	0.79	0.86	1.02	0.99	0.95	1.45	0.77	0.81	1.10
	SSP5-8.5	0.00	0.52	0.98	1.22	1.17	0.96	1.12	1.06	1.69	0.87	0.91	0.43
Resalat	SSP1-2.6	0.30	0.07	0.57	0.61	0.90	0.65	0.96	0.68	1.10	1.05	0.99	0.93
	SSP2-4.5	0.64	0.23	0.69	0.92	0.82	0.96	1.26	1.01	1.37	1.22	0.75	1.13
	SSP5-8.5	0.19	0.22	1.03	1.35	1.13	0.93	1.39	1.12	1.62	1.32	0.86	0.48

The value of the average maximum temperature has increased in different months under all scenarios compared to the base period, however, this increase varies in different months and under various scenarios (*Fig. 4*). The highest increase values are 2.38 °C and 1.86 °C for Bojnourd synoptic and Resalat stations, respectively, in April, under the SSP5-8.5 scenario. The lowest increase values, however, are 0.14 °C in January under the SSP1-2.6 scenario and 0.17 °C in February under the SSP2-4.5 scenario for Resalat station. Similarly, for Bojnourd synoptic station, the lowest increase values are 0.16 °C and 0.18 °C under two scenarios SSP1-2.6 and SSP2-4.5, respectively in February (*Table 7*). In this period, the average annual maximum temperature in Bojnourd synoptic and Resalat stations are 20.03 °C and 22.65 °C in the base period, respectively**.** The average annual maximum temperature will increase 4%, 4%, and 5% under scenarios SSP1-2.6, SSP2-4.5, and SSP5-8.5, respectively, for Bojnourd synoptic station. Similarly, for Resalat station, this increase will be 3%, 4%, and 4% under scenarios SSP1-2.6, SSP2-4.5, and SSP5-8.5, respectively. The results of this study are mainly consistent with previous studies on climate change in Iran in terms of temperature variability in the future (*Soltani et al.*, 2016; *Fallah-Gholhari et al.,* 2019). The results showed that temperature data had a better correlation with observational data (compared to precipitation data), which represents that temperature has a normal probability distribution, is less variable than that of the precipitation. However, precipitation is a discrete component and can be affected by various factors. Therefore, unlike temperature, precipitation does not have a pattern of significant changes in the study area, which is consistent with the results of studies by *Almazroui et al*. (2017), *Su et al.* (2016), and *Tan et al.* (2017).

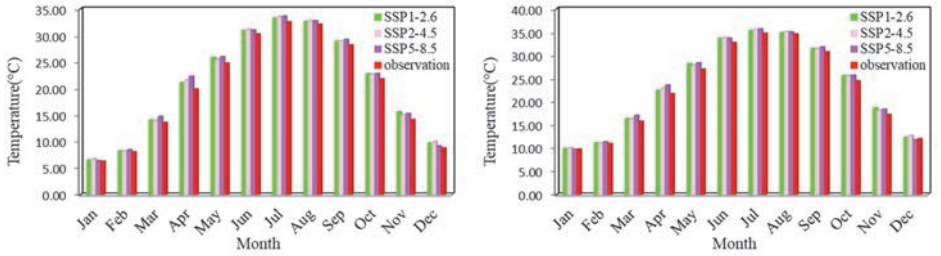

Bojnourd synoptic station Resalat station

Fig. 4. The average maximum temperature changes under different scenarios for the 2020–2049 and the base period.

Table 7. Maximum temperature changes in the period 2020–2049 compared to the base period in ° C

Station	Scenario	Jan	Feb	Mar	Apr	May	Jun	Jul	Aug	Sep	Oct	Nov	Dec
Bojnourd synoptic	SSP1-2.6	0.25	0.16	0.48	1.22	1.01	0.68	0.73	0.48	0.69	0.94	1.42	0.90
	SSP2-4.5	0.45	0.18	0.45	1.73	0.70	0.91	1.03	0.71	0.77	0.93	0.87	1.27
	SSP5-8.5	0.12	0.40	1.18	2.38	1.19	0.73	1.08	0.66	1.03	1.00	1.14	0.37
Resalat	SSP1-2.6	0.14	0.16	0.56	0.71	1.19	0.90	0.60	0.30	0.71	1.17	1.43	0.33
	SSP2-4.5	0.34	0.17	0.53	1.21	0.87	1.14	0.90	0.54	0.78	1.15	0.95	0.70
	SSP5-8.5	0.01	0.39	1.27	1.86	1.37	0.95	0.95	0.48	1.06	1.23	1.14	0

4. Conclusions

In the present study, models of the Coupled Model Intercomparison Project Phase 6 (CMIP6) are applied to assess changes in climate parameters in arid regions, which are more sensitive to climate change. Nowadays, the importance of determining the appropriate model that can make future predictions increases with the growth of research on climate change. The results showed that temperature data had a better correlation with observational data, and precipitation is a discrete component. Therefore, unlike temperature, precipitation does not have a pattern of significant changes in the study area. Precipitation will increase in the future period of 2020–2049 under three scenarios (SSP1-2.6, SSP2-4.5, and SSP5-8.5) in July, August, and September at all stations according to the results. This increase can be due to increased humidity caused by rising temperatures in the mountainous areas under the three scenarios SSP1-2.6, SSP2-4.5, and SSP5-8.5

in the future period at some stations. In general, the average precipitation will decrease as we move towards the final years of the future period in all scenarios, and this decrease occurs more in the SSP5-8.5 scenario than in the other two scenarios. Moreover, the temperature trend in the future period has increased under all scenarios compared to the base period. The highest temperature increase is in September under the SSP5-8.5 scenario, while the lowest temperature increase is in February and January under the SSP1-2.6 and SSP2-4.5 scenarios for Bojnourd synoptic and Resalat stations, respectively. Also, the highest maximum temperature increase occurs in April under the SSP5-8.5 scenario and the lowest maximum temperature increase occurs in January under the SSP1-2.6 scenario and in February under the SSP2-4.5 scenario for Resalat station. Similarly, it occurs in February under the SSP1-2.6 and SSP2-4.5 scenarios for Bojnourd synoptic station. The results of this study recommend considering temperature variability in water resources management, especially in agricultural section to avoid the possible negative effects of climate change in the region.

References

Almazroui, M., Islam, M.N., Saeed, F., Alkhalaf, A.K., and *Dambul, R.,* 2017: Assessing the robustness and uncertainties of projected changes in temperature and precipitation in AR5 Global Climate Models over the Arabian Peninsula, *Atmosph. Res. 194*, 202–213. https://doi.org/10.1016/j.atmosres.2017.05.005

Almagro, A., Oliveira, P.T.S., Rosolem, R., Hagemann, S., and *Nobre, C.A.,* 2020: Performance evaluation of Eta/HadGEM2-ES and Eta/MIROC5 precipitation simulations over Brazil. *Atmosph. Res. 244*, 105053. https://doi.org/10.1016/j.atmosres.2020.105053

Ashiq, M.W., Zhao, C., Ni, J., and *Akhtar, M.,* 2010: GIS-based high-resolution spatial interpolation of precipitation in mountain–plain areas of Upper Pakistan for regional climate change impact studies. Theoretical and *Appl. Climatol. 99*, 239–253. https://doi.org/10.1007/s00704-009-0140-y

Azari, M., Moradi, H.R., Saghafian, B., and *Faramarzi, M.,* 2016: Climate change impacts on streamflow and sediment yield in the North of Iran. *Hydrol. Sci. J. 61*, 123–133. https://doi.org/10.1080/02626667.2014.967695

Bozkurt, D., Rojas, M., Boisier, J.P., and *Valdivieso, J.,* 2018: Projected hydroclimate changes over Andean basins in central Chile from downscaled CMIP5 models under the low and high emission scenarios. *Climatic Change, 150*, 131–147. https://doi.org/10.1007/s10584-018-2246-7

Dai, A., 2011: Drought under global warming: a review. Wiley Interdisciplinary Reviews: *Climate Change, 2*, 45–65. https://doi.org/10.1002/wcc.81

de Oliveira, V.A., de Mello, C.R., Beskow, S., Viola, M.R., and *Srinivasan, R.,* 2019: Modeling the effects of climate change on hydrology and sediment load in a headwater basin in the Brazilian Cerrado biome. *Ecol. Engineer. 133*, 20–31.

Estoque, R.C., Ooba, M., Togawa, T., and *Hijioka, Y.,* 2020: Projected land-use changes in the Shared Socioeconomic Pathways: Insights and implications. *Ambio, 49*, 1972–1981. https://doi.org/10.1007/s13280-020-01338-4

Eyring, V., Bony, S., Meehl, G. A., Senior, C. A., Stevens, B., Stouffer, R. J., and Taylor, K. E. 2016. Overview of the Coupled Model Intercomparison Project Phase 6 (CMIP6) experimental design and organization. *Geoscientific Model Development, 9, 1937-1958*

Fallah-Ghalhari, G., Shakeri, F., and *Dadashi-Roudbari, A.,* 2019: Impacts of climate changes on the maximum and minimum temperature in Iran. *Theor. Appl. Climat. 138*, 1539–1562. https://doi.org/10.1007/s00704-019-02906-9

Frame, B., Lawrence, J., Ausseil, A.G., Reisinger, A., and *Daigneault, A.,* 2018: Adapting global shared socio-economic pathways for national and local scenarios. *Climate Risk Manage. 21*, 39–51. https://doi.org/10.1016/j.crm.2018.05.001

Gidden, M.J., Riahi, K., Smith, S.J., Fujimori, S., Luderer, G., Kriegler, E., ... and *Takahashi, K.,* 2019: Global emissions pathways under different socioeconomic scenarios for use in CMIP6: a dataset of harmonized emissions trajectories through the end of the century. *Geosci. Model Develop 12*, 1443–1475. https://doi.org/10.5194/gmd-12-1443-2019

Gouda, K.C., Nahak, S., and *Goswami, P.,* 2018: Evaluation of a GCM in seasonal forecasting of extreme rainfall events over continental India. *Weather Climate Extrem. 21*, 10–16. https://doi.org/10.1016/j.wace.2018.05.001

Gusain, A., Ghosh, S., and *Karmakar, S.,* 2020: Added value of CMIP6 over CMIP5 models in simulating Indian summer monsoon rainfall. *Atmosph. Res. 232*, 104680. https://doi.org/10.1016/j.atmosres.2019.104680.

Hassan, Z., Shamsudin, S., and *Harun, S.,* 2014: Application of SDSM and LARS-WG for simulating and downscaling of rainfall and temperature. *Theor. Appl. Climatol. 116*, 243–257. https://doi.org/10.1007/s00704-013-0951-8

Huang, J., Zhang, J., Zhang, Z., Xu, C., Wang, B., and *Yao, J.,* 2011: Estimation of future precipitation change in the Yangtze River basin by using statistical downscaling method. *Stoch. Environ. Res. Risk Assess. 25*, 781–792. https://doi.org/10.1007/s00477-010-0441-9

He, S., Yang, J., Bao, Q., Wang, L., and *Wang, B.,* 2019: Fidelity of the observational/reanalysis datasets and global climate models in representation of extreme precipitation in East China. *J.Climate 32*, 195–212. https://doi.org/10.1175/JCLI-D-18-0104.1

IPCC, 2013: Climate Change. 2013. The Physical Science Basis. Contribution of Working Group I to the Fifth Assessment Report of the Intergovernmental Panel on Climate Change. Cambridge University Press, Cambridge and New York.

Jones, P.D. and *Hulme, M.,* 1996: Calculating regional climatic times series for temperature and precipitation: methods and illustrations. *Int. J. Climatology 16*, 361–377. https://doi.org/10.1002/(SICI)1097-0088(199604)16:4<361::AID-JOC53>3.0.CO;2-F

Jia, K., Ruan, Y., Yang, Y., and *Zhang, C.,* 2019: Assessing the performance of CMIP5 global climate models for simulating future precipitation change in the Tibetan Plateau. *Water, 11*, 1771. https://doi.org/10.3390/w11091771.

Jiang, Z., Li, W., Xu, J., and *Li, L.,* 2015: Extreme precipitation indices over China in CMIP5 models. Part I: Model evaluation. *Journal of Climate, 28*, 8603-8619. https://doi.org/10.1175/JCLI-D-15-0099.1

Johnson, F., Westra, S., Sharma, A., and *Pitman, A.J.,* 2011: An assessment of GCM skill in simulating persistence across multiple time scales. *J. of Climate, 24*, 3609–3623. https://doi.org/10.1175/2011JCLI3732.1

Khan, A. J., Koch, M., and *Tahir, A. A.,* 2020: Impacts of climate change on the water availability, seasonality and extremes in the Upper Indus Basin (UIB). *Sustainability 12*, 1283. https://doi.org/10.3390/su12041283

Kilsby C. G. Jones P. D. Burton A. Ford A. C. Fowler H. J. Harpham C. James P. Smith A. and Wilby R. L. 2007. A daily weather generator for use in climate change studies. *Environmental Modelling & Software*. 22, 1705-1719.

Liu, Z., Mehran, A., Phillips, T.J., and *AghaKouchak, A.,* 2014: Seasonal and regional biases in CMIP5 precipitation simulations. *Climate Res. 60*, 35–50. https://doi.org/10.3354/cr01221

Liu, L., Liu, Z., Ren, X., Fischer, T., and *Xu, Y.,* 2011: Hydrological impacts of climate change in the Yellow River Basin for the 21st century using hydrological model and statistical downscaling model. *Quaternary Int. 244*, 211–220. https://doi. org/10.1016/j.quaint.2010.12.001

Lv, Y., Guo, J., Yim, S.H.L., Yun, Y., Yin, J., Liu, L., ... and *Chen, D.,* 2020: Towards understanding multi-model precipitation predictions from CMIP5 based on China hourly merged precipitation analysis data. *Atmosph. Res. 231*, 104671. https://doi.org/10.1016/j.atmosres.2019.104671

Li, Z., Wei, Z.G., Lv, S.H., Han, B., Ao, Y.H., and *Chen, H.,* 2013: Verifications of surface air temperature and precipitation from CMIP5 model in Northern Hemisphere and Qinghai-Xizang Plateau. *Plateau Meteorol. 32*, 921.

Maxino, C.C., McAvaney, B.J., Pitman, A.J., and *Perkins, S.E.*, 2008: Ranking the AR4 climate models over the Murray-Darling Basin using simulated maximum temperature, minimum temperature and precipitation. *Int. J. Climatol. 28*, 1097–1112. https://doi.org/10.1002/joc.1612

McAfee, S.A., Russell, J.L., and *Goodman, P.J.*, 2011: Evaluating IPCC AR4 cool-season precipitation simulations and projections for impacts assessment over North America. *Climate Dynam. 37*, 2271–2287. https://doi.org/10.1007/s00382-011-1136-8

Minville, M., Brissette, F., and *Leconte, R.*, 2008: Uncertainty of the impact of climate change on the hydrology of a nordic watershed. *J. Hydrology 358*, 70–83. https://doi.org/10.1016/j.jhydrol.2008.05.033

O'Neill, B.C., Kriegler, E., Ebi, K.L., Kemp-Benedict, E., Riahi, K., Rothman, D.S., ... and *Solecki, W.*, 2017: The roads ahead: Narratives for shared socioeconomic pathways describing world futures in the 21st century. *Global Environmental Change 42*, 169–180. https://doi.org/10.1016/j.gloenvcha.2015.01.004

Rivera, J.A., and *Arnould, G.*, 2020: Evaluation of the ability of CMIP6 models to simulate precipitation over Southwestern South America: Climatic features and long-term trends (1901–2014). *Atmosph. Res. 241*, 104953. https://doi.org/10.1016/j.atmosres.2020.104953

Riahi, K., Van Vuuren, D.P., Kriegler, E., Edmonds, J., O'neill, B.C., Fujimori, S., ... and *Tavoni, M.*, 2017: The shared socioeconomic pathways and their energy, land use, and greenhouse gas emissions implications: an overview. *Glob. Environ. Change 42*, 153–168. https://doi.org/10.1016/j.gloenvcha.2016.05.009

Rupp, D.E., Abatzoglou, J.T., Hegewisch, K.C., and Mote, *P.W.*, 2013: Evaluation of CMIP5 20th century climate simulations for the Pacific Northwest USA. *J. Geophys Res: Atmospheres 118*, 10,884–10,906. https://doi.org/10.1002/jgrd.50843

Rogelj, J., Popp, A., Calvin, K.V., Luderer, G., Emmerling, J., Gernaat, D., ... and *Tavoni, M.*, 2018: Scenarios towards limiting global mean temperature increase below 1.5 C. *Nat. Climate Change 8*, 325–332. https://doi.org/10.1038/s41558-018-0091-3

Semenov M. A. and Stratonovitch P. 2010. Use of multi-model ensembles from global climate models for assessment of climate change impacts. *Climate research*. 41, 1- 14.

Soltani, M., Laux, P., Kunstmann, H., Stan, K., Sohrabi, M.M., Molanejad, M., ... and *Martin, M.V.*, 2016: Assessment of climate variations in temperature and precipitation extreme events over Iran. *Theor. Appl. Climatol. 126*, 775–795. https://doi.org/10.1007/s00704-015-1609-5

Su, F., Duan, X., Chen, D., Hao, Z., and *Cuo, L.*, 2013: Evaluation of the global climate models in the CMIP5 over the Tibetan Plateau. *J. Climate 26*, 3187–3208. https://doi.org/10.1175/JCLI-D-12-00321.1

Su, B., Huang, J., Gemmer, M., Jian, D., Tao, H., Jiang, T., and *Zhao, C.*, 2016: Statistical downscaling of CMIP5 multi-model ensemble for projected changes of climate in the Indus River Basin. *Atmos. Res 178–179*, 138–149. https://doi.org/10.1016/j.atmosres.2016.03.023

Tan, M.L., Ibrahim, A.L., Yusop, Z., Chua, V.P., and *Chan, N.W.*, 2017: Climate change impacts under CMIP5 RCP scenarios on water resources of the Kelantan River Basin, Malaysia. *Atmos. Res 189*, 1–10. https://doi.org/10.1016/j.atmosres.2017.01.008

Tabor, K., and *Willams, J.*, 2010: Global downscaled climate projections for assessing the conservation impacts of climate change. *Ecol. Appl. 20*, 554–565. https://doi.org/10.1890/09-0173.1

Warnatzsch, E.A. and *Reay, D.S.*, 2019: Temperature and precipitation change in Malawi: Evaluation of CORDEX-Africa climate simulations for climate change impact assessments and adaptation planning. *Sci. Total Environ. 654*, 378–392. https://doi.org/10.1016/j.scitotenv.2018.11.098

Yazdandoost, F., Moradian, S., Izadi, A., and *Aghakouchak, A.*, 2021: Evaluation of CMIP6 precipitation simulations across different climatic zones: Uncertainty and model intercomparison. *Atmosph. Res. 250*, 105369. https://doi.org/10.1016/j.atmosres.2020.105369

DOI:10.28974/idojaras.2024.1.5

IDŐJÁRÁS

Quarterly Journal of the HungaroMet Hungarian Meteorological Service
Vol. 128, No. 1, January – March, 2024, pp. 75–98

Characteristics of annual and seasonal precipitation in North Macedonia: change analysis and correlation with the North Atlantic Oscillation (1951–2010)

Ivan Radevski[1,*], **Julia Hall** [2], **Svemir Gorin**[1], **Ana M. Petrović**[3]
Arse Kuzmanoski [1], **Emilija Manevska**[1], and **Pece Ristevski** [4]

[1]*Ss. Cyril and Methodius University*
Faculty of Natural Sciences and Mathematics, Institute of Geography,
Arhimedova 3, 1000 Skopje, North Macedonia

[2]*Interdisciplinary Centre for Complex System Science*
Meteoceanics Lisbon, Portugal

[3]*Geographical Institute "Jovan Cvijic" of the Serbian Academy of Sciences and Arts*
Djure Jakšića 9, 11000 Belgrade, Serbia

[4]*Military Academy "General Mihajlo Apostolski"*
Vasko Karangelevski bb, Skopje, North Macedonia

**Corresponding Author e-mail: radevskiivan3@gmail.com*

(Manuscript received in final form February 8, 2023)

Abstract— Studying the spatiotemporal precipitation characteristics in North Macedonia (1951–2010) is important as no spatially concurrent precipitation changes across the Balkan Peninsula have been identified. North Macedonia lies at the intersection between Mediterranean and continental climate zones and an improved understanding might help to better understand the regional precipitation patterns. The analysis shows a spatially consistent, high inter-annual variability, which makes trend detection difficult. Statistically significant decreasing trends were only found in seasonal precipitation at three stations. Changes in all other precipitation series were non-significant. Trends in winter, spring, and at annual scale are generally decreasing, whereas in summer are increasing. To better understand possible mechanisms behind the observed variability and change, correlations with the North Atlantic Ocsillation (NAO) were assessed. Significant and regionally concurrent correlations were detected. A strong correlation of the previous winter NAO-index with spring precipitation was found, which is valuable information for anticipatory water resources management in the region.

Key-words: precipitation; trends; Mann-Kendall; Sen's slope; NAO-index; North Macedonia

1. Introduction

Worldwide studies suggest a human influence on climate and hence on precipitation, which demands more advanced monitoring in the situation given the inherent climate uncertainty (*Alley et al*., 2003). Precipitation is the primary input to our water resource system, and detailed knowledge is required for water resources management. Additionally, precipitation or the lack of it and its changes require detailed analysis, as precipitation is one of the main drivers of the extreme hydrological events such as floods and droughts in Europe (e.g., *Blöschl et al.*, 2017, 2019).

There are already numerous studies about the precipitation characteristics and their changes for almost all countries in Europe, but so far, a detailed assessment for the country North Macedonia is still missing. Hence this work aims to analyze and characterize changes in annual and seasonal precipitation time series in North Macedonia. To set the regional context for the current study, below the recent scientific findings of precipitation changes for the neighboring region of North Macedonia, located on the Balkan Peninsula, are briefly summarized below.

In Bulgaria, located in the east of North Macedonia, the observed seasonal precipitation trends for summer and spring are positive. This is opposite to the negative trends found for autumn and winter over the period 1901–2001, that was used for most of the investigated stations. No conclusive country-wide change signal was reported for total annual precipitation. The mountainous region of Rila and Pirin, the highest Balkan's mountains located close the North Macedonian border, are showing non-significant downward annual trends for annual precipitation sums (significance level of α=0.05) (*Alexandrov et al*., 2004).

A study in Romania shows mixed results for annual precipitation trends over 1961–2013, based on a significance level of α=0.1. The three mountainous stations in the South Carpathians show a significant decreasing annual trend (*Marin et al*., 2014).

A hydroclimatological change analysis in Greece (south of the study region) shows that most (15 out of 17) stations exhibit a non-significant downward trend in annual precipitation (only two are statistically significant), and 5 out of 17 gauges show a statistically significant decreasing trend in winter, for the period 1961-2006 (for both α=0.1 and α=0.05) (*Mavromatis* and *Stathis*, 2011).

The annual precipitation totals in Serbia (north of the study area) have a strong spatial gradient, and generally decrease from west to east (*Milovanović et al*., 2017a). Research on temporal variability in annual precipitation in Serbia for 1961–2010 indicates a small number of gauges with a statistically significant trend (α=0.05) between -5 and +5 mm/decade. The majority of stations in western Serbia shows positive trends in annual precipitation, whereas the trends in eastern Serbia are predominately mainly negative. Overall, there is an increasing trend in annual precipitation in Serbia, although not statistically significant (α=0.05)

(*Milovanović et al*., 2017b). The obtained decreases in annual precipitation near the border with North Macedonia and Bulgaria (southern Serbia) are moderate (mostly < -15 mm/decade).

The precipitation change pattern is different for seasonal and monthly changes in Serbia. Decreasing trends in monthly precipitation sums for February (-1.5 to -3 mm/decade) and June (-1.5 to -8 mm/decade) were detected in the southern part, near the border with North Macedonia (*Milovanović et al*., 2017b). Additionally, a previous study investigating the seasonal changes in precipitation in Serbia (1961–2009), detected significant decreasing precipitation trends in winter (5/63 stations) and spring (7/63 stations), no statistically significant changes in summer, and significant increasing trends in autumn (9/63 gauges) (α=0.025). Overall, the study concluded that the majority of the precipitation changes are statistically non-significant (*Luković et al*., 2014).

In Bosnia and Herzegovina (located northwest of the study region), *Popov et al.* (2019) identified three regions with different precipitation regimes using data over the period 1961−1990. A spatial gradient with a general decrease in annual precipitation from south and west towards the northeast was also determined. The same study also showed that two of the identified sub-regions, northwest, northeast, east, and the central part of country, have statistically non-significant positive decadal trends in annual precipitation for the period 1961–2018 (2.8 – 6 mm/decade), without information about the significance level. The third region located in the south of the country is characterized by strong negative precipitation trends (-40 mm/decade).

In Croatia (also located northwest of the study region at the coast of the Adriatic Sea), different seasonal precipitation changes were detected over the period 1961–2010. A significant decreasing trend can be found in annual precipitation totals in the mountainous region and in several other regions in summer, with α=0.05 (*Gajić-Čapka et al*., 2015). The decreasing annual precipitation trends in the Mediterranean and the central part of Croatia are statistically non-significant. In the mountainous region, in summer, the trends are statistically significantly decreasing (-21 mm/decade), which is opposite to the continental region in the Pannonian Plain, which shows a statistically non-significant (α=0.05) increasing precipitation trend (*Gajić-Čapka et al.,* 2015).

Summarizing the above-mentioned studies (but not limited to these), it can be concluded that the mountainous parts of the Balkan Peninsula are affected by predominately decreasing precipitation trends. This is particularly true for western Bulgaria close to the Macedonian border for autumn, winter, and annual precipitation, Slovenia (winter), mountainous part of Croatia (summer), Southern Serbia (annual), and Greece (winter and annual).

Overall, the reviewed literature does not allow to discern any spatially consistent precipitation changes across the bordering regions of North Macedonia. This could be due to the fact that the Balkan Peninsula contains different climatic regions and are heavily modified by elevation and relief features.

North Macedonia lies at the intersection between the Mediterranean and continental climate regions. A detailed analysis of the precipitation characteristics and the observed changes in the region will fill the spatial gap and might help to provide a better context for the observed regional changes on the Balkan Peninsula.

Additionally, to improve the understanding of the drivers of observed precipitation characteristics, precipitation amounts have been correlated with the North Atlantic Oscillation (NAO) in several studies for the European region. For example, close to the current study region, North Macedonia, past research has shown that precipitation sums (over the period 1900-2010) and NAO-index have a negative correlation in Italy and Greece, as well as most of the Mediterranean gauges (some of which were statistically significant at α=0.05) (*Philandras et al.*, 2011). In Romania, winter precipitation shows a strong negative correlation with the NAO-index (*Bojariu* and *Paliu*, 2001). A study about the Vojvodina province in northern Serbia shows a statistically significant negative correlation between precipitation totals and the NAO-index for winter (α=0.1), and statistically significant negative correlations (α=0.05) for annual and autumn precipitation sums with their respective NAO-index (*Tošić et al.*, 2014). A broader study of the main Mediterranean mountains (Atlas, Pyrenees, Alps, Apennines, Dinaric Alps, Balkan Mountains, Taurus) by *López-Moreno et al.*, (2011) found a general statistically significant negative correlation (α=0.05) between the winter NAO-index and winter precipitation for the Balkan Mountains, to which the mountains of North Macedonia belong to. However, for the entire country of North Macedonia, a detailed investigation is still missing. Such an analysis might provide better context of the observed larger regional precipitation variability and changes.

1.1. Study area

The country of North Macedonia is located in Southeastern Europe (*Fig. 1*), more specifically in the central part of the Balkan Peninsula and covers an area of 25 713 km^2. The relief is predominantly hilly-mountainous, and the elevation ranges from 54 m a.s.l. (in the Gevgelija Basin) to 2 764 m a.s.l. (peak Golem Korab on the Korab Mountain), with almost 30 plains and only a few less mountain ridges.

With the help of the geographical latitude and relief conditions, North Macedonia can be roughly divided into a larger region with mainly continental climate and 2 smaller regions with sub-Mediterranean climate located in the south-eastern and southwestern parts of the country. Additionally, areas with elevation above 1 100 m a.s.l. with high mountainous climate can be found embedded in the larger region with continental climate. Generally, the climate transitions from continental to high mountainous with increasing elevation around 1 100 m a.s.l. (*Kendrovski* and *Spasenovska*, 2011; *Radevski* et al., 2018).

The larger region where the continental climate can be felt encompasses the Prespa Plain, Kichevo Plain, Kumanovo Plain, Pijanec and Slavishte Plains, Polog Plain, and the country largest Pelagonia Plain. In general, the precipitation regime of the continental climate region has two distinct precipitation maxima in late spring and middle autumn, and several minima, with a primary minimum in summer and a secondary minimum and less pronounced winter minimum. The smaller sub-Mediterranean region covers the Gevgelija-Valandovo, Dojran Plain, and Ohrid-Struga, where the Mediterranean climate influences are strongly felt. During some years, the Mediterranean influences are suppressed in certain areas, but there are also years when the Mediterranean influences are even felt along the valley of the river Vardar to Skopje, along the valley of the river Strumica in the Strumica-Radovish Plain.

The regions with mountain climate can be found in the country's highest mountains, the Shar, Korab, Jablanica, Baba, and Jakupica Mountains, which are all located in the western part of North Macedonia in parallel with the plains. In the interior of the mountain region with elevations over 2 250 meters, an alpine climate can be detected. The regions with mountain and alpine climate have the highest precipitation, generally higher than 1 000 mm/year on the highest country mountains (*Zikov*, 1995). The mountainous regions experience a precipitation maximum in winter and a precipitation minimum in late summer.

Generally, with increasing elevation the climate regimes found at the precipitation gauging stations change from sub-Mediterranean over a continental to high mountainous climate with the exception of Ohrid (station 11), located in the southwestern part of the country at the large Ohrid Lake, where even at a higher elevation a sub-Mediterranean climate can be detected.

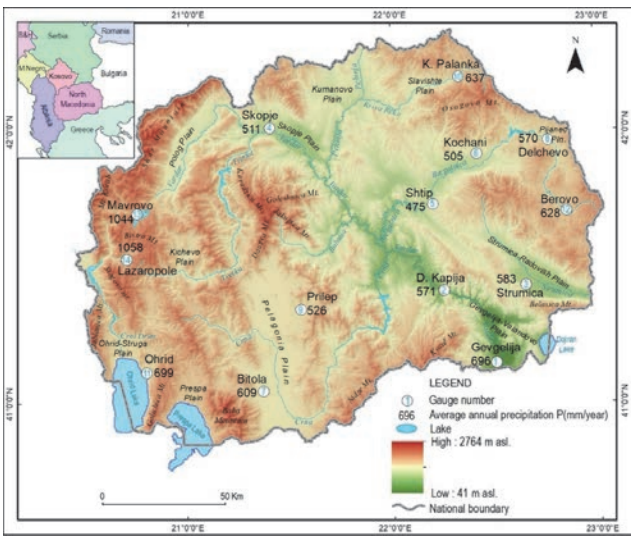

Fig. 1. Topographical map of North Macedonia showing the location of the precipitation gauges and their annual average precipitation for 1951–2010.

1.2. Data

For North Macedonia, instrumental precipitation measurements are only available for a few gauges for the first part of the 20th century. Systematic precipitation measurements are only available for a higher number of gauges after the Second World War. For the analysis, 14 precipitation gauges belonging to the Northern Macedonian National Hydrometeorological Service have been chosen that have complete data for 60 years (1951–2010). The stations were selected to ensure the best geographical coverage possible, whilst also aiming to include measurements from precipitation gauges located at a variety of different elevations and good coverage of the three climates regions in North Macedonia described above (see also *Table 1*).

Table 1. Characteristics of precipitation gauges ordered by increasing elevation

No.	Gauge	Latitude	Longitude	Elevation [m.a.s.l.]	Climatic Region
1	Gevgelija	41°09’00”	22°30’00”	59	sub-Mediterranean
2	D. Kapija	41°25’00”	22°15’00”	125	sub-Mediterranean
3	Strumica	41°26’00”	22°39’00”	224	sub-Mediterranean
4	Skopje	42°01’00”	21°24’00”	302	continental
5	Shtip	41°44’00”	22°12’00”	322	continental
6	Kochani	41°55’00”	22°25’00”	345	continental
7	Bitola	41°03’00”	21°22’00”	586	continental
8	Delchevo	41°58’00”	22°46’00”	630	continental
9	Prilep	41°21’00”	21°33’00”	661	continental
10	K. Palanka	42°12’00”	22°20’00”	691	continental
11	Ohrid	41°07’00”	20°48’00”	760	sub-Mediterranean
12	Berovo	41°42’16”	22°51’13”	827	continental
13	Mavrovo	41°42’00”	20°45’00”	1 240	high mountainous
14	Lazaropole	41°32’00”	20°42’00”	1 332	high mountainous

The 14 precipitation gauges used in this study are located at elevations ranging from 59 m a.s.l. to 1 332 m a.s.l. These gauging stations are shown in *Fig. 1*, and their main characteristics are listed in *Table 1*. The set of precipitation stations analyzed includes 2 mountain stations (>1 000 m a.s.l.) located on Bistra Mountain in the western part of the country (Lazaropole and Mavrovo).

2. Methodology

2.1. Analysed precipitation variables

As this study aims to identify precipitation characteristics and long-term changes, five different types of precipitation sum (PS) series were analyzed as indicated in *Table 2*. Note that for the calculation of the winter the precipitation totals, precipitation from the December of the previous year was used, hence the winter precipitation sum (WiPS) series start only a year later (1952).

Table 2. Analysed precipitation variables, their abbreviations as used in this study and analysis period with months and years.

Precipitation series	**Abbreviation**	**Period**
Annual precipitation sum	APS	1951–2010
Winter precipitation sum	WiPS	XII-II (1952–2010)
Spring precipitation sum	SpPS	III-V (1951–2010)
Summer precipitation sum	SuPS	VI-VIII (1951–2010)
Autumn precipitation sum	AuPS	IX-XI (1951–2010)

2.2. Test for autocorrelation

Before analyzing the changes in precipitation records, all the time series were checked for autocorrelation, as the existence of either positive or negative autocorrelation in a time series can confound the change detection, and hence it can lead to a false detection of a statistically significant trend where none may exist (*Yue* 2002). To evaluate the presence of a lag-1 serial correlation, the correlation structure of each series used in the trend assessment was assessed using plots of autocorrelation function (*ACF*) at a 10% significance level (α=0.1) (not shown).

2.3. Temporal change

Following the well-established methodology used in previous published studies on precipitation, trends were analyzed, using the widely used non-parametric Mann-Kendall (MK) trend test (*Mann*, 1945; *Kendall*, 1975) to detect monotonic trends and to assess their significance. For the basic significance testing of the trends, a significance level (α) of 0.1 was used. Increasing and decreasing trends

were detected according to the sign +/- of the statistics *S*. Further details of the MK test can be found in the Appendix.

The trend slope β over the precipitation series is estimated with the nonparametric Theil–Sen method, which is suitable to detect a nearly linear trend in the variable *x* and is also less affected by non-normal data and outliers (*Sen*, 1968, *Hirsch et al*. 1982). The slope is computed between all pairs *i* of the variable *x*:

$$\beta_i = \frac{x_j - x_k}{j - k}, \quad (1)$$

where $j>k$, $j=2,\ldots n$, $k=1,\ldots, n-1$, and $i=1\ldots N$. For *n*-values in the precipitation series *x*, it will result in $N = n(n-1)/2$ values of β (which is the median over all the combinations of record pairs for the dataset). The Sen's slope β is presented in mm per decade, with sign + for increasing and – for decreasing trend.

2.4. Temporal variability

Knowledge on the temporal variability of a time series helps in the interpretation of the trend detection results. If there is high inter-annual variability, the signal to noise ratio in the series is large, and hence trend detection needs a long time series to allow the detection of statistically significant trends (*Wilby*, 2006; *Murphy et al.*, 2013), or a strong change signal.

Here the temporal variability of the precipitation series is statistically described using the coefficient of variation (*CV*) and, for the ease of interpretation, expressed as a percentage of the mean of the series, thereby showing the long-term variability from the mean value:

$$CV = \frac{\sigma}{\mu} * 100, \quad (2)$$

where σ is the standard deviation and μ is the mean of the record of the PS series.

To evaluate the overall temporal evolution and variability of all PS series despite their differences in absolute values, the time series were standardized and expressed as standardized precipitation sum anomalies (*SPSA*):

$$SPSA = \left(\frac{ps_I - \mu}{\sigma}\right) \quad (3)$$

where PS_i is the precipitation sum (mm) aggregated over annual or seasonal timescales for an individual year (*i*), μ is the mean of the record of the PS series, and σ is the standard deviation of the PS series.

Positive/negative values of *SPSA* indicate above/below mean precipitation sum quantities for the series. For visualization purposes, the *SPSA* series were smoothed using a centered 4-year moving average. Additionally, the changes in

resulting trends calculated in Section 3.2 and their statistical significance were evaluated by varying the start and end date of the time series. If the trends changed considerably, such changes are reported in Section 3.

2.5. Atmospheric influences

As previous studies outside the study region have already shown a possible influence of the North Atlantic Oscillation (NAO) on streamflow (*Birsan*, 2015), possible connections between the different precipitation sums within the study region and the station-based North Atlantic Oscillation Index (NAOI) by Hurrell (*Hurrell*, 2018) are explored over the period 1951–2010 using the Spearman correlation. For both, annual, and seasonal analyses (for both PS and NAOI series), calculations are based on the seasonal mean values calculated from the monthly time series, which are used as input for the correlation analysis.

The NAOI has been defined as the difference in the sea level pressure between the tropical Azores high and polar Icelandic low. The index is expressed with two different phases to represent the changes in the atmospheric situations. Positive NAO phases are characterized by higher pressure differences between the Azores high and Icelandic low and are, on average, responsible for drier conditions in Southern Europe. Negative phases characterize a weaker pressure gradient between the Azores and Iceland. During this phase, storm tracks move southwards towards the Mediterranean Sea, leading to higher precipitation levels in Southern Europe (*Wallace* and *Gutzler*, 1981).

Additionally, lagged correlations (i.e., non-matching seasons) between the different seasonal NAOI and different seasonal precipitation were performed. After initial testing (not shown), the results of the correlations of the winter NAOI and the following seasonal precipitations are assessed here in detail, as winter is the season with the strongest and most clearly defined NAO patterns.

3. Results

3.1. Seasonal precipitation variations

For most of the stations (Table 3) there is no strong seasonal variations in the annual precipitation totals with no season contributions of more than 32% to the annual budget. Spring season has generally an average contribution to the annual precipitation totals with around 25%. Summer is the driest season, with the lowest contribution percentage of ~13%, except in the northeastern part of the country, where an above average precipitation contribution can be measured. The wettest season on average is autumn, with exception of the mountainous areas that have the highest seasonal precipitation contribution in winter.

Table 3. Mean annual and mean seasonal precipitation totals in mm. Seasonal values are expressed as % of the annual values. Underlined/bold letters indicate the driest/wettest seasons, respectively.

N	Gauge	Annual total	Winter %	Spring %	Summer %	Autumn %
1	Gevgelija	696	28.75	25.44	16.10	**29.61**
2	D. Kapija	571	**29.92**	26.25	17.50	26.42
3	Strumica	583	25.72	25.72	20.24	**28.30**
4	Skopje	511	25.42	25.22	22.88	**26.40**
5	Shtip	475	21.04	26.93	23.77	**28.19**
6	Kochani	505	22.17	26.13	24.94	**26.72**
7	Bitola	609	28.26	25.63	17.58	**28.42**
8	Delchevo	570	20.36	26.16	**26.68**	**26.68**
9	Prilep	526	23.59	26.64	20.93	**28.92**
10	K. Palanka	637	20.87	**27.30**	26.83	25.11
11	Ohrid	699	30.91	24.33	13.16	**31.62**
12	Berovo	628	22.46	**26.28**	25.96	25.32
13	Mavrovo	1044	**31.32**	25.19	14.08	29.50
14	Lazaropole	1058	**30.62**	24.57	14.46	30.34

3.2. Temporal change and variability

The characteristics of the annual precipitation sum (APS) and the results of the trend analysis are shown in *Table 4*. All trends obtained are non-significant (at a significance level of α=0.1). Non-significant trends range from -17.4 mm/decade at Mavrovo to + 9.8 mm/decade at Lazaropole, which are the precipitation gauges having the highest mean APS (mean > 1000 mm/year) and being located at the highest elevation in this study. However, when examining the total change observed in relation to the mean APS, the gauge at Prilep experiences the strongest negative change (-16.15%) and Mavrovo exhibits only the second strongest negative trend (-10.02% of the mean), whereas Lazaropole still shows the strongest positive trend (+5.57%). Overall, negative trends are dominating (79%).

Only 3 gauges showed a statistically significant (α=0.1) positive lag-1 serial correlation (Prilep, Ohrid, and Mavrovo), no statistically significant trends were detected in the APS series. The temporal precipitation variability found at all gauges can be classified as moderate and ranges from 17.9% at (K. Palanka) to 23.2% at Mavrovo. In the case of stronger interannual variability, the detection of statistically significant trends could be confounded.

Table 4. Annual precipitation sum series characteristics and trend analysis: mean annual sum, Theil–Sen slope β in mm/decade, total change in % of mean, and variability as in % of mean.

N	Gauge	Mean annual sum	β [mm/decade]	% Change	% Variability
1	Gevgelija	696	-6.6	-5.7	22.2
2	D. Kapija	571	-7.2	-7.57	21.6
3	Strumica	583	-8.1	-8.32	21.5
4	Skopje	511	0.4	0.41	20.9
5	Shtip	475	-6.5	-8.17	22.1
6	Kochani	505	-5.4	-6.36	19.0
7	Bitola	609	5.2	5.14	20.5
8	Delchevo	570	0	-0.02	21.3
9	Prilep	526	**-14.1**	**-16.15**	**22.8**
10	K. Palanka	637	-2.7	-2.57	17.9
11	Ohrid	699	-0.7	-0.64	21.4
12	Berovo	628	-8.6	-8.18	18.4
13	Mavrovo	1044	**-17.4**	**-10.02**	**23.2**
14	Lazaropole	1058	**9.8**	**5.57**	**18.5**

None of the seasonal PS series analyzed displayed a statistically significant (α=0.1) positive lag-1 serial correlation, hence one can assume that the detected trends are not confounded by autocorrelation.

The characteristics and possible changes in seasonal precipitation sums are listed in *Table 5*. For the WiPS, most of the trends are negative (~71%). Only the gauge at Shtip shows a statistically significant negative trend of -6.4 mm/decade or over the entire period of record a decrease of 38.91% respective to the long-term winter mean precipitation sum. This percentage change is the highest seasonal change value, as in Shtip (*Fig. 2*), the lowest winter precipitation totals are measured. Detecting such change is of importance for the region, as winter in Shtip is already the driest season, which is becoming increasingly drier. Similarly to the annual change results, Mavrovo again has the highest absolute change value (-14 mm/decade), however, the WiPS trend is not statistically significant. The positive trends in the WiPS series at a few gauges are weak and do not exceed 8.3% of the long term-mean. The interannual variability in WiPS is very high ranging from 37.5 to 55%.

Table 5. Seasonal precipitation sum characteristics and trend analysis: mean seasonal sum, Theil–Sen slope β in mm/decade, total change in % of mean, and variability as in % of mean. Trends that are statistically significant (α=0.1) are shown in bold.

N	Gauge	WiPS			SpPS			SuPS			AuPS		
		Mean sum	β	% Change	Mean sum	β	% Change	Mean sum	β	% Change	Mean sum	β	% Change
1	Gevgelija	200	-4.4	-13.27	177	-7.2	-24.52	112	0.2	1.28	206	-1.8	-5.13
2	D. Kapija	167	-0.7	-2.39	150	-2.9	-11.43	100	-0.1	-0.44	151	0.1	0.40
3	Strumica	149	0.1	0.60	150	**-4.6**	-18.30	118	3.3	16.84	165	-3.7	-13.55
4	Skopje	128	1.8	8.26	129	-4.8	-22.32	117	5.9	30.04	135	-1.5	-6.57
5	Shtip	99	**-6.4**	-38.91	128	-3.2	-14.82	113	2.7	14.54	134	-1	-4.29
6	Kochani	111	-1.7	-9.20	132	**-6.4**	-28.79	126	0.4	1.69	135	4.1	17.99
7	Bitola	172	1.2	4.15	156	1.5	5.93	107	0.2	0.89	173	3.7	12.83
8	Delchevo	116	-1.8	-9.39	149	2.0	7.97	152	1.0	3.86	152	0.6	2.27
9	Prilep	123	-6.2	-30.12	140	-3.9	-16.73	110	2.8	15.40	152	-0.5	-1.84
10	K. Palanka	132	-1.6	-7.36	174	-2.4	-8.14	171	4.3	15.15	160	4.3	16.13
11	Ohrid	216	-3.7	-10.38	170	4.4	15.42	92	1.7	11.06	221	2.6	7.00
12	Berovo	140	-3.9	-16.82	165	-3.7	-13.57	163	2.5	9.29	159	-0.8	-2.87
13	Mavrovo	326	-14	-25.83	263	-1.0	-2.30	147	-1.1	-4.52	308	-2.9	-5.63
4	Lazaropole	323	0.1	0.17	260	0.5	1.17	153	4.4	17.44	321	8.6	16.0

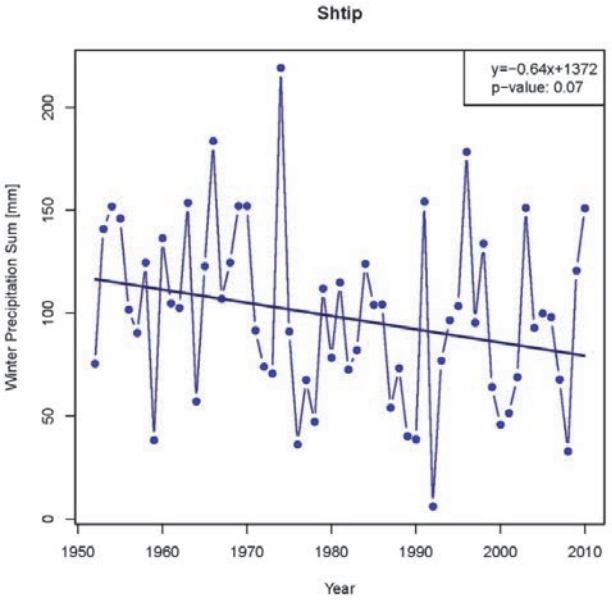

Fig. 2. WiPS series for Shtip with a statistically significant trend, Sen's slope estimate, and p-value.

In the SpPS series, two statistically significant negative trends were detected at Strumica and Kochani (*Fig. 3*). Although the two gauges do not exhibit the strongest negative trend (-4.6 and -6.4 mm/decade, respectively), which can be found at Gevgelija with -7.2 mm/decade, they show one of the highest changes relative to the long-term mean (-18.3% and -28.79% respectively). The strong decrease in Kochani is of importance, as it has the 3rd lowest spring precipitation total of the country. The non-statistically significant trends at other gauges range from -7.2 to +4.4 mm/year and from -24.52 to +15.42% of the long-term spring sum mean. Most of the trends across the country are negative (~71%) with particularly gauges that are located at lower elevation (<500 m) showing all negative trends (including the two statistically significant trends).

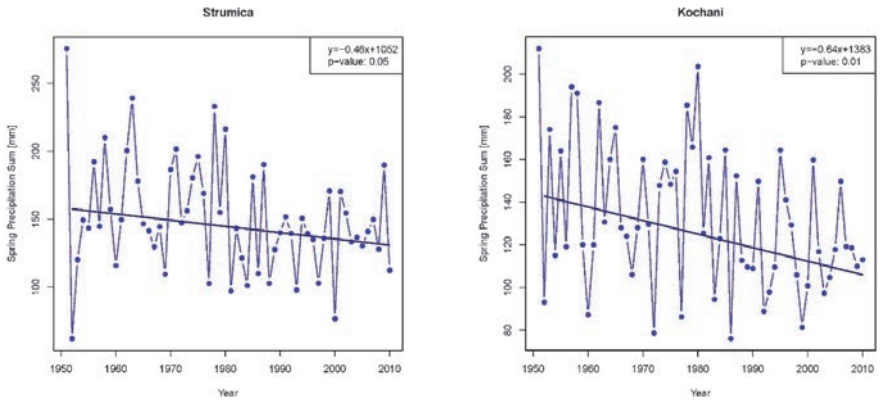

Fig. 3. SpPS series and statistically significant trends for Strumica and at Kochani with Sen's slope estimate and p-value.

In the SuPS series there are no statistically significant increasing or decreasing trends. Overall, the trends are predominately increasing (~86%), which is opposite to the WiPS and SpPS. The trends in the SuPS series range from -1.1 to +5.9 mm/year. When relating the changes to the long-term mean, the negative/positive trends have the smallest/highest percentage of change (-4.52 %, +30.04%, respectively). These results indicate, that in general there is a pattern of increasing precipitation in summer, the driest season on average, although no statistically significant trends could be detected yet. The lack of statistical significance could be partly caused by the high temporal variability found in the SuPS series (39.7 – 62.4% of the long-term mean), which is the highest found in all seasonal series.

Changes in the AuPS series are inconclusive with no statistically significant trends and half of the gauges showing increasing and the other half showing decreasing trends. However, the positive trends appear to be slightly stronger both

in terms of the absolute values and in terms of the relative changes. As the analysis of individual precipitation trends in North Macedonia showed predominately inconclusive results, the temporal evolution of the seasonal precipitation series across the country are evaluated and shown in *Fig. 4*.

The temporal evolution of the SPSA series across all series (*Fig. 4*) shows the high variability of the seasonal PS series over time, which concurs the reported statistical results and high variability of the series as listed in *Table 5*.

Additionally, from *Fig. 4*. it is also apparent that the period of record chosen has a high influence on the trends obtained (and their statistical significance), which is elaborated below (results of the detailed analysis are not shown). All examples of statistical significance refer to the significance level of α=0.1. For example, if the APS series had been analyzed until the early 2000s, statistically significant negative trends would have been detected at Gevgelija, Kapija, Strumica, Shtip, Prilep (significant until ending 2009), K. Palanka, Berovo, and Mavrovo (until 2008).

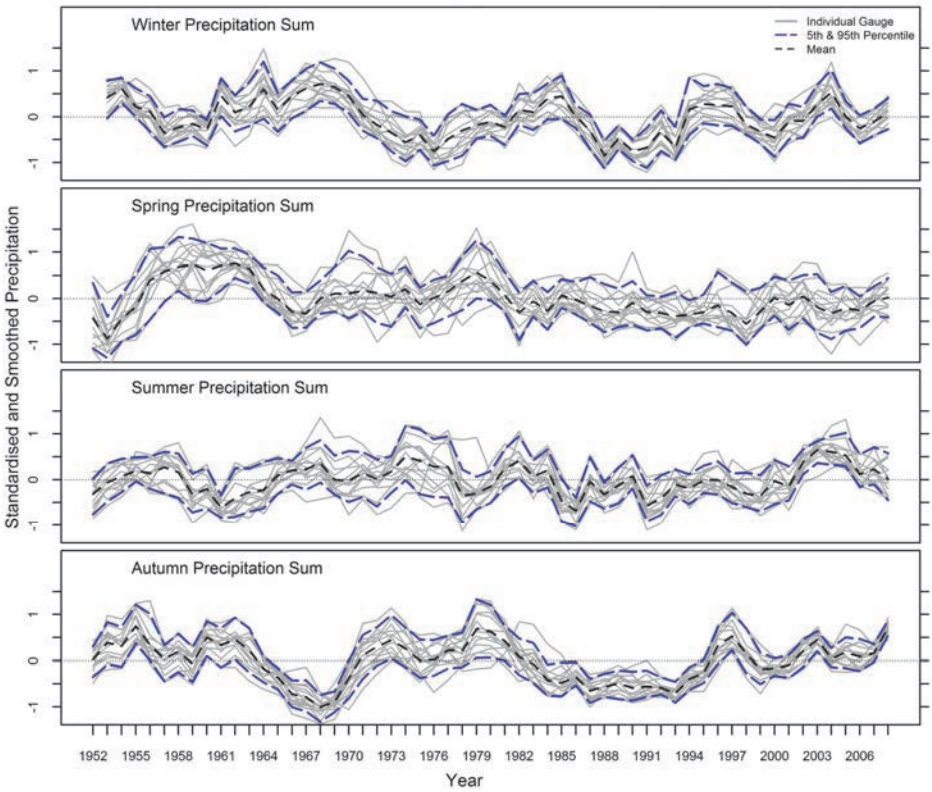

Fig. 4. Standardized and smoothed seasonal precipitation sums (SPSA). Light grey lines are the standardized and smoothed 4-year moving average series for individual gauges, blue dashed lines are the 5th and 95th percentiles of the standardized and smoothed series, and black dashed line is the average across all series.

Similar results can be obtained for the WiPS series at Prilep and Mavrovo. If the time series had been analyzed until 2009, the detected trend would have been statistically significant. The same applies to the SpPS starting 1952 at Skopje (ending 2009) and Shtip (ending 2008). If SpPS trends would had analyzed from ~1960, Gevgelija, Strumica, Skopje, Shtip, Kochani, Prilep, Berovo Marovo, and Lazaropole would have been showing statistically significant negative trends, and the analysis period would have ended in 2009 or 2010. For the SuPS series non-significant trends would have been obtained unless for few series beginning in1970 and ending around 2000 (e.g., D. Kapija, K. Palanka, and Berovo), which indicated significant negative trends for that period. Similarly, if the AuPS series had been analyzed until 1995, significant negative trends would have been found at Gevgelija, Strumica, and Mavrovo. Hence the trend results (and their statistical significance) obtained from the longest available study period, might not be representative of the shorter-term variability apparent in the data.

Furthermore, *Fig. 4* shows that (apart from a few gauges and individual years) the seasonal precipitation sums at the individual stations follow a common coherent pattern of high and low precipitations for each year and season. This indicates that there is a likely common driver behind the coherent inter-annual variability of the precipitation records.

3.3. Atmospheric influences

As discussed earlier, a possible driver of the coherent precipitation change over time could be the North Atlantic Oscillation (NAO), which in turn could cause the associated shifts in spatial and temporal precipitation patterns. For the full PS series, the relationships between the monthly NAO index (NAOI) and monthly PS series are assessed using Spearman correlations, as depicted in *Figs. 5*. and *6*. Here, negative or positive correlation between precipitation sums and NAOI series indicates a lower or higher NAOI, respectively, associated with higher precipitation values.

The correlations between the precipitation and NAOI at an annual scale are predominately negative (except for the very weak non-significant positive correlation at Bitola). Six out of the seven gauges that are located above an elevation of 600 m a.s.l. show a statistically significant negative correlation (except for Prilep, which is non-significant), with Lazaropole having the strongest Spearman's rank correlation, *rho* (*rho*=-0.114). All stations below 500 m indicate a weaker, non-significant correlation. Additionally, most of the stations with a significant negative correlation have a high mean annual PS (>620 mm) and a continental climate. The exception is Gevgelija, located in the southeast, which is the lowest lying station with a pronounced sub-Mediterranean climate.

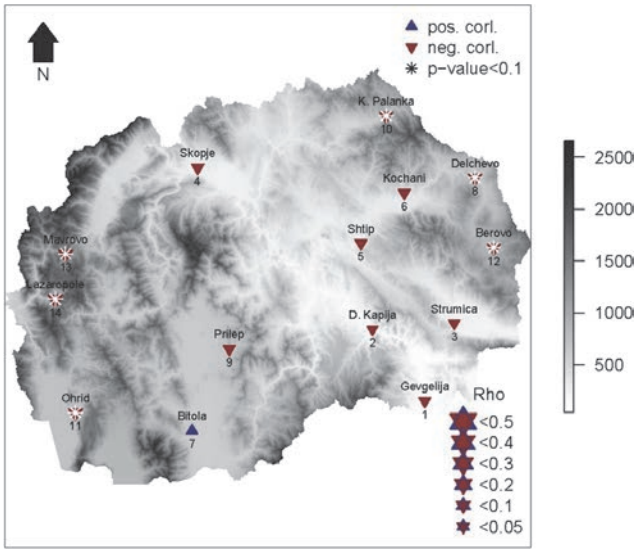

Fig. 5. Spearman's rank correlation (*rho*) between the mean of the monthly PS series and the mean of the monthly NAOI evaluated at an annual timescale. Elevation is shown in m a.s.l., blue/red color represent positive/negative correlations. Size of triangles indicates magnitude of correlations (based on upper and lower absolute correlation value), significant correlations (α=0.1) are shown by white stars.

In the seasonal correlation analysis (*Fig. 6*), the absolute correlation values are much higher than in the annual evaluation. Winter, summer, and autumn show a consistent spatial correlation pattern, having the same correlation sign countrywide. In winter and autumn, the correlations are all negative (9 and 7 gauges, respectively, are statistically significant), whereas in summer all correlations are positive (12 significant). Spring season has a more spatially distinct pattern of positive (non-significant) correlations in the central and negative correlations on the eastern and western sides of the country (3 of which are significant). As a general pattern, one can also observe that in spring, the correlations between precipitation totals and the NAO change with increasing elevation from statistically non-significant positive to significant negative correlations.

In winter, statistically significant negative correlations can be found at higher elevations. For many of these stations, winter is the season with the lowest percental precipitation (% of annual total) with exception of the stations in the western part which receive the highest amount of precipitation. In lower lying areas the correlations are non-significant. In autumn, the low-lying stations located in the centre of the country with low seasonal precipitation show a statistically significant negative correlation, although negative correlations are also found in the rest of the country.

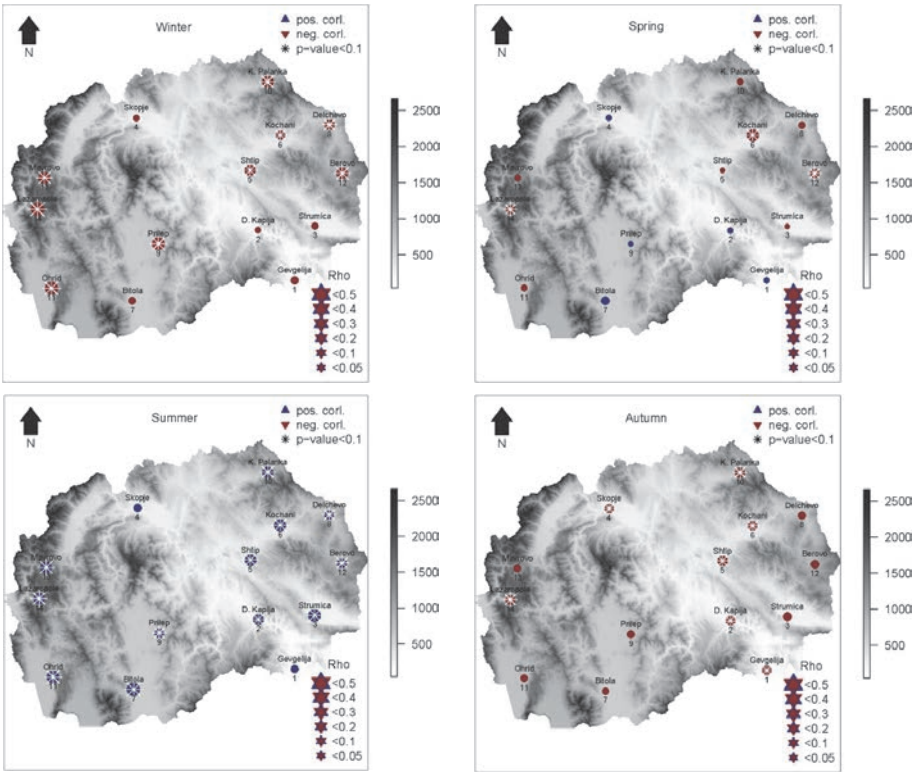

Fig. 6. Spearman's rank correlation between the mean of the monthly PS series and the mean of the monthly NAOI evaluated at a seasonal timescale. Symbols and elevation are as in *Fig. 5.*

In summer, which is generally the driest month, all correlations are positive (most of which are statistically significant). It should also be noted that at Bitola, the summer precipitation-NAOI correlation value (*rho*=0.495) is the highest obtained among all stations and seasons. Hence, the contribution of summer is strongly reflected on an annual scale leading to a positive correlation as shown in *Fig. 5*.

When performing lagged correlations, i.e., correlating the previous NAOI with the seasonal precipitations (i.e., with spring, summer and autumn), the correlation results only improve for the spring season (*Fig. 7*). Instead of having mixed spatial correlations across the study region in spring (when correlated with the same season NAOI), now spatially consistent negative correlations emerge. Also, the number of gauges showing statistically significant trend increases to 11. Overall, the strength of correlation also increases, apart from the 2 gauges (Kochani and Lazaropole) that had strong and statistically significant correlations when spring precipitation is correlated with the same season NAOI. Lazaropole (gauge located at the highest elevation) does not show a significant correlation with the NAO anymore

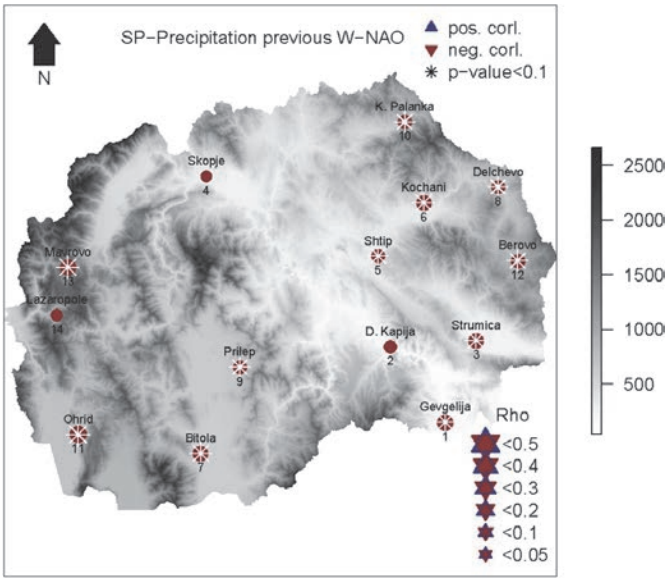

Fig. 7. Spearman's rank correlation between the mean of the monthly SpPS series and the mean of the previous monthly winter NAOI (1952–2010). Symbols and elevations are as in *Fig. 5*.

4. Discussion

The results obtained for the detailed analysis of annual and seasonal precipitation sums for the study region North Macedonia show that in the analyzed 60-year period (1951–2010), precipitation trends in North Macedonia have a spatially non-coherent pattern of predominantly significant or non-significant downward trends (except for the summer season with increasing trends) (*Tables 3* and *4*).

This outcome for North Macedonia concurs with the results of existing regional studies around the study region. This is particularly evident for the decreasing trends in annual precipitation in Croatia, Serbia, and Greece.

The study of the Mediterranean (*Philandras et al.,* 2011) shows also decreasing trend in annual precipitation sums, especially in Southern Europe. There is no spatial similarity with the other neighboring countries, especially for annual precipitation in Bulgaria and Romania, where the trend results are of mixed direction (*Marin et al*., 2014). Comparing our annual change results with those of Serbia (*Milovanović et al.,* 2017b), near the North Macedonia border, the trends are non-significantly decreasing in both countries.

The downward annual precipitation tendencies found in the southeastern moderate Mediterranean stations Gevgelija, Demir Kapija, and Strumica,

correspond to the majority of negative trends found in Greece (*Mavromatis* and *Stathis*, 2011).

This seasonal study results of North Macedonia, and a previous research of a wider region predominately have a negative trend in winter (although mostly not statistically significant), which was also noted in Romania (*Marin et al*., 2014), Bulgaria (*Alexandrov et al*., 2004), Serbia (*Luković et al.,* 2014), Dalmatia-Croatia (*Gajić-Čapka et al.*, 2015), and Greece (*Mavromatis* and *Stathis*, 2011). The spring trend results are predominantly positive in Bulgaria (*Alexandrov et al*., 2004) and Greece (*Mavromatis* and *Stathis*, 2011), negative in North Macedonia and Serbia (*Luković et al*., 2014), while predominantly positive summer trends are detected in Bulgaria (*Alexandrov et al.,* 2004) and North Macedonia, and negative trends in Croatia (*Gajić-Čapka et al.*, 2015) and Serbia (*Luković et al.*, 2014). The autumn results are miscellaneous trends in North Macedonia, positive in Serbia (*Luković et al.*, 2014), and negative in Bulgaria (*Alexandrov et al*., 2004).

Overall, the analysis of the temporal evolution of precipitation changes in North Macedonia show that there is strong inter-annual variability that has the potential to statistically influence the trend detection. Hence, one should not focus on one single time period to assess trends and their statistical significance. This strong variability could also explain why it is currently difficult to identify larger scale similarities in observed precipitation changes, when comparing with neighboring countries, as different time periods were used for the assessment. Additionally, trend signals obtained (although they are not statistically significant) should be taken into consideration, particularly if the entire country shows a spatially concurrent same sign of change, when analyzed with different start and end years.

The detailed analysis has shown that although relatively close to each other (13 km distance) and similar in mean annual and seasonal precipitation totals, the two mountainous stations (Mavrovo and Lazaropole) exhibit a very different precipitation change patterns. The only significant difference between these two mountain gauges is the direction in which the slope of the mountain faces. The mountain side on which Mavrovo station is located faces northward and Lazaropole station faces southward. The difference in slope direction and hence different climatic drivers could be the reason why different change signs and magnitudes have been detected at these stations. However, the detailed reasons for this phenomenon are beyond the scope of the current study, and should be investigated in future research. The current study also found that the North Atlantic Oscillation (NAO) seems to have an influence on the annual and seasonal precipitation sums in the region, based on the correlations obtained. To the authors knowledge, there is no study directly investigating the effects of the NAO to precipitation in the broader region in which the study region is located. However, in a study in Romania (*Birsan*, 2015), strong negative correlations between the NAOI and the mean annual streamflow have been found in western and southern

parts of the country. Positive correlations were found in plain lowland stations and no significant correlations were found for mountain gauges.

At an annual scale, the correlation of the NAOI and precipitation sums can be classified as a weaknegative correlation, which is strongest at the stations located at higher altitude (above 600 m), except Bitola, which is positively correlated. Winter and autumn are negatively correlated with the NAOI for all stations, summer is positively correlated for all stations in the country, whereas the results for spring are variable. With increasing elevation, the climate regime changes from sub-Mediterranean to mountainous. Similarly, the detected negative correlations with the NAOI become stronger in annual and winter precipitation sums and change from statistically not significant to significant. Similar change with increasing elevation can also be seen in spring, were the correlations change from statistically non-significant positive to statistically negative. In summer, there is no change across the climate regions, and all correlations are significantly positive. The negative correlations of the NAOI with winter precipitation obtained in this study are in line with previous results obtained at mountain gauges in the Mediterranean region (*López-Moreno et al.,* 2011). This is likely due to the fact that the winter NAO is stronger than that of the other seasons, which has already been pointed out in previous studies (*Hurrell*, 1995). This indicates stronger contribution of winter and autumn correlations in shaping the picture or the annual correlations.

The analysis also discovered a strong influence of the winter NAO even on the spring precipitation in North Macedonia (negative correlations) which means that for anticipating spring precipitation, the previous winter NAO might be a valuable source of information. This should be further explored in future studies.

5. Summary and conclusion

This study has provided an analysis of annual and seasonal precipitation characteristics and their changes in North Macedonia. The results are generally concurrent with the past studies for the southeastern and Mediterranean regions and time periods of study, with a few exceptions that might be due to different methods or time periods used for the different analyses.

One of the important findings is the strong, statistically significant, decreasing trend (-6.4 mm/decade) in Kochani (spring precipitation) and in Shtip (winter), as the gauges are located in the most arid mid-eastern part of the country, and low seasonal precipitation is becoming even lower. Apart from this important finding, no overarching large-scale changes could be detected. Hence, an overarching study across all the Balkan states using similar data and consistent methodology with the aim of identifying and better understanding of the precipitation characteristics and their spatiotemporal changes in the wider region will be needed. Such a larger scale study might also allow for better insights, if

the predominant statistically non-significant changes identified in this study are just locally non-significant (e.g., due to high inter-annual variability in the records at specific gauges), or if the lack of significant trends due to the high variability in precipitation is part of a larger scale regional picture. Additionally, the lack of large-scale consistent change signal could also be caused by the high variability of landscape features, which results in strong spatial gradients in the climatology of the area (three different climate regimes), making it impossible to obtain a concurrent spatial change signal. Therefore, a lack of spatial consistency in trends should not be interpreted as a lack of actual changes, but rather highlights the importance of further research in this topic.

The decreasing precipitation trends found in most of the seasons over the period 1951–2010 in North Macedonia highlight the need for improved water management lead by the state authorities, especially in the central and the eastern arid parts of the country. Future studies should hence focus on a more detailed analysis of change in additional precipitation indices (e.g., extremes and spells) to better understand the possible effects of a changing climate. Additionally, further studies are needed for informing water management and agricultural plans. Moreover, planning for new water infrastructure, to store water in winter and spring for the drier summer season is very important because of decreasing precipitation in the arid parts of the country.

This study has also shown that the annual and seasonal precipitation sums in North Macedonia show a high correlation with the North Atlantic Oscillation. A strong correlation of the previous winter NAOI with spring precipitation was also found, which indicates the possibility for anticipating the magnitude of spring precipitation one season ahead. This lagged correlation with the NAOI might be a valuable source of information for water resource management, but it needs to be further explored. However, for such future work, a wider network of meteorological stations is needed, reflecting the variety of climatological regimes in the study region. Unfortunately, the number of working meteorological stations is decreasing since the 1990s. To allow future research on this important topic, the re-establishing of the meteorological and precipitation gauging network in North Macedonia for obtaining high-quality climatological data is needed.

References

Alexandrov, V., Schneider, M., Koleva, E., and *Moisselin, J.M.,* 2004: Climate variability and change in Bulgaria during the 20th century. *Theor. Appl. Climatol. 79*, 133–149. https://doi.org/10.1007/s00704-004-0073-4

Alley, R.B., Marotzke, J., Nordhaus, W.D., Overpeck, J.T., Peteet, D.M., Pielke, R.A., Pierrehumbert, R.T., Rhines, P.B., Stocker, T.F., Talley, L.D. and *Wallace, J.M.,* 2003: Abrupt climate change. Science 299 (5615), 2005–2010. https://doi.org/10.1126/science.1081056

Birsan, M.V., 2015: Trends in monthly natural streamflow in Romania and linkages to atmospheric circulation in the North Atlantic. *Water Resour. Manage. 29*, 3305–3313. https://doi.org/10.1007/s11269-015-0999-6

Blöschl, G., Hall, J., Parajka, J., Perdigão, R. A. P., Merz, B., Arheimer, B., Aronica G.T, Bilibashi, A., Bonacci, O., Borga, M., Čanjevac, I., Castellarin, A., Chirico, G.B., Claps, C., Fiala, K., Frolova, K., Gorbachova, L., Gül, A., Hannaford, J., Harrigan, S., Kireeva, M., Kiss, A., Kjeldsen, T. R., Kohnová, S., Koskela, J. J., Ledvinka, O., Macdonald, N., Mavrova-Guirguinova, M., Mediero, L., Merz, R., Molnar, P., Montanari, A., Murphy, C., Osuch, M., Ovcharuk, V., Radevski, I., Rogger, M., Salinas, J. L., Sauquet, E., Šraj, M., Szolgay, J., Viglione, A., Volpi, E., Wilson, D., Zaimi, K. and *Živković, N*., 2017: Changing climate shifts timing of European floods. Science 357 (6351), 588–590. https://doi.org/10.1126/science.aan2506

Blöschl, G., Hall, J., Viglione, A., Perdigão, R.A.P., Parajka, J., Merz, B., Lun, D., Arheimer, B., Aronica, G. T., Bilibashi, A., Boháč, M., Bonacci, O., Borga, M., Čanjevac, I., Castellarin, A., Chirico, G.B., Claps, P., Frolova, N., Ganora, D., Gorbachova, L., Gül, A., Hannaford, J., Harrigan, S., Kireeva, M., Kiss, A., Kjeldsen, T. R., Kohnová, S., Koskela, J. J., Ledvinka, O.,Macdonald, N., Mavrova-Guirguinova, M., Mediero, L., Merz, R., Molnar, P., Montanari, A., Murphy, C., Osuch, M., Ovcharuk, V., Radevski, I., Salinas, J. L., Sauquet, E., Šraj, M., Szolgay, J., Volpi, E., Wilson, D., Zaimi, K. and *Živković, N*., 2019: Changing climate both increases and decreases European river floods. Nature 573, 108–111. https://doi.org/10.1038/s41586-019-1495-6

Bojariu, R. and *Paliu, D.*, 2001: North Atlantic Oscillation projection on Romanian climate fluctuations in the cold season. In: (eds. *M. Brunet, D. Lopez*) Detecting and Modelling Regional Climate Change and Associated Impacts. Berlin-Heidelberg: Springer, 345–356. https://doi.org/10.1007/978-3-662-04313-4_29

Gajić-Čapka, M., Cindrić, K., and *Pasarić, Z.*, 2015: Trends in precipitation indices in Croatia, 1961–2010. *Theor. Appl. Climatol. 121*, 167–177. https://doi.org/10.1007/s00704-014-1217-9

Hirsch, R.M., Slack, J.R. and *Smith, R.A.*, 1982: Techniques of trend analysis for monthly water quality data. *Water Resour. Res. 18*, 107–121. https://doi.org/10.1029/WR018i001p00107

Hurrell, J.M., 1995: Decadal trend in the North Atlantic oscillation: regional temperature and precipitation. *Science 269*, 676–679. https://doi.org/10.1126/science.269.5224.676

Hurrell, J.M. & NATIONAL CENTER FOR ATMOSPHERIC RESEARCH STAFF (eds). Last modified 04 Aug 2018 "The Climate Data Guide: Hurrell North Atlantic Oscillation (NAO) Index (station-based)." Available from: https://climatedataguide.ucar.edu/climate-data/hurrell-north-atlantic-oscillation-nao-index-station-based [Accessed on 17 November 2020].

Kendall, M.G., 1975: Rank correlation methods. London: Griffin.

Kendrovski, V. and *Spasenovska, M.*, 2011: The Effects on Health of Climate Change in the Republic of Macedonia. (2011) [online] pp. 31–76. Ministry of Health: Skopje, the Former Yugoslav Republic of Macedonia. Available from: http://www.un.org.mk/en-publications-full/items/the-effects-on-health-of-climate-change-in-the-republic-of-macedonia.pdf [Accessed on 26 March 2021].

López-Moreno, J.I., Vicente-Serrano, S.M., Morán-Tejeda, E., Lorenzo-Lacruz, J., Kenawy, A. and *Beniston, M.*, 2011: Effects of the North Atlantic Oscillation (NAO) on combined temperature and precipitation winter modes in the Mediterranean mountains: Observed relationships and projections for the 21st century. *Glob. Planet. Change 77*, 62–76. https://doi.org/10.1016/j.gloplacha.2011.03.003

Luković, J., Bajat, B., Blagojević, D, et al., 2014: Spatial pattern of recent rainfall trends in Serbia (1961–2009). *Reg. Environ. Change 14*, 1789–1799. https://doi.org/10.1007/s10113-013-0459-x

Mann, H.B., 1945: Nonparametric tests against trend. Econometrica: *J. Econometric Soc. 13*, 245–259. https://doi.org/10.2307/1907187

Marin, L., Birsan, M.V., Bojariu, R., Dumitrescu, A., Micu, D.M. and *Manea, A.*, 2014: An overview of annual climatic changes in Romania: trends in air temperature, precipitation, sunshine hours, cloud cover, relative humidity and wind speed during the 1961–2013 period. *Carpathian J. Earth Environ. Sci. 9* (4), 253–258.

Mavromatis, T. and *Stathis, D.*, 2011: Response of the water balance in Greece to temperature and precipitation trends. *Theor. Appl. Climatol. 104*, 13–24. https://doi.org/10.1007/s00704-010-0320-9

Milovanović, B., Radovanović, M., Stanojević, M., Pecelj, M. and *Nikolić, J.*, 2017a: Climate of Serbia. In: M. Radovanović, ed. Geografija Srbije [in Serbian]. Belgrade: Geographical Institute "Jovan Cvijić" SASA, 95–159.

Milovanović, B., Schuster, P., Radovanović, M., Vakanjac, V.R. and *Schneider, C.*, 2017b: Spatial and temporal variability of precipitation in Serbia for the period 1961–2010. *Theor. Appl. Climatol.* 130, 687–700. https://doi.org/10.1007/s00704-017-2118-5

Murphy, C. Harrigan, S. Hall, J., and *Wilby R.*, 2013: Climate-driven trends in mean and high flows from a network of reference stations in Ireland. *Hydrol. Sci. J. 58*, 755–772. https://doi.org/10.1080/02626667.2013.782407

Philandras, C.M., Nastos, P.T., Kapsomenakis, J., Douvis, K.C., Tselioudis, G., and *Zerefos, C.S.*, 2011: Long term precipitation trends and variability within the Mediterranean region. *Nat. Hazards Earth Syst. Sci. 11*, 3235–3250. https://doi.org/10.5194/nhess-11-3235-2011

Popov, T., Gnjato, S., Bajić, D., and *Trbić, G.*, 2019: Spatial Patterns of Precipitation in Bosnia and Herzegovina. Journal of the Geographical Institute "Jovan Cvijić" SASA, 69 (3), 185–195. https://doi.org/10.2298/IJGI1903185P

Radevski, I., Gorin, S., Taleska, M. and *Dimitrovska, O.*, 2018: Natural regime of streamflow trends in Macedonia. *Geografie, 123*(1), 1–20. https://doi.org/10.37040/geografie2018123010001

Sen, P.K., 1968: Estimates of the regression coefficient based on Kendall's tau. *J. Amer. Stat. Assoc. 63*, 1379–1389. https://doi.org/10.1080/01621459.1968.10480934

Tošić, I., Hrnjak, I., Gavrilov, M.B., Unkašević, M., Marković, S.B., and Lukić, T., 2014: Annual and seasonal variability of precipitation in Vojvodina, Serbia. Theor. Appl. Climatol. 117, 331–341. https://doi.org/10.1007/s00704-013-1007-9

Wallace, J.M. and *Gutzler D.S.*, 1981: Teleconnections in the geopotential height field during the Northern Hemisphere Winter. *Month. Weather Rev. 109*, 784–812. https://doi.org/10.1175/1520-0493(1981)109<0784:TITGHF>2.0.CO;2

Wilby, R.L., 2006: When and where might climate change be detectable in UK river flows?. *Geophys. Res. Lett. 33*, L19407. https://doi.org/10.1029/2006GL027552

Yue, S., 2002: The influence of autocorrelation on the ability to detect trend in hydrological series. *Hydrol. Process. 16*, 1807–1829. https://doi.org/10.1002/hyp.1095

Zikov, M., 1995: Клима и климатска регионализација на Република Макеоднија, *Geograph. Rev. 30*, 13–23 [in Macedonian].

Appendix

The Mann-Kendall (MK) test allows testing two hypotheses: H0 - There is no significant trend in the time series and Ha - there is a significant trend in the time series. To test the hypotheses the computation of MK S statistics is required, which is determined as follows:

$$S = \sum_{i=1}^{n-1} \sum_{j=i+1}^{n} sgn\left(T_j - T_i\right), \tag{1}$$

where

$$\mathrm{sgn}\left(T_j - T_i\right) = \begin{cases} 1 \; if \; T_j - T_i > 0 \\ 0 \; if \; T_j - T_i = 0 \\ -1 \; if \; T_j - T_i < 0 \end{cases}. \tag{2}$$

In the formula T_j and T_i are the time series of annual/seasonal values of precipitation sums in years $j=i+1, i+2, i+3$, and $i=1, 2, 3,\ldots, n-1$, where $j>i$, and n is the last year of the time series. A positive value of S indicates an increasing

trend and a negative value indicates a decreasing trend in the precipitation time series.

$$Z = \begin{cases} \frac{S-1}{\sigma} \; or \; S > 0 \\ 0 \; or \; S = 0 \\ \frac{S+1}{\sigma} \; or \; S < 0 \end{cases}, \tag{3}$$

where Z is normalized/standard test statistics, $\sigma 2$ is the variance of a near normally distributed statistics S for $n \geq 10$. For measuring the significance of the precipitation trend, the p-value was computed (significance level α=0.1). Hence, if the p-value is lower than 0.1 Ha is accepted, and a positive or negative trend is considered to be statistically significant. If p>0.1, H0 is accepted, which means there is no statistically significant monotonic trend in the precipitation time series.

$$p = [1 - f(Z)]. \tag{4}$$

DOI:10.28974/idojaras.2024.1.6

IDŐJÁRÁS

Quarterly Journal of the HungaroMet Hungarian Meteorological Service
Vol. 128, No. 1, January – March, 2024, pp. 99–120

Vulnerability of Central Serbian national parks to wildfires

Stanimir Živanović [1], **Milena Gocić** [2,*], and **Ivana Tošić** [3]

[1]*Emergency Management Sector of Serbia*
11000 Belgrade, Serbia

[2]*University of Niš, Faculty of Science and Mathematics*
Department of Geography
18000 Niš, Serbia

[3]*University of Belgrade-Faculty of Physics*
Institute for Meteorology
11000 Belgrade, Serbia

**Corresponding Author e-mail: milena.nikolic@pmf.edu.rs*

(Manuscript received in final form February 23, 2023)

Abstract— National parks in Serbia are sensitive to various types of natural hazards that are becoming more frequent and having a significant negative impact on the environment. The present study examines the effects of weather conditions on wildfires in the national parks (NPs) Tara, Djerdap, and Kopaonik using data from meteorological stations and applying climate indices based on air temperatures and precipitation. It examines the variability of fire occurrence dynamics, which depend on changes in the forest aridity index (*FAI*), the De Martonne aridity index (I_{DM}), and the Lang's rain factor (AI_{Lang}) during the period 2005–2021.

The highest number of fire occurrences was recorded in NP Tara and NP Djerdap, and the lowest in NP Kopaonik. The risk of fire was greatest during September (27.5%) and August (18.1%), when air temperatures were high and precipitation was low. The fire season was longest in NP Djerdap (February–December) and NP Tara (March–November), and shortest in NP Kopaonik (April–August).

Due to the weak correlation between the annual number of fires and individual values of climate variables and climate indices, multiple linear regression (MLR) models were developed. The highest correlation and coefficient of determination were obtained using temperature, precipitation, I_{DM}, and AI_{Lang} as predictors for NP Tara and NP Djerdap but not NP Kopaonik, where only three wildfires were recorded.

Key-words: climatic conditions, fire in nature, national park, Serbia

1. Introduction

The natural resources of national parks are of exceptional importance, so more and more attention is being given to their preservation and protection. Protected natural areas contribute to society by preserving biological diversity and providing areas for recreation, science, and education. Efforts are, therefore, being made to ensure that this remains the case (*Rada* and *Marquina*, 2008).

The forest ecosystems of national parks are increasingly sensitive to changes that occur as a result of numerous natural and anthropogenic factors. The sustainability of a forest ecosystem depends to a significant extent on these influences. For instance, certain stress factors, by their intensity and frequency, can lead to a weakening of the vitality of certain plant species and eventually cause them to become extinct. As pointed out by the Centre for Research on the Epidemiology of Disasters (CRED), the Munich Reinsurance Company, and the Swiss Re Group, forest fires are generally classified into a group of natural climatological disasters, where wildfires are perceived as forest fires and land fires (*Lukić et al., 2*013). Therefore, wildfires are potentially the most destructive type of natural disaster in forested areas (*Bowman et al*., 2009). Climate conditions play a key role in the determination of the fire regime in the given area. The pronounced effects of climate change on forest fires were also highlighted by *Rosavec et al.* (2022). During 2022, the Intergovernmental Panel on Climate Change (IPCC) indicated that global warming effects tend to increase the number of forest fires around the world (*IPCC*, 2022), and there are many studies outlining the potential impacts of climate change on the risk of forest fires in the southeast Europe (e.g., *Novković et al.*, 2021).

According to *Gigović et al.* (2019), positive trends in both the number of forest fire events and burned areas have been confirmed in Europe during the last few decades. In relation with climate variability, during the high air temperature summer months, the number of forest fires in Serbia has been increasing as well (*Novković et al.*, 2021). Since forest area in the Republic of Serbia covers approximately 31.1% (27,200 km^2), protected natural areas are particularly vulnerable to forest fires and require special scientific attention (*Gigović et al.*, 2019).

National parks in Serbia are threatened by various natural hazards. *Dragićević et al*. (2011) state that this risk varies according to the territory. *Tošić et al*. (2019) point out that Serbia is susceptible to wildfires, and their number is increasing. Fires in nature often have unpredictable and far reaching consequences (*Tošić et al*., 2019). Several studies (*Abatzoglou* and *Kolden*, 2013; *Bessie* and *Johnson*, 1995; *Littell et al*., 2009) have shown that weather is the most variable and biggest driver of fire hazard. *Skvarenina et al*. (2003) claim that meteorological factors play a key role in affecting wildfire occurrence and behavior. For *de Angelis et al*. (2015), fire regimes are strongly related to weather conditions that directly and indirectly influence ignition and propagation.

Meteorological conditions such as long periods without precipitation help create conditions for the development of forest fires (*Cane et al*., 2008). The frequency, size, intensity, periodicity, and type of fire depend on the weather and climate, along with the structure and composition of the forest (*Dale et al.*, 2001). Weather alone can cause a forest fire, and when it does, can control its behaviour (*Van Wagner*, 1987).

Flannigan et al. (2016) suggest that weather and climatic elements (e.g., temperature, precipitation, wind, and atmospheric moisture) are critical aspects of fire activity. Climate has a strong influence on the activity, frequency, and probability of the occurrence of fire in nature (*Urbieta et al*., 2015; *Jolly et al*., 2015; *Pérez-Sánchez et al*., 2017).

Large forest fires are more frequent in areas with natural value. These have the highest level of state protection precisely because they are characterised by disasters. A case study of NP Djerdap in 2011 showed that the occurrence of large forest fires was strongly influenced by climatic conditions (*Živanović* and *Tošić*, 2020). When the dry season is longer, especially in periods when the air temperature is extremely high, the risk of fire is higher (*Živanović et al*., 2020b; *Živanović*, 2017, *Tošić et al*., 2020). By contrast, the danger of fire is lower during extremely wet periods (*Chandler et al*., 1983; *Dimitrakopoulos et al*., 2011; *Ćurić* and *Živanović*, 2013; *Tošić et al*., 2019; *Živanović*, 2021; *Živanović et al*., 2020).

The present study aimed to determine the vulnerability of national parks in the territory of Serbia from fires in nature based on the dynamics of forest fires and selected climate indices. It is hoped that the findings will help the relevant services to develop an effective forest fire prevention system.

2. Materials and methods

2.1. Study area and data

The territory of Serbia is located in the southeastern part of Europe and covers an area of 88 499 km^2. The total forest coverage in the Republic of Serbia is 29.1% (*Banković et al*., 2009), 1.8% of which comprises national parks. The present study examined parks in central Serbia: NP Djerdap, NP Tara, and NP Kopaonik (*Fig. 1*). Basic data on all three are presented in *Table 1*.

Fig. 1. Location of NP Tara, Djerdap, and Kopaonik in the Republic of Serbia.

Table 1. Basic data of selected national parks Djerdap, Tara and Kopaonik

National park	Forest area (ha)		Altitude (m)	Relative height (m)	Forest cover (%)
	Forest (all)	State forest			
Djerdap	63 786	45 455	45 – 803	758	64
Tara	24 992	13 589	291 – 1591	1,300	80
Kopaonik	11 969	9 863	640 – 2 017	1 377	62

National park Djerdap is located in the northeastern part of central Serbia. It includes some of the Djerdap Gorge and the Severni Kučaj, Miroč, and Štrbac massifs. It covers the municipalities of Golubac, Majdanpek, and Kladovo (*Law on National Parks*, 2018).

National park Tara is located in the western part of Serbia. It covers an area limited by the Drina river, between Višegrad and Bajina Bašta, and includes the Zvezda, Crni vrh, and Ravna Tara mountains (*Law on National Parks*, 2018).

National park Kopaonik is located in the southern-central part of the country and covers the highest parts of the Kopaonik mountain and the basins of the Samokovska, Gobeljska, Brzećka, and Barska rivers. It extends to the municipalities of Raška and Brus (*Law on National Parks*, 2018).

The location of meteorological stations and their latitude, longitude, and altitude are listed in *Table 2*.

Table 2. Location of meterological stations in the national parks (latitude, longitude, and altitude)

National park	Meteorological station	Latitude (N)	Longitude (E)	Altitude (m)
Djerdap	Veliko Gradište	44° 45’	21° 31’	82
Tara	Bajina Bašta	43º 58’	19º 34’	270
Kopaonik	Kopaonik	43º 17’	20º 48’	1 711

To consider the climatic characteristics of the NPs, we used the average monthly and annual values of air temperature and precipitation from three main meteorological stations for the period 2005–2021. The data were retrieved from the Republic Hydrometeorological Service of Serbia (*RHSS*, 2021). Fire data were retrieved from the competent fire protection services in each of the NPs.

2.2. Methods

2.2.1. Climate indices

Selected climate indices such as the De Martonne aridity index (I_{DM}), Lang aridity index (AI_{Lang}) and the Forestry Aridity Index(*FAI*) based on air temperature and precipitation data were used since these indices are the most suitable for analysis of climate conditions over the territory of the Republic of Serbia (based on previous studies) (e.g., *Hrnjak et al.*, 2014; *Gavrilov et al.*, 2019; *Radaković et al.*, 2018; *Bačević et al.*, 2017).

The annual values of I_{DM} (*de Martonne*, 1925), AI_{Lang} (*Lang*, 1920), and *FAI* (*Führer et al*., 2011), are obtained from the following equations:

$$I_{DM} = \frac{P}{T+10}, \tag{1}$$

$$AI_{Lang} = \frac{P}{T}, \tag{2}$$

$$FAI = \frac{T_{\text{VII–VIII}}}{P_{\text{V–VII}} + P_{\text{VII–VIII}}} c, \quad (3)$$

where P is the annual precipitation (mm), T is the annual mean temperature (°C), $T_{\text{VII– VIII}}$ is the average temperature in July and August (°C), $P_{\text{V–VII}}$ is the precipitation total from May to July (mm), $P_{\text{VII–VIII}}$ is the precipitation total for July–August (mm), and $c = 100$ mm/°C is the constant. The classification of climate according to Lang is given in *Table 3*. The classification of the I_{DM} is given in *Table 4*. The *FAI* and the average weather conditions of four different climate categories are shown in *Table 5*. Unlike the I_{DM}, humidity rises with a decrease in the value of *FAI* and vice versa (*Gavrilov et al.*, 2019). The monthly aridity index values are determined using AI_{Lang} and I_{DM} indices. AI_{Lang} index is based on the hypothesis that warmer air temperatures lead to soil and air dryness if there is not enough precipitation and/or groundwater recharge. On the other hand, the I_{DM} is one of the best known and widely used aridity/humidity indices in applied climatology for climate classification (*De Martonne* 1925; *Croitoru et al.*, 2012). The *FAI* is a very good parameter for presenting climate conditions during the yearly forests' growth, which is very important for forestry management (*Gavrilov et al.*, 2019).

Table 3. Climate classification according to *Lang* (1920)

Value of AI_{Lang}	Types of climate
0 – 20	Arid
20 – 40	
40 – 60	Semi-arid
60 – 100	Semi-humid
100 – 160	Humid
> 160	Perhumid

Table 4. The De Martonne index (I_{DM}) classification

Values of I_{DM}	Types of climate
$I_{DM} < 10$	Arid
$10 \leq I_{DM} < 20$	Semi-arid
$20 \leq I_{DM} < 24$	Mediterranean
$24 \leq I_{DM} < 28$	Semi-humid
$28 \leq I_{DM} < 35$	Humid
$35 \leq I_{DM} < 55$	Very humid
$I_{DM} > 55$	Extremely humid

Table 5. Meteorological features of forestry climate categories

***FAI* values**	**Forestry climate categories**
< 4.75	Beech climate
4.75 – 6.00	Hornbeam-oak climate
6.00 – 7.25	The sessile oak/Turkey oak climate
> 7.25	Forest-steppe climate

2.2.2. Multiple linear regression (MLR) models

Multiple linear regression models were used to establish the relationship between the number of fires and climate variables and indices. Meteorological variables and climate indices were used as predictors (independent variables), and the data on forest fires as the predicted variable. The models were calibrated for the first 10 years (from 2005 to 2015) and validated for the remaining five years (from 2016 to 2021). The model efficiency coefficient (*MEF*), Pearson's correlation coefficient (r), and coefficient of determination (R^2) were used to assess the predictive power of the model (*Cohen et al*., 2002). The Nash–Sutcliffe efficiency can range from -∞ to 1. The model is perfect when the efficiency is 1 (*Nash* and *Sutcliffe*, 1970). The R^2 ranges from 0 to 1, with a perfect fit being equal to 1.

2.3. Climate characteristics of national parks

2.3.1. Basic characteristics of air temperature

The temperature regime is a basic feature of the climate of an area and has a direct and/or indirect influence on the values of other climatic elements. Periods of high air temperature represent a very pronounced danger for the occurrence of fires in nature (*Živanović et al*., 2015). Average monthly and annual values of air temperature in Serbian NPs are given in *Table 6* (www.hidmet.gov.rs). The following conclusions can be drawn from the data on their mean monthly and annual air temperature values:

– The highest annual air temperature values were recorded in NP Djerdap (12.3 °C) and the lowest in NP Kopaonik (4.6 °C). The difference in average annual air temperatures of 7.7 °C may have had a significant impact on the frequency and intensity of forest fires in both parks.

– The highest mean monthly air temperatures were during July in NP Tara (21.9 °C) and NP Djerdap (23.2 °C), and in August in NP Kopaonik (13.3 °C).

Table 6. Mean monthly and annual air temperature in national parks of Serbia during the period 2005–2021

Met. station	Month												Annual
	1	2	3	4	5	6	7	8	9	10	11	12	
Veliko Gradište	0.9	2.7	7.1	12.7	17.0	21.1	23.2	22.4	17.7	12.0	7.6	2.4	12.3
Bajina Bašta	1.2	3.5	7.3	12.2	16.2	20.0	21.9	20.4	16.4	11.8	7.1	2.4	11.9
Kopaonik	-4.7	-3.7	-1.5	3.3	7.5	11.6	13.1	13.3	9.6	5.3	1.8	-2.9	4.6

2.3.2. Basic characteristics of precipitation

Precipitation was irregularly distributed in time and space with regard to atmospheric processes and relief features. *Trabaud* (1980) states that the amount and distribution of precipitation is an important climatic element that affects the occurrence of fires. The number of fires decreases exponentially with the height of precipitation. The latter, whether in surplus or deficit, directly influences the state of fuel material in the forest, thereby reducing the risk of fire and vice versa (*Ćurić et al.*, 2013). *Table 7* shows the mean monthly and annual precipitation total at meteorological stations in the NPs under study for the period 2005–2021 (www.hidmet.gov.rs). The annual precipitation totals, which reflected the differences in altitude, were highest in NP Kopaonik (1087.3 mm) and lowest in NP Djerdap (684.2 mm). *Table 7* shows that precipitation was at its highest during May and June. Winter was drier than summer in all three NPs.

Table 7. Mean monthly and annual precipitation in national parks of Serbia during the period 2005–2021

Met. station	Month												Annual
	1	2	3	4	5	6	7	8	9	10	11	12	
Veliko Gradište	55.8	48.6	51.4	52.6	87.3	69.3	81.3	54.1	44.5	90.0	43.5	55.2	684.2
Bajina Bašta	46.2	60.0	65.4	55.6	95.6	94.8	74.1	70.8	58.2	66.1	52.8	66.4	720.3
Kopaonik	86.7	68.0	101.2	88.4	128.9	115.7	94.0	77.7	72.6	91.3	73.1	89.0	1087.3

3. Results and discussion

3.1. Analysis of climate indices

With the help of different drought indices, dry periods (in terms of humidity) can be determined, particularly, when the occurrence of forest fires is pronounced (*Živanović*, 2021). *Tošić et al.* (2020) argue that the risk of fire is greater when the dry season is longer, especially during periods, when the air temperature is extremely high. The values of the climate indices in terms of aridity for 2005–2021 can be seen in *Table 8*.

Table 8. Climate classification according to the aridity index

Climate index	**Meteorological station**		
	Veliko Gradiše	**Kopaonik**	**Bajina Bašta**
Lang's rain factor (AI_{Lang})	Semi-arid (AI_{Lang} = 57.1)	Perhumid (AI_{Lang} = 244.8)	Semi-humid (AI_{Lang} = 68.6)
De Martonne aridity index (I_{DM})	Humid (I_{DM} = 31.3)	Extremely humid (I_{DM} = 74.9)	Very humid (I_{DM} = 37.2)
Forest aridity index (*FAI*)	Forest-steppe climate (*FAI* = 7.6)	Beech climate (*FAI* = 3.0)	Forest-steppe climate (*FAI* = 6.0)

Figs. 2, *3*, and *4* show the values of the climate indices during the period 2005–2021. The multiannual values of the drought index for the period 2005–2021 indicate an exceptional diversity of climatic conditions and a relatively large variation in values during certain years. On the basis of AI_{Lang} (*Fig. 2*), it may be concluded that a semi-arid climate prevailed in NP Djerdap during 2005–2021. The lowest values of this index were recorded in NP Djerdap in 2011 (AI_{Lang} = 33.4), and the highest in NP Kopaonik in 2005 (AI_{Lang} = 340.5).

High *FAI* values were recorded in 2012, 2013, and 2015 (*Fig. 3*), and small values in 2014. The *FAI* values were extremely high for NP Kopaonik, which indicates that its forest ecosystems were the least affected of the three.

Fig. 4 shows that the I_{DM} was low for 2011 indicating extremely dry conditions. Extremely wet conditions pertained in 2014, with I_{DM} values ranging from 41.8 in Veliko Gradište to 89.5 in Kopaonik (*Fig. 4*). According to the De Martonne's aridity index, the humidity conditions for 2011 corresponded to the conditions of a semi-arid climate at the Veliko Gradište measuring site (*Fig. 4*). In NP Kopaonik, 2011 was extremely humid.

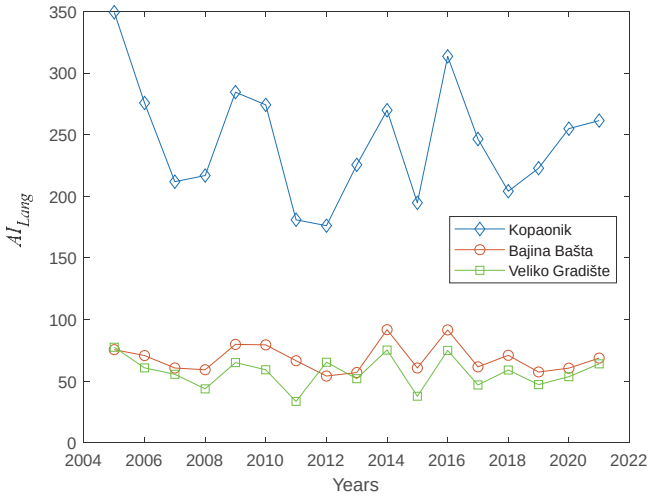

Fig. 2. Values of the Lang's rain factor (AI_{Lang}) at the meteorological stations in the national parks of Serbia during the period 2005–2021.

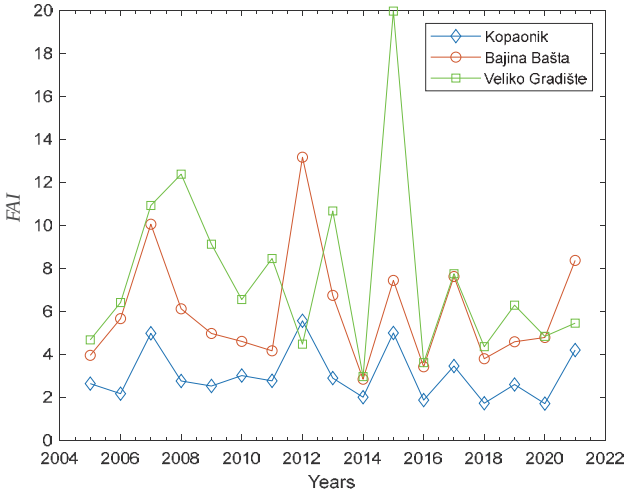

Fig. 3. Values of the forest aridity index (*FAI*) at the meteorological stations in the national parks of Serbia during the period 2005–2021.

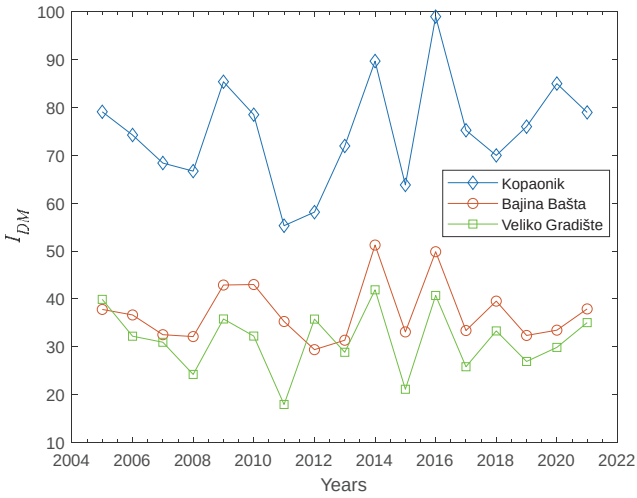

Fig. 4. Values of the De Martonne aridity index (I_{DM}) at the meteorological stations in the national parks of Serbia during the period 2005–2021.

Figs. 2, 3, and *4* show that favorable conditions for fire existed in 2007, 2012, and 2015. These were warm years, as was confirmed by the climatic conditions on the synoptic scale (*Fig. 5*). Annual temperature anomalies across Serbia were positive: 0.9 °C in 2007 (*Fig. 5a*), 1 °C in 2012 (*Fig. 5c*), and 1.25 °C in 2015 (*Fig. 5d*) when compared with the period as a whole. The only negative temperature anomaly was in 2011 (*Fig. 5b*). In the same year, a negative precipitation anomaly was registered over the central area of the Balkans (up to –40 mm), and –20 mm in Serbia (*Fig. 6a*). In contrast with 2011, conditions in 2014 did not favor the development of fires: excessive precipitation was registered over the Balkans (more than 40 mm), as well as in Serbia itself (along the Sava and Danube river valleys; *Fig. 6b*).

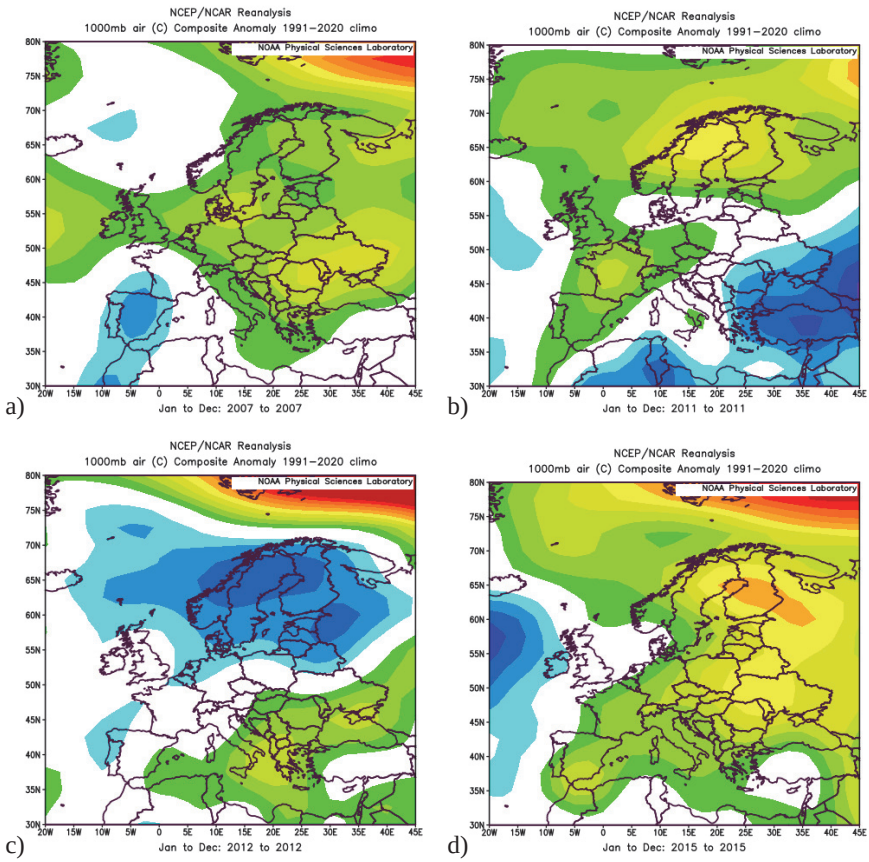

Fig. 5. Composite anomaly of 1000 hPa air temperature (°C) for: a) 2007, b) 2011, c) 2012, and d) 2015 compared to the period 1991–2020.

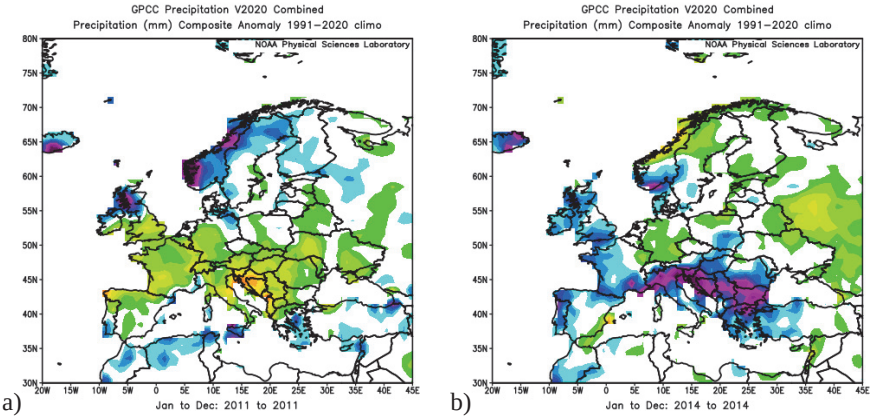

Fig. 6. Composite anomaly of precipitation (mm) for: a) 2011 and b) 2014 compared to the period 1991–2020.

According to *Gračanin* (1950), the adjusted AI_{Lang} for monthly values of precipitation and air temperature indicates that in each of the meteorological stations, the highest values are during the cold period of the year (*Fig. 7*). The lowest values of the monthly rain factor are in summer, that is, the growing season, when plants are in most need of precipitation. It should be noted that August and September were arid in the NP Djerdap area (Veliko Gradište). Based on the multiannual mean for NP Kopaonik, each month was defined as humid, and April, May, October, and November as perhumid.

The monthly values of the De Martonne (I_{DM}) aridity index (*Fig. 8*) indicate that the driest month was August. Values of I_{DM} for NP Tara and NP Djerdap for July, August, and September indicate a Mediterranean type of climate. A humid type of climate was determined for NP Kopaonik during all months.

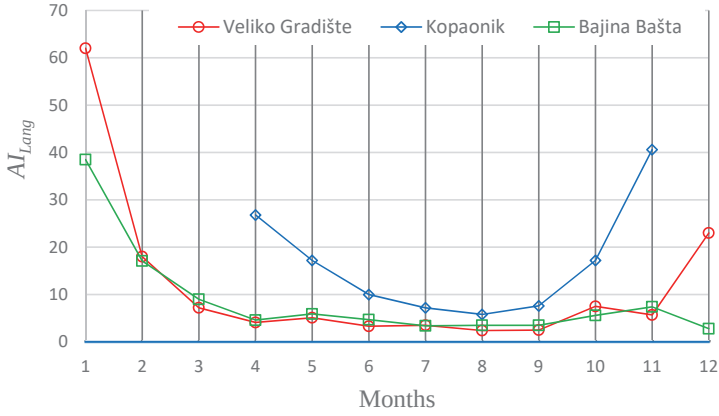

Fig. 7. Monthly values of the AI_{Lang} index during the period 2005–2021.

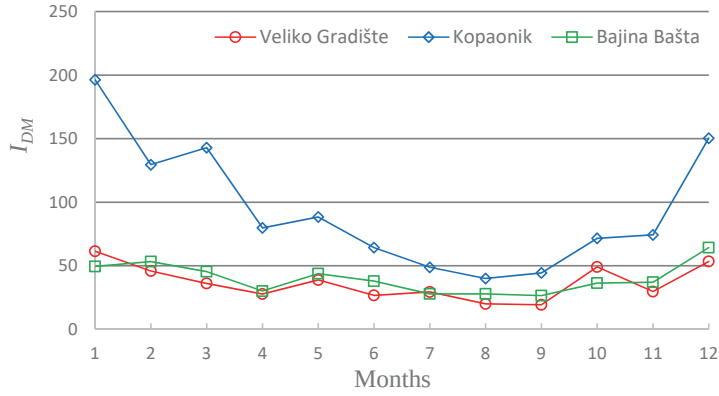

Fig. 8. Monthly values of the I_{DM} index during the period 2005–2021.

3.2. Dynamics of fire occurrence

The dynamics of the occurrence of fires in open spaces in the NPs between 2005–2021 can be seen in *Fig. 9*. The largest number of fires occurred in NP Tara (272 fires, that is, 58.2% of the total number). The lowest number of fires occurred in NP Kopaonik (three fires, that is, 0.6% of the total number of fires). The highest number of fires was recorded in 2007 (85 fires), and the lowest in 2018 and 2020 (four fires). Air temperatures were extremely high and precipitation was unevenly distributed during 2007, which affected the drying of fuel material in the forest and on forest land, creating suitable conditions for the occurrence and development of fires. The heat waves in Serbia that lasted 6–12 days in 2007 were extreme climatic events.

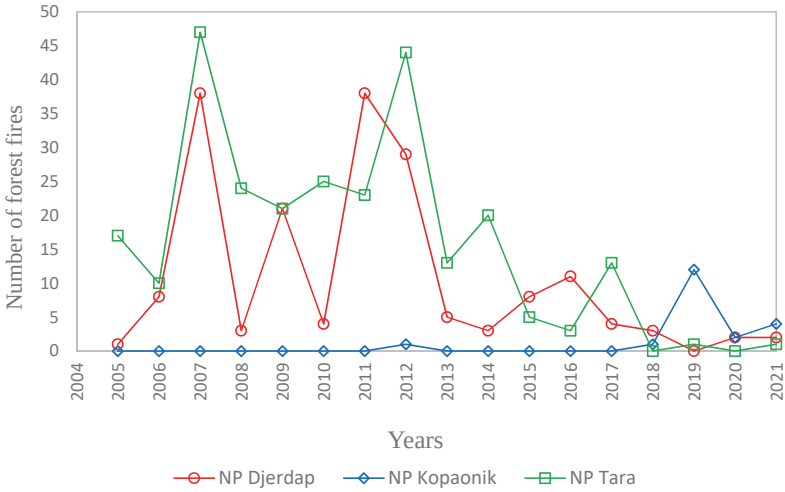

Fig. 9. Number of forest fires per year during the period 2005–2021.

Characteristic fires (in terms of intensity and duration) occurred between September 13 and September 16, 2011 in NP Djerdap and between August 23 and September 5, 2012 in NP Tara. *Lukić et al.* (2017) recorded a significant correlation between meteorological parameters and forest fires on Tara Mountain. In case study of NP Djerdap in 2011, *Živanović* and *Tošić* (2020) stated that the occurrence of fires was strongly influenced by climatic conditions.

The highest degree of vulnerability to fire was in September (27.5% of the total annual number of fires) and August (18.1%; *Fig. 10*). There was a significant frequency of fires occurring in March and April, though the air temperature was not high. No fires occurred in any of the NPs in January. The longest fire periods were in NP Djerdap (February–December) and NP Tara (March–November), and the shortest in NP Kopaonik (April–August). The frequency of fires at the beginning and the end of these seasons suggest that the fire season may last longer in the future.

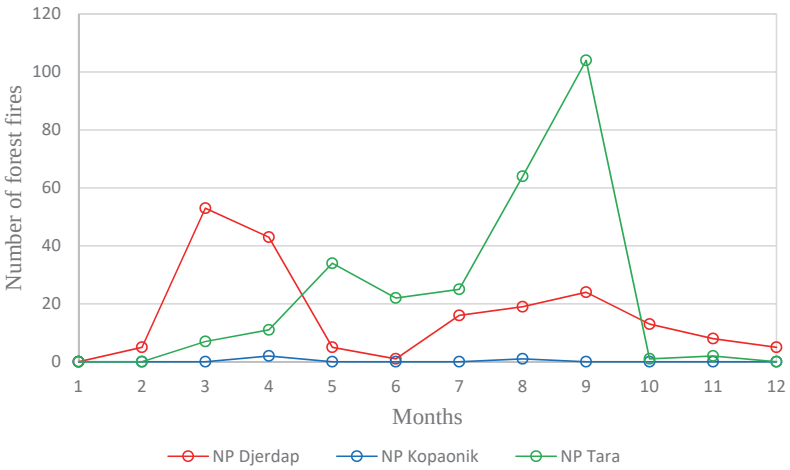

Fig. 10. Number of forest fires in national parks according to months of origin during the period 2005–2021.

The high number of fires in September 2011, 2012, 2015, and 2018 may be explained by the very warm conditions that prevailed. *Fig. 11a* shows that the temperature anomaly in September 2011 was around 3 °C higher in the Balkans and Serbia, while in 2012, the maximum temperature was in northeast Serbia (where the anomaly was 2.5 °C) (*Fig. 11b*). September 2015 and 2018 were less warm than in 2011 and 2012. In September 2015, the positive temperature anomaly was about 2 °C (*Fig. 11c*), while in 2018, it was about 1.0 °C (*Fig. 11d*).

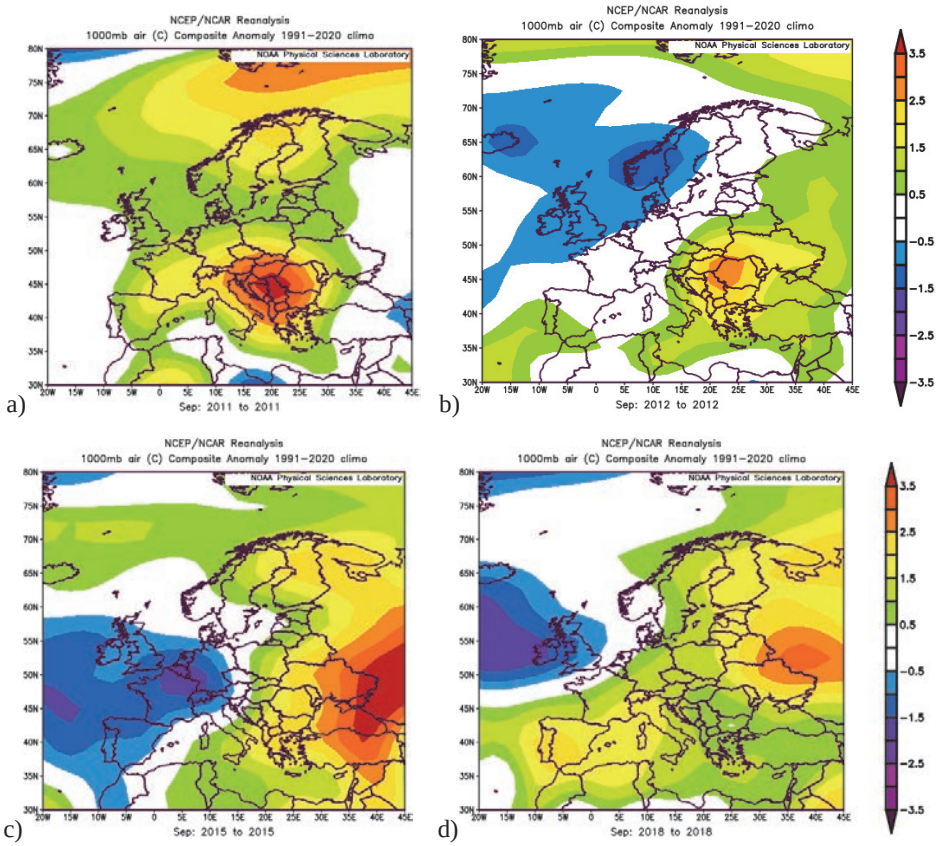

Fig. 11. Composite anomaly of 1000 hPa air temperature (°C) for: a) 2011, b) 2012, c) 2015, and d) 2018 compared to the period 1991–2020.

3.3. Correlation between fire occurrence and climate indices

A possible connection between the number of fires and climate indices during 2005–2021 was investigated using linear correlations. *Table 9* shows the linear correlations of the mean annual values of temperature, precipitation, AI_{Lang}, I_{DM}, and *FAI* with the occurrence of forest fires.

The results are shown for NP Djerdap and Tara and not for NP Kopaonik, because only three fires were recorded in the latter (in 2012, 2019, and 2021). There was a positive relationship between the annual number of fires and *FAI* and a negative relationship for other predictors. The strongest correlation between the number of fires and *FAI* was found in NP Tara (0.5503), while for NP Djerdap,

the strongest correlation was between the number of fires and precipitation (*Table 9*). The R^2 for NP Tara was 0.3029, which means that 30.29% of the variation in the number of forest fires was explained by *FAI* alone.

Table 9. Results from linear regression models for the number of forest fires in national parks of Serbia with annual precipitation sum (*Prec*), mean annual temperature (*Temp*), forest aridity index (*FAI*), De Martonne aridity index (I_{DM}), and Lang's rain factor (AI_{Lang})

Location	Equation	*r*	R^2	Predictor
NP Djerdap	y = -2.818x + 727.8	-0.2438	0.0594	*Prec*
	y = -0.003x + 12.27	-0.0600	0.0036	*Temp*
	y = -0.241x + 59.83	-0.2355	0.0554	AI_{Lang}
	y = -0.129x + 32.8	-0.2399	0.0576	I_{DM}
	y = 0.050x + 7.013	0.1495	0.0224	*FAI*
NP Tara	y = -2.463x + 853.2	-0.2390	0.0571	*Prec*
	y = -0.015x + 12.13	-0.3081	0.0949	*Temp*
	y = -0.127x + 70.6	-0.1524	0.0232	AI_{Lang}
	y = -0.088x + 38.59	-0.1952	0.0381	I_{DM}
	y = 0.105x + 4.337	0.5503	0.3029	*FAI*

Because low correlation was found between the annual number of fires and individual indices, MLR models were developed for the stations in NP Djerdap (*Table 10*) and NP Tara (*Table 11*). They were evaluated using three goodness-of-fit estimates (*r*, R^2, and *MEF*). First, in the case of NP Djerdap, both climate variables, temperature and precipitation, were kept as predictors, but the result did not improve (*Table 10*). The contribution of all climate indices was then examined, and again there was no change. However, the inclusion of AI_{Lang} along with temperature and precipitation increased the correlation to –0.8171, as well as R^2 to 0.6677. In addition, an improvement was noted when the I_{DM} was included in combination with precipitation and temperature (r = –0.9111, R^2 = 0.8301). The highest coefficients of correlation and determination (r = –0.9128, R^2 = 0.8333) were obtained using temperature, precipitation, I_{DM}, and AI_{Lang} as predictors

(*Table 10*). This indicates that about 83.3% of the forest fire variability in NP Djerdap could be explained by these four variables. For all three cases, values of MEF (model officiency coefficient) were about –4, also indicating the best estimates.

Table 10. Results from multiple linear regression models for the number of forest fires in NP Djerdap with retained predictors: annual precipitation total (*Prec*), mean annual temperature (*Temp*), forest aridity index (*FAI*), De Martonne aridity index (I_{DM}), and Lang's rain factor (AI_{Lang})

Location	Predictor	*r*	R^2	*MEF*
	Temp, Prec	0.0265	0.0070	-10.60
	I_{DM}, AI_{Lang}	-0.0290	0.0080	-10.70
	I_{DM}, *FAI*	-0.1202	0.0145	-8.36
	AI_{Lang}, *FAI*	-0.1817	0.0330	-9.96
	I_{DM}, AI_{Lang}, *FAI*	-0.2293	0.0526	-13.17
	Temp, AI_{Lang}	-0.0007	0	-10.17
	Temp, FAI	0.1900	0.0361	-6.81
NP Djerdap	*Prec*, AI_{Lang}	-0.0270	0.0007	-10.73
	Prec, FAI	-0.0265	0.0007	-6.90
	Temp, Prec, I_{DM}	-0.9111	0.8301	-4.45
	Temp, Prec, AI_{Lang}	-0.8171	0.6677	-4.27
	Temp, Prec, FAI	-0.1547	0.0239	-14.79
	Temp, Prec, I_{DM}, AI_{Lang}	-0.9128	0.8333	-4.72
	Temp, Prec, AI_{Lang}, *FAI*	-0.2198	0.0483	-7.05
	Temp, Prec, I_{DM}, AI_{Lang}, *FAI*	-0.2782	0.0774	-5.68

According to *Table 11*, a stronger relationship between the number of fires and the combination of *FAI* and I_{DM} was observed for NP Tara (r = 0.4268, R^2 = 0.1822), that is, *FAI* and AI_{Lang} (r = 0.4441, R^2 = 0.1972), compared with NP Djerdap. A higher correlation (r = 0.4356) was obtained using *FAI* with temperature and precipitation as predictors, as well as with added the AI_{Lang} and I_{DM} (r = 0.5934; Table 11). As was the previous case with NP Djerdap, the highest correlation (r = 0.7452) and R^2 (0.5553) were obtained using temperature, precipitation, I_{DM}, and AI_{Lang} as predictors (*Table 11*).

Table 11. Results from multiple linear regression models for the number of forest fires in NP Tara with retained predictors: annual precipitation total (*Prec*), mean annual temperature (*Temp*), Forest aridity index (*FAI*), De Martonne aridity index (I_{DM}), and Lang's rain factor (AI_{Lang})

Location	Predictor	*r*	R^2	*MEF*
NP Tara	*Temp, Prec*	-0.1032	0.0107	-39.06
	I_{DM}, AI_{Lang}	-0.0427	0.0018	-38.06
	I_{DM}, *FAI*	0.4268	0.1822	-22.97
	AI_{Lang}, *FAI*	0.4441	0.1972	-21.30
	I_{DM}, AI_{Lang}, *FAI*	0.4258	0.1813	-23.10
	Temp, AI_{Lang}	-0.0734	0.0054	-38.44
	Temp, FAI	0.4064	0.1651	-26.84
	Prec, AI_{Lang}	-0.0513	0.0026	-38.21
	Prec, FAI	0.4156	0.1728	-24.58
	Temp, Prec, I_{DM}	0.2235	0.0499	-30.10
	Temp, Prec, AI_{Lang}	0.5818	0.3385	-21.99
	Temp, Prec, FAI	0.4356	0.1897	-22.29
	Temp, Prec, I_{DM}, AI_{Lang}	0.7452	0.5553	-18.57
	Temp, Prec, AI_{Lang}, *FAI*	0.5780	0.3341	-16.67
	Temp, Prec, I_{DM}, AI_{Lang}, *FAI*	0.5934	0.3521	-15.80

Lower correlation and determination coefficient values were obtained for NP Tara, except when *FAI* was used as a predictor. Lower values were also obtained for *MEF* (*Table 11*), which means that a better model was obtained for NP Djerdap.

The results of the study suggest a connection between fires in nature and weather conditions. This accords with the findings of *Flannigan* and *Harrington* (1988), *Viegas* and *Viegas* (1994), *Westerling et al*. (2006), *Won et al*. (2010), amongst others.

4. Conclusions

The present study has revealed that the NPs were at different levels of vulnerability from wildfires during the period in question. The findings indicate that the highest degree of threat occurred during the months of August and September.

Data on the number of fires for the period 2005–2021 indicated that the highest number of fires was recorded in NP Tara and the lowest number in NP

Kopaonik. The number of registered fires was higher in the NPs at a lower altitude. Climate variables, as well as climate indices calculated using air temperature and precipitation, correlated with the dynamics of fire occurrence. The correlation with *FAI* was positive and it was negative for precipitation, temperature, AI_{Lang}, and I_{DM}. A linear correlation of 0.5503 was obtained between the number of fires and *FAI* for NP Tara and −0.2438 between the number of fires and precipitation for NP Djerdap. The best MLR model was obtained using temperature, precipitation, I_{DM}, and AI_{Lang} as predictors for both NP Djerdap (where the coefficient of correlation was −0.9128) and NP Tara (where it was −0.7452).

Obtained results by this study can be applied for adequate forest fire risk management and monitoring in the Republic of Serbia. Future investigation should strive to derive forest fire susceptibility maps which can be used by decision makers for better preparedness, coordination, and intervention in the national parks area vulnerable to wildfires.

References

Abatzoglou, J.T. and *Kolden, C.A.*, 2013: Relationships between climate and macroscale area burned in the western United States. *Int. J. Wildland Fire 22*, 1003–1020. https://doi.org/10.1071/WF13019.

Banković, S., Medarević, M., Pantić, D. and *Petrović, N.*, 2009: National Forest Inventory of the Republic of Serbia - Forest Fund of the Republic of Serbia. Ministry of Agriculture, Forestry and Water Management of the Republic of Serbia. Planeta print Belgrade (1–244).

Bačević, N., Vukoičić, D., Nikolić, M., Janc, N., Milentijević, N. and Gavrilov, M.B. 2017: Aridity in Kosovo and Metohija, Serbia. *Carpathian J. Earth Environ. Sci. 12*, 563–570.

Bessie, W.C. and *Johnson, E.A.*, 1995: The relative importance of fuels and weather on fire behaviour in subalpine forests. *Ecology 76*, 747–762. https://doi.org/10.2307/1939341

Bowman, D.M., Balch, J.K., Artaxo, P., Bond, W.J., Carlson, J.M., Cochrane, M.A., D'Antonio, C.M., DeFries, R.S., Doyle, J.C. and *Harrison, S.P.*, 2009: Fire in the Earth system. *Science 324*, 481–484. https://doi:10.1126/science.1163886

Cane, D., Gottero, F., Francesetti, A., Pelfini, F. and *Pelosini, R.*, 2008: Fire weather index application in north-western Italy. *Adv. Sci. Res. 2*, 77–80. https://doi.org/10.5194/asr-2-77-2008

Chandler, C., Cheney, P., Thomas, P., Trabaud, L. and *Williams, D.*, 1983: Fire in Forestry. Vol. 1: Forest Fire Behaviour and Effects, John Wiley and Sons, New York.

Cohen, J., Cohen, P., West, S.G. and *Aiken, L.S.*, 2002: Applied Multiple Regression/Correlation Analysis for the Behavioral Sciences. 3rd ed. Routledge, New York, NY, USA. https://doi.org/10.4324/9781410606266

Croitoru, A., Piticar, A., Imbroane, and *A., Burada, C.*, 2012: Spatiotemporal distribution of aridity indices based on temperature and precipitation in the extra-Carpathian regions of Romania. *Applied Climatology 109*, 1–2. https://doi:10.1007/s00704-012-0755-2

Ćurić, M. and *Živanović, S.*, 2013: Dependence between Deficit and Surplus of Precipitation and Forest Fires. *Disaster Advances 6*, 64–69.

Dale, V.H., Joyce, L.A., McNulty, S., Neilson, R.P., Ayres, M.P., Flannigan, M.D., Hanson, P.J., Irland, L.C., Lugo, A.E., Peterson, C.J., Simberloff, D., Swanson, F.J., Stocks, B.J. and *Wotton, B.M.*, 2001: Climate Change and Forest Disturbances. *BioScience 51*(9), 723–734. https://doi.org/10.1641/0006-3568(2001)051[0723:CCAFD]2.0.CO

de Angelis, A., Ricotta, C., Conedera, M. and *Pezzatti, G.B.*, 2015: Modelling the Meteorological Forest Fire Niche in Heterogeneous Pyrologic Conditions. *PLoSONE 10*, e0116875. https://doi.org/10.1371/journal.pone.0116875

de Martonne, E., 1925: Traité de géographie physique. Vol. I: Notions generals, climat, hydrographie. *Geogr. Rev. 15*, 336–337.

Dimitrakopoulos, A.P., Vlahou, M., Anagnostopoulou, C.G. and *Mitsopoulos, I.D.*, 2011: Impact of drought on wildland fires in Greece: implications of climatic change? *Climatic Change 109*, 331–347. https://doi.org/10.1007/s10584-011-0026-8

Dragićević, S., Filipović, D., Kostadinov, S., Ristić, R., Novković, I., Živković, N., Andjelković, G., Abolmasov, B., Sećerov, V. and *Djurdjić, S.*, 2011: Natural hazard assessment for land-use planning in Serbia. *Int. J. Environ. Res. 5*, 371–380.

Flannigan, M.D., Wotton, B.M., Marshall, G.A., de Groot, W.J., Johnston, J., Jurko, N. and *Cantin, A.S.*, 2016: Fuel moisture sensitivity to temperature and precipitation: climate change implications. *Climatic Change 134*, 59–71. https://doi.org/10.1007/s10584-015-1521-0

Flannigan, M.D. and *Harrington, J.B.*, 1988: A study of the relation of meteorological variables to monthly provincial area burned by wildfire in Canada 1953–80. *J. Appl. Meteorol. 27*, 441–452. https://doi.org/10.1175/1520-0450(1988)027<0441:ASOTRO>2.0.CO;2

Führer, E., Horváth, L., Jagodics, A., Machon, A. and *Szabados, I.*, 2011: Application of new aridity index in Hungarian forestry practice. *Időjárás 115*, 205–216.

Gavrilov, M.B., Wenling, A., Chenxi, X., Radaković, M.G., Qingzhen, H., Fan, Y., Zhengtang, G., Perić, Z., Gavrilov, G. and Marković S.B., 2019: Independent Aridity and Drought Pieces of Evidence Based on Meteorological Data and Tree Ring Data in Southeast Banat, Vojvodina, Serbia. Atmosphere 10, 586. https://doi.org/10.3390/atmos10100586

Gigović, L., Pourghasemi, H.R., Drobnjak, S., Bai, S. 2019: Testing a new ensemble model based on SVM and random forest in forest fire susceptibility assessment and its mapping in Serbia's Tara National Park. *Forests*, 10, 408. https://doi.org/10.3390/f10050408

Gračanin, M., 1950: Mjesečni kišni faktori i njihovo značenje u pedološkim istraživanjima. *Poljoprivredno znastvena smotra 12*, 51–67. (in Slovenian)

Hrnjak, I., Lukić, T., Gavrilov, M.B., Marković S., Unikašević M. and *Tošić I.*, 2014: Aridity in Vojvodina, Serbia. *Theor Appl Climatol* 115, 323–332. https://doi.org/10.1007/s00704-013-0893-1

IPCC, 2022: Climate Change 2022: Mitigation of Climate Change. Contribution of Working Group III to the Sixth Assessment Report of the Intergovernmental Panel on Climate Change; Shukla, P.R., Skea, J., Slade, R., al Khourdajie, A., van Diemen, R., McCollum, D., Pathak, M., Some, S., Vyas, P., Fradera, R., Eds.; Cambridge University Press: Cambridge, UK; New York, NY, USA.

Jolly, W.M., Cochrane, M.A., Freeborn, P.H., Holden, Z.A., Brown, T.J., Williamson, G.J. and *Bowman, D.M.J.S.*, 2015: Climate-induced variations in global wildfire danger from 1979 to 2013. *Nat. Commun. 6*, 7537. https://doi.org/10.1038/ncomms8537

Littell, J.S., McKenzie, D., Peterson, D.L. and *Westerling, A.L.*, 2009: Climate and wildfire area burned in western US ecoprovinces, 1916-2003. *Ecol. Appl. 19*, 1003–1021. https://doi.org/10.1890/07-1183.1

Lang, R., 1920: Verwitterrung und Bodenbildung als Eifuhrung die Bodenkunde. Stuttgart.

Law on National Parks, 2018: Official Gazette of RS No. 84/2015-15 and 95/2018-267 https://www.paragraf.rs/propisi/zakon_o_nacionalnim_parkovima.html (accessed on July 20, 2022). (in Serbian)

Lukić, T., Marić, P., Hrnjak, I., Gavrilov, M.B., Mlađan, D., Zorn, M., Komac, B., Milošević, Z., Marković, S.B., Sakulski, D., Jordan, A., Đorđević, J., Pavić, D. and *Stojsavljević, R.*, 2017: Forest fire analysis and classification based on a Serbian case study. *Acta Geogr. Slov. 57*, 51–63. https://doi.org/10.3986/AGS.918

Lukić, T., Gavrilov, M. B., Marković, S. B., Komac, B., Zorn, M., Mladjan, D., Đorđević, J., Milanović, M., Vasiljević, Dj. A., Vujičić, M. D., Kuzmanović, B., and Prentović, R., 2013: Classification of the natural disasters between the legislation and application: experience of the Republic of Serbia. *Acta geographica Slovenica* 53, 149–164. https://doi.org/10.3986/AGS53301

Nash, J. and *Sutcliffe, J.*, 1970: River flow forecasting through conceptual models part I—A discussion of principles. *J. Hydrol. 10*, 282–290. https://doi.org/10.1016/0022-1694(70)90255-6

Pérez-Sánchez, J., Senent-Aparicio, J., Díaz-Palmero, J.M. and *Cabezas-Cerezo, J.D.*, 2017: A comparative study of fire weather indices in a semiarid south-eastern Europe region. Case of study: Murcia (Spain). *Sci. Total Environ. 590–591*, 761–774. https://doi.org/10.1016/j.scitotenv.2017.03.040

RHSS, 2021: Republic Hydrometeorological Service of Serbia: Retrieved from: http://www.hidmet.gov.rs (accessed on May 5th 2021)

Rada, B. and *Marquina, L.*, 2008: Forest fire prevention plans in National Parks: Ordesa National Park and Monte Perdido. In Proceeding of the Second International Symposium on Fire Economics, Planning and Policy: A global View. April 10-22. Cordoba, Spain. https://www.fs.fed.us/psw/publications/documents/psw_gtr208en/psw_gtr208en_053-062_rada.pdf

Radaković, M.G., Tošić, I., Bačević, N., Mladjan D., Gavrilov M., Marković S., 2018: The analysis of aridity in Central Serbia from 1949 to 2015. *Theor Appl Climatol* 133, 887–898 https://doi.org/10.1007/s00704-017-2220-8

Rosavec, Roman, Damir Barčić, Željko Španjol, Milan Oršanić, Tomislav Dubravac, and Alan Antonović 2022: Flammability and Combustibility of Two Mediterranean Species in Relation to Forest Fires in Croatia. *Forests* 13, no. 8: 1266. https://doi.org/10.3390/f13081266

Skvarenina, J., Mindas, J., Holecy, J. and *Tucek, J.*, 2003: Analysis of the natural and meteorological conditions during two largest forest fire events in the Slovak Paradise National Park. In Proceeding of the Int. Scientific Workshop on Forest Fires in the Wildland-Urban Interface and Rural areas in Europe, May 15-16, Athens, Greece.

Tošić, I., Živanović, S. and *Tošić, M.*, 2020: Influence of extreme climate conditions on the forest fire risk in the Timočka Krajina region (northeastern Serbia). *Időjárás 124*, 331–347. https://doi.org/10.28974/idojaras.2020.3.2

Tošić, I., Mladjan, D., Gavrilov, M.B., Živanović, S., Radaković, M.G., Putniković, S., Petrović., P., Krstić Mistridželović, I. and *Marković, S.B.*, 2019: Potential influence of meteorological variables on forest fire risk in Serbia during the period 2000–2017. *Open Geosci. 11*, 414–425. https://doi.org/10.1515/geo-2019-0033

Trabaud, L., 1980: Impact biologique et écologique des feux de la végétation des zones de garrigues du bas-Languedoc. Thesis, Université des Sciences et Techniques du Languedoc, France.

Urbieta, I.R., Zavala, G., Bedia, J., José, M., Gutiérrez, J.M., San-Miguel-Ayanz, J., Camia, A., Keeley, J.E. and *Moreno, J.M.*, 2015: Fire activity as a function of fire–weather seasonal severity and antecedent climate across spatial scales in southern Europe and Pacific Western USA. *Environ. Res. Lett. 10*, 114013. https://doi.org/10.1088/1748-9326/10/11/114013

Van Wagner, C.E., 1987: Development and structure of the Canadian forest fire weather index system. *For. Tech. Rep., 35*, Canadian Forestry Service, Ottawa, Canada.

Viegas, D.X. and *Viegas, M.T.*, 1994: A relationship between rainfall and burned area for Portugal. *Int. J. Wildland Fire 4*, 11–16. https://doi.org/10.1071/WF9940011

Westerling, A.L., Hidalgo, H.G., Cayan, D.R. and *Swetnam, T.W.*, 2006: Warming and Earlier Spring Increase Western U.S. Forest Wildfire Activity. *Science 313*, 940–943. https://doi.org/10.1126/science.1128834

Won, M.S., Danesh Miah, M., Koo, K.S., Lee, M.B. and *Shin, M.Y.*, 2010: Meteorological Determinants of Forest Fire Occurrence in the Fall, South Korea. *J. Korean For. Soc. 99*, 163–171.

Živanović, S., 2021: Influence of forest humidity on the distribution of forest fires on the territory of Serbia. *Disaster Advances 14*, 8–14. https://doi.org/10.25303/149da0814

Živanović, S., *Ivanović* R., *Nikolić* M., *Đokić* M. and Tošić I., 2020: Influence of air temperature and precipitation on the risk of forest fires in Serbia. *Meteorol Atmos Phys. 132*, 869–883. https://doi.org/10.1007/s00703-020-00725-6

Živanović, S., 2017: Impact of drought in Serbia on fire vulnerability of forests. *Int. J. Bioautomation 21*, 217–226.

Živanović, V.S. and *Tošić A.I.*, 2020: Influence of climatic conditions on fire risk in Djerdap National Park (Serbia): A case study of September 2011. *Thermal Sci. 24*, 2845–2855. https://doi.org/10.2298/TSCI190905094Z

Živanović, S., Gocić M., Ivanović R. and *Martić-Bursać N.*, 2015: The effect of air temperature on forest fire risk in the municipality of Negotin. *Bull. Serbian Geograph. Soc. 95*, 67–76. https://doi.org/10.2298/GSGD1504067Z

DOI:10.28974/idojaras.2024.1.7

IDŐJÁRÁS

Quarterly Journal of the HungaroMet Hungarian Meteorological Service
Vol. 128, No. 1, January – March, 2024, pp. 121–141

Thermal assessments at local and micro scales during hot summer days: a case study of Belgrade (Serbia)

Stevan Savić [1,*], **Boško Milovanović** [2], **Dragan Milošević** [1], **Jelena Dunjić** [1], **Milica Pecelj** [2,3], **Milica Lukić** [4], **Miloš Ostojić** [5], and **Renata Fekete** [5]

[1]*University of Novi Sad, Faculty of Sciences*
Chair of Geoecology, Novi Sad, Serbia

[2]*Serbian Academy of Sciences and Arts,*
Geographical Institute "Jovan Cvijić", Belgrade, Serbia

[3] *University of East Sarajevo, Faculty of Philosophy, Department of Geography,*
East Sarajevo, Bosnia and Herzegovina

[4]*University of Belgrade, Faculty of Geography, Belgrade, Serbia*

[5]*University of Novi Sad, Faculty of Sciences,*
Department of Geography, Tourism and Hotel Management, Novi Sad, Serbia

**Corresponding Author e-mail: stevan.savic@dgt.uns.ac.rs*

(Manuscript received in final form January 11, 2023)

Abstract— Increasing thermal risk in cities is endangering the health and well-being of urban population and is driven by climate change and intensive urbanization. Therefore, if we plan to enlarge the capacities of cities to be more climate resilient in the 21st century, more detailed monitoring of urban climate on local and micro scales is needed. For this research we performed two microclimate measurement campaigns in urban area of Belgrade, during hot summer days in 2021. In total, five measurement sites were chosen in different urban designs and different local climate zones (LCZs). For thermal monitoring (air temperature – *Ta* and globe temperature – *Tg*) the Kestrel heat stress tracker sensor with 1-min measurement resolution was used, but we used 10-min average values. Obtained results showed distinct thermal differences (up to 7 °C on average) between densely built-up areas and green areas. Differences between built-up LCZs are lower with values from 2 to 4 °C. Important part of this research was microclimate monitoring on sites within the same LCZ (intra-LCZ variability). Results showed that shadows and short- and longwave radiation play a paramount role in thermal variability. Direct and reflected radiations on one measurement site increased *Ta* up to 6 °C and *Tg* up to 12 °C when compared to other measurement site (in a similar urban design), which was in the shadow.

Key-words: urban climate, temperature values, local climate zone; microclimate condition, urban design; city

1. Introduction

Numerous studies argued that different thermal conditions are driven by various urban designs, both on local scale (*Lehnert et al.,* 2021a) and microscale (*Middel* and *Krayenhoff,* 2019). Urban areas, characterized with predominant impervious surfaces and surface roughness, have higher thermal signal, lower evaporation, and a general disbalance in radiation and convection efficiency. Thus, urbanization directly affects temperature (air and surface), air humidity, wind speed, solar radiation, and other meteorological parameters, creating a city-specific urban climate. Furthermore, based on the modified pervious natural surfaces and the artificialization processes, thermoradiative and energetic processes are altered in cities (*Manoli et al.,* 2019). Based on the mentioned geometric/surface and thermal/radiative properties in cities, *Stewart* and *Oke* (2012) created a climate-based local climate zone (LCZ) classification system for urban and non-urban areas in order to standardize the research framework for thermal observations and assessments. Using LCZ concept, the heat load assessment could be performed at local scale that corresponds to areas (from hundreds of square meters to several kilometers on a horizontal scale) with uniform surface cover, urbanization structure, building materials, traffic, and human activities (*Stewart* and *Oke*, 2012). However, thermal differences can be uncovered on microscale, i.e., on sites that are located in the same LCZ, not only in different LCZs (*Shi et al.,* 2016; *Skarbit et al.,* 2017; *Quanz et al.,* 2018; *Shi et al.,* 2018; *Milošević et al.,* 2022a).

Climate projection outcomes displaying more frequent and severe heat waves (HWs) in Europe as a consequence of climate change (*Fischer* and *Schär,* 2010*; Jacob et al.,* 2018*; Geletič et al.,* 2020), and that will continue to occur during the 21st century (*Leconte et al.,* 2020; *IPCC,* 2021). According to previous publications, HWs in summer periods are generally connected with negative effects on public health in cities based on intensive outdoor thermal loads (*Tong et al.,* 2021*; Tuholske et al.,* 2021), but some results show potential positive influence of HWs in winter time in European regions that characterized with highly urbanized and populated areas/cities (*Macintyre et al.,* 2021). A combination of intense HWs and single hot days in summer and urbanization process in cities will modify urban thermal conditions more than the climate in rural/non-urbanized environments (*Oke et al.,* 2017). As a consequence, these urban-rural and intra-urban thermal differences will be intensified during intense HW periods and single hot days in summer.

The global climate change impacts force the cities to be more climate-resilient and climate-adaptable, and this task is of paramount importance (*Jänicke et al.,* 2021). Therefore, in situ and mobile measurements of climate conditions on the local and micro scales help to understand the climate processes and apply resilient/adaptable measures in cites. Previous research papers already highlighted the importance of urban networks and mobile measurements, e.g., *Konstantinov*

et al. (2018), *Dian et al.* (2019), *Šećerov et al.* (2019), *Lehnert et al.* (2021b), *Skarbit et al.* (2017), *Alonso* and *Renard* (2020) and *Milošević et al.* (2022a; 2022b).

Belgrade's urban heat island (UHI) and outdoor thermal comfort (OTC) indices have been identified so far in relation to the surrounding cities (*Milovanović,* 2015; *Milovanović et al.,* 2020), or based on offical meterological station datasets (*Pecelj et al.,* 2021; *Lukić et al.,* 2021). However, this study presents the first micrometeorological measurement campaigns that were performed in Belgrade (capital of Serbia), during hot summer days in 2021, in diverse urban environments. This kind of climate monitoring can be valuable for future climate-sensitive urban design and planning strategies. Based on that, the main goals of this research are as follows: a) monitoring of micrometeorological conditions in diverse urban environments, such as densely built-up areas, industrial areas, urban or forest parks, during hot summer days; b) detailed spatial and temporal analysis of thermal conditions (air temperature – *Ta* and globe temperature – *Tg*, which is a measure of the heat stress in district sunlight) obtained from the field measurements; and c) discussion of obtained thermal condition results in Belgrade in order to contribute to better climate change adaptation.

2. Research area, materials and methods

2.1. Description of research area

Belgrade is a capital city of the Republic of Serbia located in Southeast Europe (*Fig. 1*). City coordinates are 44°49`N and 20°27`E, with an average absolute elevation of about 117 m. The urban area of 3 222 km^2 has a population of about 1.6 million people. The downtown and its nearest surrounding are characterized by densely built-up urban design. Towards the suburban areas, there are more detached multi-storey buildings and one-storey houses with higher ratio of green areas. There are forest parks on the southern and northeastern parts of the urban area (*Fig. 1*). Obviously, a strongly modified climate and significant thermal differences between Belgrade urban area and its natural surroundings can be expected.

Belgrade has a *Cfa* climate (*Milovanović et al.,* 2017) according to the Köppen-Geiger climate classification system (*Kottek et al.,* 2006). During the 1991–2020 period, the mean annual temperature was 13.2 °C, the mean annual maximum temperature was 18.2 °C, the mean annual minimum temperature was 9.1 °C, and the mean annual precipitation is 698.9 mm (*Republic Hydrometeorological Service,* 2022).

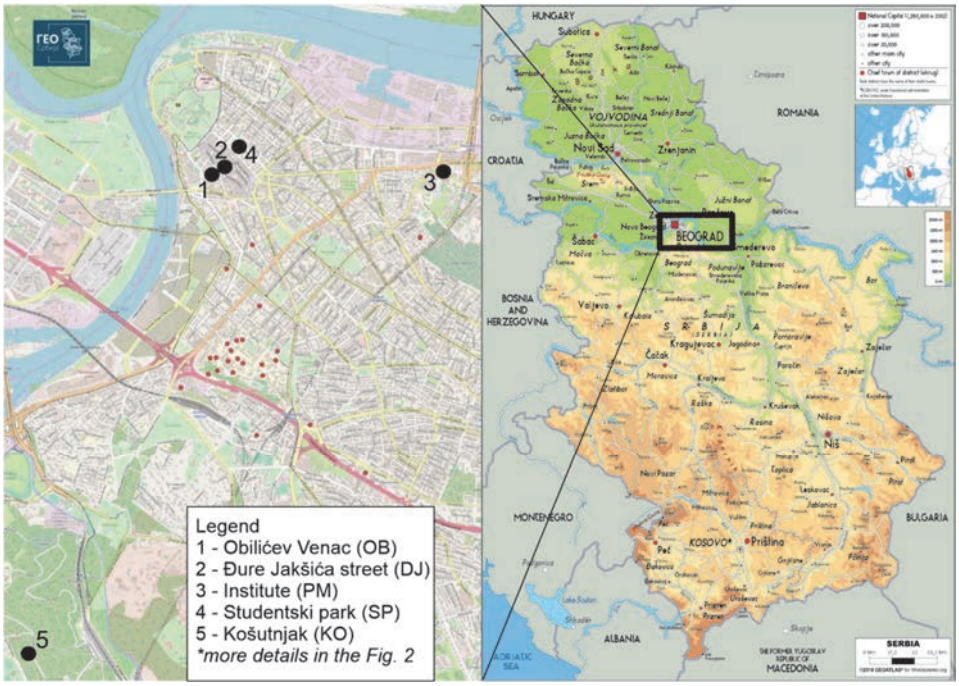

Fig. 1. Locations of micrometeorological measurement campaigns in summer 2021, and position of Belgrade in Serbia. Source of maps: *https://a3.geosrbija.rs/* (urban map of Belgrade) and *https://www.worldometers.info/img/maps/serbia_physical_map.gif* (Serbia/Europe).

2.2. Measurement locations and datasets

Micrometeorological monitoring has been performed through organization of two measurement campaigns in the urban area of Belgrade. Measurement campaigns were performed on June 18 and August 23, 2021 on five locations with different urban environments (*Fig. 2*). Both measurement campaigns were realized on hot summer days, i.e., during intensive HW periods. The HW period is defined as period with minimum three consecutive days with maximum temperature 5 °C or more comparing to average for this part of the year. In our case, in Belgrade, the average *Ta* is 22.0 °C in June and 24.0 °C in August (*Republic Hydrometeorological Service*, 2022), so days with maximum temperature of 29 °C or higher can be considered as adequate. Selected hot summer days, for our research, were characterized with maximum daily air temperature higher than 30 °C, no precipitation, low cloud cover, low wind speed, and intense solar radiation. Measurement campaigns were conducted at five sites with different urban designs: 1) Obilićev Venac (OV) is characterized by an open square with combination of pavement and green area with trees, and surrounded by densely built-up area that is equivalent to LCZ 2

according to *Stewart* and *Oke* (2012) classification system of local climate zones (LCZs). This location is a popular pedestrian and relaxation area in the city; 2) Đure Jakšića street (DJ) is an urban canyon street with multi-storey buildings on both sides and without green areas. The street is 100% covered by artificial surfaces and oriented northeast-southwest. This location is part of LCZ 2 and is a very intensive pedestrian corridor; 3) Institute for Biological Research „Siniša Stanković" (PM) is characterized by the combination of parking lots and green areas (on microlevel) and surrounded by light industrial buildings and residential areas. This measurement location is a synergy between LCZ 8 and LCZ 3; 4) Studentski park (SP) is characterized by an urban park with scattered trees (LCZ B). This park is about 200 m long and with width of about 100 m (based on Google Earth data). The central part of the park is an open square, while other parts of the park are a combination of green areas with trees and pedestrian footpaths. This park is surrounded by densely built-up areas that represent LCZ 2; and 5) Košutnjak (KO) presents a forest park in the suburban area with dense trees (LCZ A), and this location is characterized by 100% of pervious surfaces and green areas. Locations SP and KO are popular relaxation areas. Locations of measurement sites are presented in *Fig. 1* and *Fig. 2*, and more microenvironmental characteristics of each site are shown in *Table 1*.

Table 1. Basic descriptions of the microenvironment around the five measurement locations

Date of measurement	Name of location	Abbreviation of location	Latitude (N) longitude (E)	Altitude (m)	Urban area feature	LCZ
June 18 /August 23, 2021	Obilićev Venac	OV	44°48'59"; 20°27'18"	113	downtown; densely built	2
August 23, 2021	Đure Jakšića street	DJ	44°49'02"; 20°27'23"	116	downtown; densely built	2
June 18, 2021	Institute for Biological Research „Siniša Stanković"	PM	44°49'03"; 20°29'12"	94	industrial; residential	8_3
August 23, 2021	Studentski park	SP	44°49'09"; 20°27'29"	111	downtown; urban park	B
June 18, 2021	Košutnjak	KO	44°46'10"; 20°25'43"	220	outskirt; forest park	A

LCZ – local climate zone classification (based on *Stewart* and *Oke*, 2012)

Fig. 2. Locations of micrometeorological measurements (performed on June 18 and August 23, 2021) in Belgrade (Serbia): (1) Obilićev Venac – OV; (2) Đure Jakšića street – DJ; (3) Institute for Biological Research „Siniša Stanković" – PM; (4) Studentski park – SP; and (5) Košutnjak - KO.

Measurement campaign on June 18 was performed from 12:00 to 18:00 in Central European Summer Time – CEST at three locations (OV, PM, and KO). On August 23, the measurements were conducted from 12:00 to 21:00 (CEST) at OV, DJ, and SP. The goal was to monitor thermal differences in various urban designs during the hottest parts of the day and during the sunset period, when the highest thermal differences are expected in different urbanization types.

Three Kestrel 5400 Heat Stress Tracker sensors (*Fig. 2*, *Table 2*) were used to obtain one-minute measurements of *Ta* – air temperature measured at 1.1 m from the surface (in °C) and *Tg* – globe temperature measured at 1.1 m from the surface (in °C), during both measurement campaigns. The *Tg* is referred as the globe temperature or black globe temperature and resembles the thermal values of surroundings, and that means that *Tg* simulates the thermal conditions felt by the human body (*available at: https://www.designingbuildings.co.uk/wiki/Globe_temperature*). For further statistical analysis, we used 10-minute average values of the measured variables. Usage of 10-minute average values of meteorological variables showed to be sufficiently frequent for this kind of urban thermal analysis (*Unger et al.*, 2018; *Milošević et al.*, 2022a; 2022b). The Kestrel Heat Stress Tracker sensors were deployed at least 15 minutes before the start of the measurement in order to allow the sensors to equilibrate to the atmospheric conditions. Furthermore, the equipment is calibrated in accordance with the manufacturer's specifications (*available at: https://kestrelinstruments.com/mwdownloads/download/link/id/14/*).

Table 2. Accuracy, resolution, and range of Kestrel 5400 Heat Stress Tracker sensors used for outdoor thermal condition measurements in Belgrade (Serbia)

Sensors	Accuracy (+/-)	Resolution	Range
Air temperature (*Ta*)	0.5 °C	0.1 °C	-29.0 to 70.0 °C
Relative humidity (*RH*)	±2%RH	0.1%RH	10 to 90% 25 °C non-condensing
Wind speed (*v*)	larger of 3% of reading, least significant digit or 0.1 m/s	0.1 m/s	0.6 to 40.0 m/s
Globe temperature (*Tg*)	1.4 °C	0.1 °C	-29.0 to 60.0 °C

Note: available at: https://kestrelinstruments.com/mwdownloads/download/link/id/14/

2.3. Statistical methods

The description of the measured data is given using central tendency and dispersion (mean value, standard deviation, absolute maximum, and absolute minimum values of *Ta* and *Tg* – *Table 3*). Daily fluctuations of measured variables

in the period from 12:00 to 18:00 CEST and 12:00 to 21:00 CEST is shown graphically (*Fig. 3* and *Fig. 4*). We defined our research question as: Is there any significant difference between *Ta/Tg* values measured at different locations in Belgrade during the hot summer days? To test the null hypothesis H0 – there is no statistically significant difference between the *Ta* values measured at the mentioned locations; and H0 – there is no statistically significant difference between the *Tg* values measured at the mentioned locations; the one-way analysis of variance was used. Finally, following the results of the Levene test of homogeneity of variances, Hochberg and Games-Howell post-hoc tests were used to compare the values of the measured variables between possible pairs of locations. Those tests are considered appropriate if some of the assumptions for the application of one-way analysis of variance are not appropriate (*Tamhane*, 1979; *Stoline*, 1981; *Shingala and Rajyaguru*, 2015). To conduct the mentioned analysis, we used SPSS v. 14.

Table 3. Main statistical characteristics of air temperature (*Ta*) and globe temperature (*Tg*) in diverse urban environments of Belgrade (Serbia) during the measurement campaigns

Date of measurement	Locations	*Ta* (°C)				*Tg* (°C)			
		max.	min.	aver.	st. dev.	max.	min.	aver.	st. dev.
June 18, 2021	OV	34.7	26.8	30.8	1.9	48.5	35.4	42.5	3.3
	PM	36.1	29.6	32.6	1.7	50.3	34.1	42.6	3.8
	KO	29.4	25.8	27.8	0.9	37.6	26.9	29.5	1.3
August 23, 2021	OV	36.5	23.5	31.0	3.7	47.5	23.2	35.7	8.6
	DJ	40.6	25.4	32.1	3.8	49.1	25.6	34.1	6.9
	SP	33.4	23.6	30.3	3.1	39.1	23.7	31.6	4.0

max. – maximum; min. – minimum; aver. – average; st. dev. – standard deviation.

3. Results

3.1. Temperature measurements

During the two days measurement campaigns, the highest *Ta* values were recorded in the most densely built-up areas (OV, PM, DJ) and the lowest values were measured in green areas (KO and SP) (*Table 3*). The highest average *Ta* and *Tmax* values were measured in the compact mid-rise zone – LCZ 2 (OV, DJ) and large low-rise zone with small area and houses – LCZ 8_3 (PM). *Tmax* ranged from

34.7 °C (OV on June 18) to 40.6 °C (DJ on August 23). In the dense trees zone – LCZ A (KO – forest park) and scattered trees zone – LCZ B (SP – urban park), *Tmax* values are about 7 °C lower compared to the densely built-up zones (LCZ 2/LCZ 8_3). Similar tendencies are visible in the averaged *Ta* values, but with a smaller temperature difference (about 2 °C to 5 °C) between various LCZ types. Contrary to average *Ta* and *Tmax*, *Tmin* values are quite similar at all measurement locations, except the location PM. The *Tmin* is about 2 °C higher in PM in both measurement days, which can be explain with very intensive traffic in the morning in the industrial surroundings. The values of the standard deviation show 50% lower value at the location of KO (forest park) in relation to OV and PM (in June 18) and about 20% lower value at the location of SP (urban park) in relation to OV and DJ (in August 23) (*Table 3*).

Fig. 3 shows 10-minute *Ta* differences between measurement locations and provide detailed insights into the temporal variability of *Ta* in different urban designs in Belgrade. During the whole period of measurement (from 12:00 to 18:00, on June 18 CEST), *Ta* differences are positive when comparing densely built-up areas (OV and PM) with green area (KO). The highest intra-urban differences were recorded at 16:30 (8.7 °C) between PM and KO, and at 18:00 (7.1 °C) between OV and KO. Generally, the differences between OV/PM and KO constantly increased from 16:30 towards 18:00, but quite high differences can be also noticed before 15:30. The intra-urban comparison between LCZ 2 (OV) and LCZ 8_3 (PM) show lower *Ta* values on OV location during most of the time, with a few exceptions (*Fig. 3a*).

Temporal variability based on 10-minute *Ta* values during the measurement campaign on August 23 (from 12:00 to 21:00 CEST) present constantly higher values in the densely built-up area (LCZ 2) with locations OV and DJ, when compared to the urban park (SP). Only during the sunset and nighttime, the differences between OV and SP are negligible. The highest intra-urban differences are measured between DJ and SP, with differences higher than 7 °C (form 14:20 to 15:20), and OV-SP with the highest difference of 4.6 °C (at 12:30). The micro-location differences within the LCZ 2 zone (OV-DJ) show higher *Ta* values at OV location from 12:00 to 14:00, but during the rest of the measurement time, DJ location was warmer, particularly from 14:00 to 16:00 CEST (*Fig. 3b*).

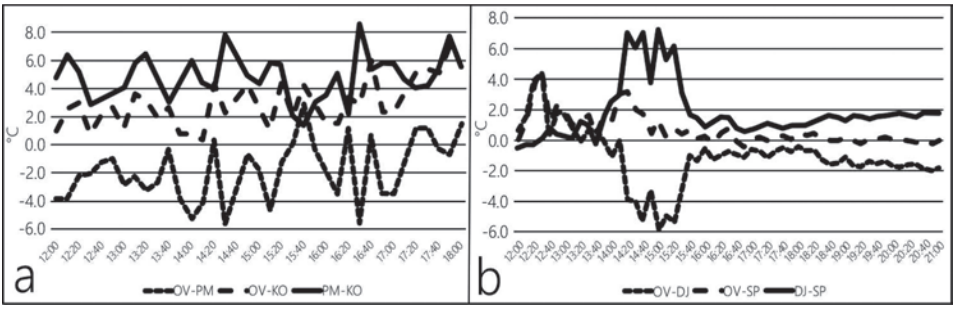

Fig. 3. Temporal variation of *Ta* in Belgrade (Serbia) during the measuring campaigns: (a) on June 18 – measurement time 12:00-18:00 CEST; and (b) August 23 – measuring time 12:00-21:00 CEST). The OV-PM – represents *Ta* differences between the diverse densely built-up types (LCZ 2/LCZ 8_3); OV-KO – represents *Ta* differences between the densely built-up type (LCZ 2) and forest park (LCZ A); and PM-KO – represents *Ta* differences between the densely built-up type (LCZ 8_3) and forest park (LCZ A).

The highest values of *Tg*, during both measurement campaigns are recorded at densely built-up zones (OV, PM, DJ), and the lowest values are noticed in forest and urban parks (KO and SP). The differences between built-up zones (OV, PM, DJ) and green areas (KO, SP) are from about 10 °C to 13 °C – *Tgmax*, about 2 °C to 9 °C – *Tgmin*, and about 4 °C to 13 °C – average *Tg*. The highest differences are recorded between densely built-up zones (LCZ 2/LCZ 8_3) and forest park (LCZ A) during the measurement campaign on June 18. Contrarily to that, significantly smaller differences were observed between compact mid-rise built-up zone (LCZ 2) and urban park (LCZ B) during the measurement campaign on August 23. The values of the standard deviation are three times lower in the forest park (KO), i.e., twice lower in the urban park (SP) compared to the urbanized parts of the city (*Table 3*).

Temporal variations of *Tg* (*Fig. 4*), during the measurement campaign on June 18 (*Fig. 4a*) show positive differences between OV/PM and KO during the whole measurement time, with a substantially hotter period between 14:00 and 15:30 CEST. During that time, *Tg* is higher from 12 °C to 17 °C in densely urbanized zones compared to the green area of forest park. Furthermore, *Tg* values are higher in large low-rise zone with small area of houses – LCZ 8_3 (PM) then in compact mid-rise zone – LCZ 2 (OV) during most of the measurement time (between 12:00 and 18:00). Only during a few short periods, *Tg* values are higher at OV location.

Fig. 4b presents *Tg* intra-urban differences during the measurement campaign on August 23 (form 12:00 to 21:00 CEST). On all three micro-locations (OV, DJ, and SP), after 16:00 CEST, *Tg* differences are around 0 °C (2 °C or less). On the other hand, significant differences between the densely built-up zone (OV

and DJ) and urban park (SP) are recorded from 12:00 to 16:00, particularly in the period from 14:00 to 16:00. In these hours, locations in LCZ 2 are substantially hotter than the urban park with *Tg* differences up to 15 °C. Also, the interesting outcome is that DJ location has substantially higher *Tg* values compared to OV location in the period from 14:00 to 15:40. In the period between 12:00 and 14:00, OV location has noticeable higher *Tg* values compared to DJ location. In both cases, *Tg* differences are up to 12 °C.

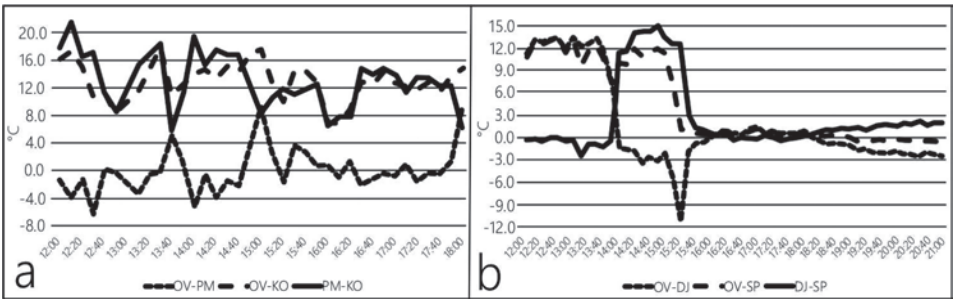

Fig. 4. Temporal variation of *Tg* in Belgrade (Serbia) during the measuring campaigns: (a) on June 18 – measurement time 12:00-18:00 CEST; and (b) on August 23 – measurement time 12:00-21:00 CEST). OV-DJ – represents *Tg* differences within the same densely built-up type (LCZ 2); OV-SP – represents *Tg* differences between the densely built-up type (LCZ 2) and urban park (LCZ B); and DJ-SP – represents *Tg* differences between the densely built-up type (LCZ 2) and urban park (LCZ B).

3.2. Statistical outcomes

To examine whether there is a statistically significant difference between *Ta* and *Tg* on all three locations during the measurement campaign on June 18, a one-way analysis of variance was applied. It was shown that there are statistically significant differences (r = 0.05) in *Ta* (*Table 4*) and *Tg* (*Table 5*) between the measurement locations.

Table 4. Results of the one-way analysis of *Ta* variance during the measurement campaign on June 18 (measurement time 12:00–18:00 CEST)

	Sum of squares	df	Mean square	F	Sig.
Between groups	432.486	2	216.243	88.210	0.000
Within groups	264.757	108	2.451		
Total	697.243	110			

df – degree of freedom; F – F-value; Sig. - significance

Table 5. Results of the one-way analysis of *Tg* variance during the measurement campaign on June 18 (measurement time 12:00–18:00 CEST)

	Sum of squares	df	Mean square	F	Sig.
Between groups	4039.694	2	2019.847	209.242	0.000
Within groups	1042.541	108	9.653		
Total	5082.234	110			

df – degree of freedom; F – F-value; Sig. - significance

Hochberg and Games-Howell post-hoc tests were used to determine which pairs of measurement locations had a statistically significant differences in *Ta* and *Tg*, respectively. These tests were chosen because the Levene test showed that there was no homogeneity of variance in the analyzed variables (*Table 6* and *Table 7*).

Table 6. Results of the Levene test of homogeneity of variance for *Ta* measured during the measurement campaign on June 18 (measurement time 12:00–18:00 CEST)

Levene statistic	df1	df2	Sig.
8.139	2	108	0.001

df1 and df2 – degreases of freedom; Sig. - significance

Table 7. Results of the Levene test of homogeneity of variance for *Tg* measured during the measurement campaign on June 18 (measurement time 12:00–18:00 CEST)

Levene statistic	df1	df2	Sig.
6.772	2	108	0.002

df1 and df2 – degreases of freedom; Sig. - significance

Regarding *Ta*, both tests showed that there are statistically significant differences between each of the pairs of locations (KO-OV; KO-PM, OV-PM), i.e., that *Ta* in KO is significantly lower than that in PM, i.e., OV, and that *Ta* on OV is significantly lower than that in PM (*Table 8*). In terms of *Tg*, there is a statistically significant difference only between KO and OV, i.e., KO and PM, where *Tg* value in KO is lower by about 12.8 °C than at PM and OV. The difference in *Tg* between PM and OV is negligible (0.027 °C) and not statistically significant (*Table 9*).

Table 8. Results of post-hoc tests for *Ta* measured during the measurement campaign on June 18 (measurement time 12:00–18:00 CEST)

Post-hoc test	Location	Location	Mean difference (°C)	Std. error	Significance
Hochberg	KO	PM	-4.784	0.36402	0.000
		OV	-3.000	0.36402	0.000
	PM	KO	4.784	0.36402	0.000
		OV	1.784	0.36402	0.000
Games-Howell	KO	PM	-4.784	0.319217	0.000
		OV	-3.000	0.344469	0.000
	PM	OV	1.784	0.420683	0.000

Significance values marked with grey areas are statistically significant.

Table 9. Results of post-hoc tests for *Tg* measured during the measurement campaign on June 18th (measurement time 12:00–18:00 h CEST)

Post-hoc test	Location	Location	Mean difference (°C)	Std. error	Significance
Hochberg	KO	PM	-12.784	0.698	0.000
		OV	-12.811	0.629	0.000
	PM	KO	12.784	0.698	0.000
		OV	-0.027	0.826	0.999
Games-Howell	KO	PM	-12.784	0.698	0.000
		OV	-12.811	0.629	0.000
	PM	OV	-0.027	0.826	0.999

Significance values marked with grey areas are statistically significant.

Analysis of variance for the measurement campaign on August 23 showed that there is a statistically significant difference in *Ta* and *Tg* between the measurement locations, i.e., OV, SP, and DJ (*Tables 10* and *11*). Furthermore, Levene test showed that there is a homogeneity of variance in *Ta*, while it is absent for *Tg* (*Tables 12* and *13*).

Table 10. Results of one-way analysis of *Ta* variance during the measurement campaign on August 23 (measurement time 12:00–21:00 CEST)

	Sum of squares	df	Mean square	F	Sig.
Between groups	90.703	2	45.352	3.570	0.030
Within groups	2058.109	162	12.704		
Total	2148.812	164			

df – degree of freedom; F – F-value; Sig. - significance

Table 11. Results of one-way analysis of *Tg* variance during the measurement campaign on August 23 (measurement time 12:00–21:00 CEST)

	Sum of squares	df	Mean square	F	Sig.
Between groups	514.521	2	257.261	5.627	0.004
Within groups	7406.473	162	45.719		
Total	7920.994	164			

df – degree of freedom; F – F-value; Sig. - significance

Table 12. Results of the Levene test of homogeneity of variance for *Ta* measured during the measurement campaign on August 23 (measurement time 12:00–21:00 CEST)

Levene Statistic	df1	df2	Sig.
0.523	2	162	0.594

df1 and df2 – degreases of freedom; Sig. - significance

Table 13. Results of the Levene test of homogeneity of variance for *Tg* measured during the measurement campaign on August 23 (measurement time 12:00–21:00 CEST)

Levene Statistic	df1	df2	Sig.
17.014	2	162	0.000

df1 and df2 – degreases of freedom; Sig. - significance

A statistically significant difference in *Ta* (1.8 °C) exists only between DJ and SP (*Table 14*). According to the Hochberg post-hoc test, a statistically significant difference in *Tg* exists only between OV and SP. However, according to the Games-Howell post-hoc test, there is a statistically significant difference between OV and SP, but also between DJ and SP (*Table 15*).

Table 14. Results of post-hoc tests for *Ta* measured during the measurement campaign on August 23 (measurement time 12:00–21:00 CEST)

Post-hoc test	Location	Location	Mean difference (°C)	Std. error	Significance
Hochberg	OV	DJ	-1.109	0.680	0.281
		SP	0.691	0.680	0.671
	DJ	OV	1.109	0.680	0.281
		SP	1.800	0.680	0.026
Games-Howell	OV	DJ	-1.109	0.720	0.276
		SP	0.691	0.650	0.539
	DJ	OV	1.109	0.720	0.276
		SP	1.800	0.667	0.022

Significance values marked with grey areas are statistically significant.

Table 15. Results of post-hoc tests for *Tg* measured during the measurement campaign on August 23 (measurement time 12:00–21:00 CEST)

Post-hoc test	Location	Location	Mean difference (°C)	Std. error	Significance
Hochberg	OV	DJ	1.673	1.289	0.480
		SP	4.291	1.289	0.003
	DJ	OV	-1.673	1.289	0.480
		SP	2.618	1.289	0.126
Games-Howell	OV	DJ	1.673	1.483	0.499
		SP	4.291	1.280	0.004
	DJ	OV	-1.673	1.483	0.499
		SP	2.618	1.072	0.043

Significance values marked with grey areas are statistically significant.

4. Discussion and conclusions

Micrometeorological measurement campaigns performed in Belgrade during hot summer days confirmed general statement that different urban designs have specific thermal patterns. The obtained results showed that densely built-up areas with multi-storey buildings (OV and DJ locations), densely built-up areas with light industrial buildings and residential areas (PM location), and green areas with trees (SP and KO locations) have different thermal conditions during the day/evening/sunset hours, and in the most cases, these differences are statistically

significant, as it was presented in results. Therefore, it can be concluded that the LCZ classification system created by *Stewart* and *Oke* (2012) based on different built-up and land cover types is appropriate method for thermal difference assessments in cities on the local scale.

Results from this study showed that temperature differences between densely built-up areas and green areas are about 7 °C, while differences between various built-up zones (LCZ 2 – LCZ 8_3) are about 2–4 °C. Previous studies focused on *Ta* showed that the highest *Ta* values are usually found in more urbanized areas of the city. For example, in Lisbon (Portugal), the more compact urban areas had the highest temperature conditions (*Oliveira et al.*, 2021), and in Banja Luka (Bosnia & Herzegovina), the downtown area with densely built-up design had highest thermal conditions in daytime and nighttime hours during the hot summer days (within HW period), when compared to urban park and riverside (*Milošević et al.*, 2022a). Research studies also analyzed urban shadows and green areas as elements that drive thermal conditions. *Lelovics et al.* (2016) recognized urban cool island with temperature lower by 1 °C (in Szeged, Hungary) or 2 °C (in Novi Sad, Serbia) in densely built-up zones during the summer days caused by shadowing conditions. Furthermore, urban parks that are close to/or within downtown areas could lower temperature conditions with up to 1 °C or more, that is noticed in Ghent (Belgium) (*Top et al.*, 2020). Therefore, a few research studies related of green infrastructures and its cooling potential in cities are published already. *Tan et al.* (2016; 2017) highlighted the impact of trees in Sky View Factor values, and some authors (*Morakinyo et al.*, 2020; *Gál et al.*, 2021) pronounced different spatial characteristics of green areas and content of species as elements that driving to cooler thermal conditions in hot periods. Also, we can conclude that hot summer days that occur within the heat wave periods represent higher concern based on general accumulation of heat during the consecutive hot summer days and obtained intensive outdoor thermal load (surplus of the heat) in built-up areas, as well as in rural/non-urbanized areas.

Our research also showed temperature differences between the locations in the same LCZ (OV and DJ locations), i.e., these outcomes emphasize that urban areas are characterized by specific thermal conditions on the microscale. OV and DJ locations are only 150 m away from each other, both are in the LCZ 2, but OV site is the open square with pavement and green area, while DJ is in a narrow street canyon with no green area (*Fig. 2*). During the measurement day, the OV site was sunny, while street canyon was in the shade from 12:00 to 14:00 CEST, which lead to higher *Ta* (about 4 °C) and *Tg* values (about 12 °C) on the OV site. Completely different thermal conditions at these two locations occur from 14:00 to 15.30 CEST. During this time, DJ site is entirely sunny, and the OV location is mostly in shadows because of trees and high buildings on the south part of the square. In this one and a half hour, the maximum measured *Ta* difference (DJ-OV) is 6 °C, and the maximum measured *Tg* difference is 12 °C. After 15.30 until the end of the measurement, both sites are in shadow, and differences are from

0 °C to 2–3 °C. These outcomes are in general in accordance with the results of *Geletič et al.* (2021), where is pronounced that direct and reflected radiation intensified thermal conditions in urban surroundings. On the other hand, we have to be aware of technical issues in Kestrel Heat Stress Trackers i.e., when the black globe is under direct radiation, this could lead to overestimation of *Tg* values (*Kántor* and *Unger*, 2011; *Middel et al.*, 2016). Intra-LCZ variability was analyzed by others, too, and *Skarbit et al.* (2017) found small differences (less than 1 °C) in Szeged (Hungary) between sites in LCZ 5, 6 and 9. *Shi et al.* (2018) confirmed thermal differences from LCZ 1 to LCZ 6 in Hong Kong, and the range is from 2 °C to 3 °C. *Quanz et al.* (2018) analyzed thermal conditions within LCZ 2_B and found that average daily differences are generally about 1 °C, but during clear, calm, and dry days, the daytime differences are rising about 3 °C.

During the same campaign in August, the results show that there are no differences of more than 3 °C between the OV/DJ locations and the SP site (urban park) in the period after 15:00 CEST. All three sites are in the shade after 15:00 CEST, but due to the green area in the urban park, lower values are expected. However, this is not the case, which may be due to several factors, such as the size of the park, which is approximately 100×200 m, characterized by scattered trees and urban environment around the park that is densely built-up (LCZ 2). Such a statement is in accordance with other studies that highlighted spatial characteristics of green areas as thermal conditions regulator (*Morakinyo et al.*, 2020; *Gál et al.*, 2021).

Finally, to prepare cities to be more resilient to climate change and heat risks, detailed thermal conditions monitoring on the microscale is needed, and therefore, further thermal assessments could be based on crowd-sourcing techniques using citizen weather stations (CWS), smart-phone records, web-based tools (*Fenner et al.*, 2017, 2019; *Venter et al.*, 2020), or purpose-designed mobile/portable instruments with specifically-numbered and high-accuracy sensors, particularly for radiation measurements (*Middel* and *Krayenhoff*, 2019; *Schnell et al.*, 2021). These kind of monitoring can contribute to achieving the SDGs (Sustainable Development Goals) within the Agenda 2030 through: a) raise awareness of heat load stress and to improve the public health care for vulnerable groups (under age or poverty groups) of the population in cities (SDG 3); b) contribute to a better implementation of climate-conscious urbanization that can improve the microclimate conditions, increase quality of life of the population, and adapt cities to climate change (SDG 11); and c) contribute to further adaptation to climate change, especially in urban areas where the microclimate and local climate are additionally modified due to the impact of urbanization (SDG 13). Obviously, the interaction of the process of "climate change-urbanization-urban climate" and its direct impact on the tendencies of atmospheric changes in cities should be incorporated into the development of climate action policies, as it becomes a serious issue in the twenty-first century (*Savić et al.*, 2022).

The potential shortcoming of this research can be defined in the number of days when measurements were taken, considering that during the summer of 2021, there were significantly more hot days. However, the two hot summer days that were analyzed in this study may well represent a realistic picture of the micro-scale thermal conditions in Belgrade, and each one must take into account both technical and human capacities when planning field measurements. The further development of these investigations will develop both on temporal and spatial levels, and it will be particularly interesting to implement a campaign of measurements in different urban micro conditions during tropical nights and to monitor the differences in thermal conditions.

Acknowledgements: This research was supported by the financial support of the Ministry of Education, Science and Technological Development of the Republic of Serbia (Grant No. 451-03-47/2023-01/200125). We would like to thank the Institute for Biological Research "Siniša Stanković" for the location provided for field measurements.

References

Alonso, L. and *Renard, F.*, 2020: A new approach for understanding urban microclimate by integrating complementary predictors at different scales in regression and machine learning models. *Remote Sens-Basel 12(15)*, 2434. https://doi.org/10.3390/rs12152434

Dian, C., Pongrácz, R., Incze, D., Bartholy, J., and *Talamon, A.*, 2019: Analysis of the urban heat island intensity based on air temperature measurements in a renovated part of Budapest (Hungary). *Geographica Pannonica 23*, 277–288. https://doi.org/10.5937/gp23-23839

Fenner, D., Meier, F., Bechtel, B., Otto, M., and *Scherer, D.*, 2017: Intra and inter 'local climate zone' variability of air temperature as observed by crowdsourced citizen weather stations in Berlin, Germany. *Meteorol. Z. 26*, 525–547. doi: 10.1127/metz/2017/0861

Fenner, D., Holtmann, A., Meier, F., Langer, I., and *Scherer, D.*, 2019: Contrasting changes of urban heat island intensity during hot weather episodes. *Environ. Res. Lett. 14*, 124013. https://doi.org/10.1088/1748-9326/ab506b

Fischer, E.M. and *Schär, C.*, 2010: Consistent geographical patterns of changes in high-impact European heatwaves. *Nat. Geosci. 3*, 398–403. https://doi.org/10.1038/ngeo866

Gál, T., Mahó, S. I., Skarbit, N., and *Unger, J.*, 2021: Numerical modelling for analysis of the effect of different urban green spaces on urban heat load patterns in the present and in the future. *Comput. Environ. Urban 87*, 101600. https://doi.org/10.1016/j.compenvurbsys.2021.101600

Geletič, J., Lehnert, M., and *Jurek, M.*, 2020: Spatiotemporal variability of air temperature during a heat wave in real and modified landcover conditions: Prague and Brno (Czech Republic). *Urban Clim. 31*, 100588. https://doi.org/10.1016/j.uclim.2020.100588

Geletič, J., Lehnert, M., Krč, P., Resler, J., and *Krayenhoff, E.S.*, 2021: High-resolution modelling of thermal exposure during a hot spell: a case study using PALM-4U in Prague, Czech Republic. *Atmosphere-Basel 12(2)*, 175. https://doi.org/10.3390/atmos12020175

IPCC, 2021: Summary for Policymakers. In: Climate Change 2021: The Physical Science Basis. Contribution of Working Group I to the Sixth Assessment Report of the Intergovernmental Panel on Climate Change [Masson-Delmotte V, P Zhai, A Pirani, SL Connors, C Péan, S Berger, N Caud, Y Chen, L Goldfarb, MI Gomis, M Huang, K Leitzell, E Lonnoy, JBR Matthews, TK Maycock, T Waterfield, O Yelekçi, R Yu, B Zhou (eds.)]. Cambridge University Press, Cambridge, United Kingdom and New York, NY, USA, 3−32. https://doi.org/10.1017/9781009157896.001

Jacob, D., Kotova, L., Teichmann, C., Sobolowski, S.P., Vautard, R., Donnelly, C., Koutroulis, A.G., Grillakis, M.G., Tsanis, I.K., Damm, A., and *Sakalli, A.*, 2018: Climate impacts in Europe under +1.5 C global warming. Earths Future 6, 264–285. https://doi.org/10.1002/2017EF000710

Jänicke, B., Milošević, D., and *Manavvi, S.*, 2021: Review of User-Friendly Models to Improve the Urban Micro-Climate. *Atmosphere-Basel 12(10)*, 1291. https://doi.org/10.3390/atmos12101291

Kántor, N. and *Unger, J.*, 2011: The most problematic variable in the course of human-biometeorological comfort assessment—the mean radiant temperature. *Cent. Eur. J. Geosci. 3*, 90–100. https://doi.org/10.2478/s13533-011-0010-x

Konstantinov, P., Varentsov, M., and *Esau, I.*, 2018: A high density urban temperature network deployed in several cities of Eurasian Arctic. *Environ. Res. Lett. 13(7)*, 075007. https://doi.org/10.1088/1748-9326/aacb84

Kottek, M., Grieser, J., Beck, C., Rudolf, B., and *Rubel, F.*, 2006: World Map of the Köppen-Geiger climate classification updated, *Meteorol. Z. 15(3)*, 259–263. https://doi.org/10.1127/0941-2948/2006/0130

Leconte, F., Bouyer, J., and *Claverie, R.*, 2020: Nocturnal cooling in Local Climate Zone: Statistical approach using mobile measurements. *Urban Clim. 33*, 100629. https://doi.org/10.1016/j.uclim.2020.100629

Lehnert, M., Savić, S., Milošević, D., Dunjić, J., and *Geletič, J.*, 2021a: Mapping local climate zones and their applications in European urban environments: A systematic literature review and future development trends. *ISPRS Int. J. Geo-Inf. 10*, 260. https://doi.org/10.3390/ijgi10040260

Lehnert, M., Brabec, M., Jurek, M., Tokar, V., and *Geletič, J.*, 2021b: The role of blue and green infrastructure in thermal sensation in public urban areas: A case study of summer days in four Czech cities. *Sustain. Cities Soc. 66*, 102683. https://doi.org/10.1016/j.scs.2020.102683

Lelovics, E., Unger, J., Savić, S., Gál, T.M., Milošević, D., Gulyás, Á., Marković, V., Arsenović, D., and Gál, C.V., 2016: Intra-urban temperature observations in two Central European cities: a summer study. Időjárás 120, 283–300.

Lukić M., Filipović, D., Pecelj, M., Crnogorac, L., Lukić, B., Divjak, L., Lukić, A., and *Vučićević, A.*, 2021: Assessment of Outdoor Thermal Comfort in Serbia's Urban Environments during Different Seasons. *Atmosphere-Basel 12(8)*, 1084. https://doi.org/10.3390/atmos12081084

Manoli, G., Fatichi, S., Schläpfer, M., Yu, K., Crowther, T.W., Meili, N., Burlando, P., Katul, G.G., and *Bou-Zeid, E.*, 2019: Magnitude of urban heat islands largely explained by climate and population. *Nature 573*, 55–60. https://doi.org/10.1038/s41586-019-1512-9

Macintyre, H.L., Heaviside, C., Cai, X., and *Phalkey, R.*, 2021: The winter urban heat island: Impacts on cold-related mortality in a highly urbanized European region for present and future climate. *Environ. Int. 154*, 106530. https://doi.org/10.1016/j.envint.2021.106530

Middel, A., Selover, N., Hagen, B., and *Chhetri, N.*, 2016: Impact of shade on outdoor thermal comfort—a seasonal field study in Tempe, Arizona. *Int. J. Biometeorol. 60(*, 1849–1861. https://doi.org/10.1007/s00484-016-1172-5

Middel, A. and *Krayenhoff, E.S.*, 2019: Micrometeorological determinants of pedestrian thermal exposure during record-breaking heat in Tempe, Arizona: Introducing the MaRTy observational platform. *Sci. Total Environ. 687*, 137–151. https://doi.org/10.1016/j.scitotenv.2019.06.085

Milošević, D., Trbić, G., Savić, S., Popov, T., Ivanišević, M., Marković, M., Ostojić, M., Dunjić, J., Fekete, R., and *Garić, B.*, 2022a: Biometeorological conditions during hot summer days in diverse urban environments of Banja Luka (Bosnia and Herzegovina). *Geographica Pannonica 26(4)*, 29–45. https://doi.org/10.5937/gp26-35456

Milošević, D., Middel, A., Savić, S., Dunjić, J., Lau, K., and *Stojsavljević, R.*, 2022b: Mask wearing behavior in hot urban spaces of Novi Sad during the COVID-19 pandemic. *Sci. Total Environ. 815*, 152782. https://doi.org/10.1016/j.scitotenv.2021.152782

Milovanović, B. 2015: Air Temperature Changes in Serbia and Belgrade Heat Island. Journal of the Geographical Institute "Jovan Cvijić" SASA 65(1), 33–42. https://doi.org/10.2298/IJGI1501033M

Milovanović, B., Ducić, V., Radovanović, M., and *Milivojević, M.*, 2017: Climate regionalization of Serbia according to Köppen climate classification. *Journal of the Geographical Institute "Jovan Cvijic" SASA 67(2)*, 103-114. https://dais.sanu.ac.rs/123456789/12570

Milovanović, B., Radovanović, M., and *Schneider, C.*, 2020: Seasonal Distribution of Urban Heat Island Intensity in Belgrade Serbia. *Journal of the Geographical Institute "Jovan Cvijić" SASA 70(2)*, 163–170. https://doi.org/10.2298/IJGI2002163M

Morakinyo, T.E., Ouyang, W., Lau, K.K.L., Ren, C., and *Ng, E.*, 2020: Right tree, right place (urban canyon): Tree species selection approach for optimum urban heat mitigation-development and evaluation. *Sci. Total Environ. 719*, 137461. https://doi.org/10.1016/j.scitotenv.2020.137461

Oke, T., Mills, G., Christen A, and *Voogt, J.*, 2017: Urban Climates. Cambridge University Press, Cambridge, UK.

Oliveira, A., Lopes, A., Correia, E., Niza, S., and *Soares, A.*, 2021: An urban climate-based empirical model to predict present and future patterns of the Urban Thermal Signal. *Sci. Total Environ. 790*, 147710. https://doi.org/10.1016/j.scitotenv.2021.147710

Pecelj, M., Matzarakis, A., Vujadinović, M., Radovanović, M., Vagić, N., Đurić, D., and *Cvetković M.*, 2021: Temporal Analysis of Urban-Suburban PET, mPET and UTCI Indices in Belgrade (Serbia). *Atmosphere-Basel 12(7)*, 916. https://doi.org/10.3390/atmos12070916

Quanz, J.A., Ulrich, S., Fenner, D., Holtmann, A., and *Eimermacher, J.*, 2018: Micro-scale variability of air temperature within a local climate zone in Berlin, Germany, during summer. *Climate 6*, 5. https://doi.org/10.3390/cli6010005

Republic Hydrometeorological Service 2021: Republic Hydrometeorological Service, Belgrade, Serbia. available at: https://www.hidmet.gov.rs/ciril/meteorologija/klimatologija_produkti.php

Republic Hydrometeorological Service 2022: Republic Hydrometeorological Service, Belgrade, Serbia. *available at: https://www.hidmet.gov.rs/ciril/meteorologija/klimatologija_srednjaci.php*

Savić, S., Trbić, G., Milošević, D., Dunjić, J., Ivanišević, M., and *Marković, M.*, 2022: Importance of assessing outdoor thermal comfort and its use in urban adaptation strategies: a case study of Banja Luka (Bosnia and Herzegovina). *Theor. Appl. Climatol. 150*, 1425–1441. https://doi.org/10.1007/s00704-022-04237-8

Shi, Y., Ren, C., Zheng, Y., and *Ng, E.*, 2016: Mapping the urban microclimatic spatial distribution in a sub-tropical high-density urban environment. *Architectural Science Review 59(5)*, 370–384. https://doi.org/10.1080/00038628.2015.1105195

Shi, Y., Lau, K.K.L., Ren, C., and *Ng, E.*, 2018: Evaluating the local climate zone classification in high-density heterogeneous urban environment using mobile measurement. *Urban Clim. 25*, 167–186. https://doi.org/10.1016/j.uclim.2018.07.001

Shingala, M. and *Rajyaguru, A.*, 2015: Comparison of Post Hoc Tests for Unequal Variance. *Int. J. New Technol. Sci. Engin. 2(5)*, 22–33.

Skarbit, N., Stewart, I. D., Unger, J., and *Gál, T.*, 2017: Employing an urban meteorological network to monitor air temperature conditions in the 'local climate zones' of Szeged, Hungary. *Int. J. Climatol. 37*, 582–596. https://doi.org/10.1002/joc.5023

Schnell, I., Cohen, P., Mandelmilch, M., and *Potchter, O.*, 2021: Portable - trackable methodologies for measuring personal and place exposure to nuisances in urban environments: Towards a people oriented paradigm. *Comput. Environ. Urban 86*, 101589. https://doi.org/10.1016/j.compenvurbsys.2020.101589

Stewart, I.D. and *Oke, T.R.*, 2012: 'Local Climate Zones' for urban temperature studies. *Bull. Amer. Meteorol. Soc. 93*, 1879–1900. https://doi.org/10.1175/BAMS-D-11-00019.1

Stoline, M.R., 1981: The Status of Multiple Comparisons: Simultaneous Estimation of All Pairwise Comparisons in One-Way ANOVA Designs. *The American Statistician 35(3)*, 134–141. https://doi.org/10.1080/00031305.1981.10479331

Šećerov, I., Savić, S., Milošević, D., Arsenović, D., Dolinaj, D., and *Popov, S.*, 2019: Progressing urban climate research using a high-density monitoring network system. *Environ. Monit. Assess. 191*, 89. https://doi.org/10.1007/s10661-019-7210-0

Tamhane, A.C., 1979: A Comparison of Procedures for Multiple Comparisons of Means with Unequal Variances. *J. Am. Stat. Assoc. 74(366)*, 471–480. https://doi.org/10.1080/01621459.1979.10482541

Tan, Z., Lau, K.K.L., and *Ng, E.*, 2016: Urban tree design approaches for mitigating daytime urban heat island effects in a high-density urban environment. *Energ. Buildings 114*, 265–274. https://doi.org/10.1016/j.enbuild.2015.06.031

Tan, Z., Lau, K.K.L., and *Ng, E.*, 2017: Planning strategies for roadside tree planting and outdoor comfort enhancement in subtropical high-density urban areas. *Build. Environ. 120*, 93–109. https://doi.org/10.1016/j.buildenv.2017.05.017

Tong, S., Prior, J., McGregor, G., Shi, X., and *Kinney, P.*, 2021: Urban heat: an increasing threat to global health. *BMJ-Brit. Med/ J. 375*, n2467. https://doi.org/10.1136/bmj.n2467

Top, S., Milošević, D., Caluwaerts, S., Hamdi, R., and *Savić, S.*, 2020: Intra-urban differences of outdoor thermal comfort in Ghent on seasonal level and during record-breaking 2019 heat wave. *Build. Environ. 185*, 107103. https://doi.org/10.1016/j.buildenv.2020.107103

Tuholske, C., Caylor, K., Funk, C., Verdin, A., Sweeney, S., Grace, K., Peterson, P., and *Evans, T.*, 2021: Global urban population exposure to extreme heat. *PNAS 118*, e2024792118. https://doi.org/10.1073/pnas.2024792118

Uger, J., Skarbit, N., and *Gál, T.*, 2018: Evaluation of outdoor human thermal sensation of local climate zones based on long-term database. *Int. J. Biometeorol. 62*, 183–193. https://doi.org/10.1007/s00484-017-1440-z

Venter, Z.S., Brousse, O., Esau, I., and *Meier, F.*, 2020: Hyperlocal mapping of urban air temperature using remote sensing and crowdsourced weather data. *Remote Sens. Environ. 242*, 111791. https://doi.org/10.1016/j.rse.2020.111791